Measuring and modeling the effects of temperature on the amphibian chytrid fungus and assessing amphibian skin bacterial communities

Zachary John Gajewski

Dissertation submitted to the Faculty of the
Virginia Polytechnic Institute and State University
in partial fulfillment of the requirements for the degree of

Doctor of Philosophy
in
Biological Science

Leah R. Johnson, Chair
Lisa K. Belden
Eric P. Smith
Meryl C. Mims

July 27, 2021
Blacksburg, Virginia

Keywords: Amphibian Chytrid Fungus, Amphibian Skin Bacteria, Thermal Performance Curves, Varying Temperature Performance

Measuring and modeling the effects of temperature on the amphibian chytrid fungus and assessing amphibian skin bacterial communities

Zachary John Gajewski

Abstract

Emerging infectious diseases are a threat to wildlife populations and conservation efforts. One example of this is the amphibian chytrid fungus, *Batrachochytrium dendrobatidis* (Bd), which causes the disease chytridiomycosis and has been linked to amphibian populations declines worldwide. There have been numerous attempts to mitigate the effects of Bd on amphibians, all with mixed results. Two factors that have previously been found to correlate with Bd infection intensity and prevalence are the amphibian skin bacterial communities and environmental temperatures. Some naturally occurring bacteria on the skin of amphibians and warmer temperatures can limit Bd infection. For my dissertation research, I aimed to 1) assess the amphibian skin bacterial communities across species, developmental stage, infection status, and different local environments, and 2) understand and predict the effect of a natural, varying temperature regime on the growth of Bd from constant temperature data. In Chapter 1, I reviewed the amphibian chytrid fungus and the effects of varying temperature on organisms' performance or trait rates. In Chapter 2, I sampled bacterial communities on ranid tadpoles and three ranid frog species at Mianus River Gorge Preserve in Bedford, New York, USA. I found that tadpoles had significantly different bacterial alpha diversity measurements than adult frogs, with higher Faith's phylogenetic diversity, Shannon diversity, and amplicon sequence variant (ASV) richness. Bacterial communities between the three different adult frogs species were not different. Additionally, infected frogs did not have significantly different bacterial communities than uninfected frogs. In Chapter 3, I predicted Bd growth in three varying temperature environments with Bayesian hierarchical models assuming different thermal performance curves. My predictions overestimated the growth of Bd in varying temperature environments, and the choice of thermal performance curve used in the models strongly impacted the predictions by altering the implied relationship between Bd's growth rate and temperature. In Chapter 4, I aimed to improve modeling methods for predicting *in vitro* Bd growth in varying temperature environments by adding additional features to the model based on observed biological phenomena, specifically a temperature-dependent delay period for Bd development. However, the model parameters were unidentifiable with this added complexity when only optical density data are available to quantify growth, highlighting the need to match the appropriate data to the complexity of the model. In Chapter 5, I created a mechanistic model that was parameterized by a combination of optical density, MTT assays (a metabolic assay), and zoospore count data to learn more about Bd growth dynamics. I also examined how many days of zoospore count data are needed to fit the mechanistic model. By combining these three data sources, I increased the ability to estimate most model parameters. My dissertation added to both the amphibian skin bacterial community literature, supporting differences between tadpoles and

adult frog bacterial communities, and added new data from a previously unsurveyed area. Attempts are being made to use bacterial communities to limit diseases in many wildlife populations, through a probiotic. To use skin bacterial communities, factors that shape these communities need to be understood to ensure the successful application of a probiotic. My dissertation also added to the thermal ecology literature, showing that current methods and my optical density Bayesian hierarchical model do not accurately predict performance in varying temperature environments. As temperatures are changing around the world and temperature variability is expected to increase in many places, predicting how organisms will perform in new thermal environments is becoming increasingly important.

Measuring and modeling the effects of temperature on the amphibian chytrid fungus and assessing amphibian skin bacterial communities

Zachary John Gajewski

General Audience Abstract

Infectious diseases around the world have led to wildlife population declines. Chytridiomycosis is a disease in amphibians caused by the amphibian chytrid fungus, *Batrachochytrium dendrobatidis* (Bd). Bd infects the skin of amphibians and can cause death. The composition of amphibian skin bacterial communities, bacteria that live on the skin of amphibians, can limit the growth of Bd on amphibians and reduce disease. Due to some species of bacteria inhibiting Bd growth, attempts have been made to try to use bacteria to limit disease in amphibians. But, we still do not know to what extent some host and environmental factors influence host bacterial communities, and how this might influence disease in amphibians. Warmer environmental temperatures have also been associated with reduced chytridiomycosis in amphibians. However, the effect of temperature is often studied at constant temperatures instead of natural, varying temperatures. The impact of varying temperature on Bd growth dynamics is still not fully understood. My dissertation research examined 1) differences in amphibian bacterial communities in different species and at different developmental stages (tadpoles vs. frogs), and 2) whether I can accurately predict Bd growth in varying temperature environments. First, I examined skin bacterial communities of three frog species at Mianus River Gorge, in Bedford, NY. I found that tadpoles had more diverse bacterial communities than adult frogs and that adults from the three species had similar bacterial communities, and that Bd infection status did not correlate with skin bacterial community composition. Second, I examined how temperature impacts the growth of Bd and whether we can predict how Bd grows in natural, fluctuating temperature conditions. Specifically, I used data from lab experiments in which I grew Bd at constant temperatures to fit a model and then predict how Bd grew in temperatures that fluctuate over the day as they would in nature. I found that current methods that use constant temperature data to predict how Bd grows in natural temperature scenarios are not accurate. Third, I attempted to improve modeling methods to predict Bd growth in natural temperature scenarios by specifying that Bd development is dependent on temperature. I found that the increasing model complexity without the correct type or amount of data leads to not being able to fit the model. Lastly, I combined three different types of Bd growth data to fit a new model that describes Bd growth. Fitting this new model with three data sources, I learned more about Bd growth and was more certain about the values of the parameters in the model. Additionally, this model has parameters and model components directly related to Bd growth, unlike in the previous Chapters' models. Using this model will allow us to examine how temperature influences specific Bd growth stages in future studies. My dissertation examined host and environmental factors that influence skin bacterial communities. Determine how these factors shape and change host bacterial communities will allow scientists to successfully use bacteria to reduce

disease in amphibians and other wildlife. Additionally, I examined methods in the literature and built my own model to predict Bd growth in varying temperature environments. I found that taking constant temperature data from the lab to predict Bd growth in more natural varying temperature environments is not accurate and future studies need to improve these methods. Developing these methods is becoming more important as temperatures change around the world and organisms are exposed to new temperatures. Improving these methods would allow more accurate predictions about organisms' performance in new environmental conditions.

Acknowledgments

I would first like to thank both of my advisors, Dr. Leah R. Johnson and Dr. Lisa K. Belden, for their support and help throughout my PhD. Thank you to Lisa for all of your guidance through both undergraduate and graduate school, and for giving me the opportunity to learn about research. Thank you to Leah for giving me the opportunity to learn more about statistical methods, and for all of your patience as I learned new quantitative methods. I would also like to thank my committee members, Dr. Eric Smith and Dr. Meryl Mims, for all the discussion and feedback they gave on my research.

Thank you to all of my friends both at and outside of Virginia Tech for always being willing to listen to my talk about my research and providing your thoughts. Thank you for all the support that you have given me through my PhD, and for making graduate school so memorable.

Next, I would like to thank Roderick G. Christie, Chris Nagy, Budd Veverka, and everyone at the Mianus River Gorge for funding my research and providing an excellent location for field work. I would also like to give special thanks to Daniel Medina and Jenifer Walke for all of their feedback on my field work and help with processing my field samples. Thank you to the IDEAS RCN for funding travel to Reno, NV, to collect some data for my dissertation. I would also like to thank Dr. Jamie Voyles for allowing me to travel to her lab and run some growth experiments. Additionally, I would like to thank the Voyles lab members for helping me run all of my growth experiments and for being so welcoming. A special thanks to Ciara Sheets for all her help in the lab and for continuing to run some experiments in my absence.

Lastly, I would like to thank my parents and sister for all of the love and support they provided me throughout my PhD. Thank you for always being there for me and for all of your words of encouragement, without you I would not be where I am today.

Contents

Chapter 1

Introduction

Several new emerging infectious diseases have been identified that severely impact wildlife populations. These include chytridiomycosis [71], white-nose syndrome [34], snake fungal disease [56], chronic wasting disease [30], Tasmanian Devil facial tumor disease [57], and coral black band disease [69]. One of the more devastating diseases has been chytridiomycosis. This disease is caused by the amphibian chytrid fungus *Batrachochytrium dendrobatidis* (Bd) and has been linked to significant amphibian populations declines around the world [25, 71].

Preventing the loss of any species is important for ethical reasons, but, amphibians often provide a first way for people to connect to nature, through catching or listening to frogs as kids. Additionally, the loss of amphibians from ecosystems can impact nutrient cycles, pest species populations, and predator populations (reviewed in [33]). For example, amphibians are vital members of some ecosystem food chains, both as prey and predators [20, 33, 93]. Loss of amphibians could also have consequences for vector-borne disease as tadpoles are often important biotic controls for mosquito populations [20]. Additionally, the loss of amphibians will reduce the food availability of species that commonly prey on amphibians. Recently, a study on neotropical snake populations showed that snake biodiversity decreased and some snake species had decreased body condition after amphibian populations declined in the area [93]. The impact on communities from the loss of amphibians highlights the importance of amphibians within a community and the need to understand and protect them from the amphibian chytrid fungus.

1.1 The Amphibian Chytrid Fungus

The amphibian chytrid fungus, Bd, is a zoosporic fungus belonging to the phylum Chytridiomycota (class Chytridiomycetes). The fungal pathogen has two life stages: zoospores and zoosporangia. Bd starts as an aquatic mobile zoospore. The zoospore encysts in keratinized cells in the epidermis of amphibians where it develops into a zoosporangium. As the zoosporangium matures in the epidermis an amphibian, zoospores develop inside of it; these are eventually released back into the water [7]. The new zoospores can either reinfect the same host or find a new host to infect. Infection by Bd can disrupt vital amphibian skin functions, and at a high enough infection intensity, this can lead to death [82, 85].

The severity of Bd and its negative impact on amphibian populations has led to a significant amount of research into how to control and mitigate its effects. Anti-fungal baths, which

have worked in zoos, have been considered, but all individuals in a population or globally would have to be treated [27, 28]. Individuals would also have to be treated repeatably due to the ability for Bd to persist in the environment for long periods of time [40]. The use of zooplankton as a biological control has been considered to control Bd in the environment. There has been some limited success in using some zooplankton species to limit Bd in laboratory experiments, but there has been no large scale experiment [15, 73]. Development of a vaccine has been attempted, with limited success, by exposing amphibians to dead zoospores to build up an immune reaction [58]. However, the viability of a vaccine is still debated in the literature [77].

1.2 Skin Microbial Communities and the Amphibian Chytrid Fungus

Research on the amphibian skin microbiome has yielded promising results with some bacterial species limiting the growth of Bd on amphibians. Microbial communities provide several benefits to the organisms that they grow on or in. These can range from digestive benefits from microbes found in the host digestive system to skin microbes providing some resistance to invading pathogens [18, 79]. This resistance to pathogens has been studied in many systems including corals [44], fish [19], plants [92], bats [35], and amphibians [68]. Amphibian skin bacterial communities have been extensively studied and certain bacterial species can provide some resistance to Bd (reviewed in [68]).

Many anti-Bd bacterial species have been identified that produce metabolites that limit the growth of Bd [4, 88]. For example, *Janthinobacterium lividum*, an anti-Bd bacterial species, produces metabolites violacein and I3C that limit the growth of Bd [13, 14]. In the lab, these metabolites can deter zoospores from settling on cells through negative chemotaxis [49]. Additionally, the application of naturally occurring anti-Bd microbes to the skin of certain amphibians has led to reduced mortality and morbidity in amphibians [4, 31, 32]. Wild amphibian populations with more anti-Bd microbes have been found to be less affected by Bd [16, 48, 90].

Successes in mitigating disease with skin microbial communities have led to a considerable amount of research on the amphibian skin microbiome to find more anti-Bd microbes, and determine if the application of anti-Bd microbes, aa probiotics, to at-risk amphibians is a feasible solution [68]. There have been several studies that have successfully implemented bioaugmentation strategies, adding or amplifying a beneficial microbe to a microbial community, to enhance host resistance to Bd [4, 31, 32]. A probiotic can be applied to soil and be transferred to amphibians [59], but, how long the probiotic lasts in the soil and how widely the probiotic can be spread is still not fully understood. The ability to spread the treatment through soil would allow amphibians to passively acquire the probiotic and amphibians would not have to be treated individually. However, the application of an anti-Bd

microbe does not seem to work universally across multiple species. For example, *Janthinobacterium lividum*, an anti-Bd microbe, mitigates the effects of Bd on *Rana muscosa*, the Mountain Yellow-legged frog, but similar effects were not seen in *Atelopus zeteki*, the Panamanian Golden frog [5]. To implement an effective probiotic strategy, when the probiotic should be applied and how host and environmental factors might alter the probiotic should be determined. Understanding these factors will ensure that the introduced microbe would persist on the amphibian and produce the desired outcome.

Amphibian skin microbial community research can be directly applied to disease and conservation efforts. Additionally, amphibians have served as useful model systems for understanding the environmental and host factors that influence microbial community composition. Amphibian skin microbial communities are different from environmental bacterial communities, hinting that hosts may have a way to influence their bacterial communities [86] or that already established bacterial communities outcompete new bacteria. Additional host factors, such as phylogeny and development, from tadpoles to adults, are associated with bacterial community differences [1, 6, 47, 63]. However, some studies find that phylogenic differences become less distinct at lower taxonomic levels (i.e., genus and species) and habitat differences and environmental factors are more important [10, 11, 22]. Previous studies have found environmental factors, such as elevation, temperature, pH, precipitation, and salinity, can influence amphibian skin microbial communities [2, 23, 37, 55, 80]. Pathogen effects on microbial communities can also be examined in amphibians due to Bd. Some field studies have shown Bd infection is associated with differences in skin microbial communities, while other studies have found no association [6, 39, 45, 67]. However, using field studies to examine the effect of a pathogen on host microbial communities can be difficult due to the lack of prior history of sampled amphibians. The relationship between Bd infection and microbial community has been demonstrated in the lab, but Bd infection is not always associated with community changes [41, 87]. Although there have been studies that have investigated host, environmental, and pathogen factors that influence host microbial communities, there is still more basic survey research needed to collect amphibian microbial community data to understand the relative importance of each factor.

1.3 Environmental Temperatures and the Amphibian Chytrid Fungus

Temperature is an environmental factor that influences amphibian microbial communities [46, 54, 55]. Temperature is also a critical environmental factor that impacts the growth and virulence of Bd [26, 75, 83, 89]. Early on in the literature, there was a debate on the importance of temperature, and climate change, to amphibian population declines and Bd dynamics [17, 51, 62, 70]. As more papers were published, the significance of environmental temperatures on Bd became clear. For example, prevalence and infection intensity of Bd is lower in warmer seasons and environments [8, 26, 64]. In the lab, Bd can grow at tem-

peratures between 3°C and 27°C [61, 75, 84]. Although there are strain differences in the thermal preference, the optimum growth temperature for Bd is around 21°C [84]. Warmer environments and habitats can offer a refuge from the fungal pathogen. Even though the relationship between Bd growth and temperature has been well established, there are other ways that temperature can influence Bd dynamics. For example, temperature can influence zoospore settling rate or the size of the zoospore, which could influence Bd dynamics. Studying the thermal preferences of the fungal pathogen can offer insights into the future spread of Bd and what amphibian populations might be vulnerable.

Studies that examine the relationship between an organism, such as Bd, and temperature often do so in controlled constant environments where an organism's trait is examined over several constant temperatures [75, 84]. The data are then fitted with a thermal performance curve, which is a mathematical function that relates a trait to constant temperatures, to understand how an organism's performance changes over temperature [3, 36, 75, 84]. Although most studies are at controlled constant temperatures, environmental temperatures are not constant and can fluctuate significantly at many temporal scales. Recently, more research has gone into examining an organism's performance, including Bd, in more natural varying temperature environments [29, 60, 65, 76]. These variations can have an impact on an organism's performance, such as Bd growth, amphibian development, and amphibian skin microbial communities [29, 55, 60, 76]. However, organisms can experience a wide range of varying environmental temperature regimes, and testing each regime individually to determine the effect on performance would impossible.

Using constant temperature to accurately predict varying temperature performance would limit the number of varying temperature studies needed. Methods that try to predict varying temperature performance from constant temperature data often use thermal performance curves (TPC) to adjust performance and integrate over time-varying temperatures to determine performance [9, 24, 42, 60]. One common method that does this is rate summation, which integrates across time-varying temperature to solve for performance [91]. However, the accuracy of these methods is still debated in the literature [9, 52, 60]. Additionally, there are many thermal performance curves in the literature to choose from. Each thermal performance curve varies in complexity, number of parameters, and form/shape of the function. Thus, the choice of TPC could impact varying temperature predictions under any projection methods.

A number of the different thermal performance curves were developed in the field of entomology with studies of temperature-dependent growth rates of larval and pupal stages in insects [12, 43, 53]. These curves have now been taken and fit in a wide variety of systems, including bacteria, phytoplankton, and amphibians [53, 60, 66] There are two approaches to constructing thermal performance curves, empirical and mechanistic. Empirical models, such as Logan 10, Stinner, and Briere, can be used for the temperature and trait data, however, the model provides no biological explanation for the data [12, 53, 78]. More mechanistic models have been developed based on enzyme kinetics to describe why a trait performance is low at non-optimal temperatures. Common mechanistic models include Schoolfield, Sharpe

and DeMichele, and Ikemoto [38, 72, 74]. These mechanistic models typically have taken the previous mechanistic model and improved it, incorporating new knowledge or ideas.

Understanding how thermal performance curves impact varying temperature predictions is important in making accurate predictions about varying temperature performance or disease dynamics. This will become increasingly important to understand as the temperature around the world continues to change and temperature variability increases with climate change [21, 81]. Temperature fluctuations can have significant impacts on species performance and biotic interactions, such as disease dynamics [29, 50, 60, 81]. This has been demonstrated in amphibian systems, where varying temperatures impact both amphibian host developmental rates and Bd growth rates [29, 50, 60]. Therefore, only making predictions based on an average environmental temperature could miss the important consequences that temperature fluctuations could have, leading to inaccurate predictions about an organism or disease dynamics in the natural environment.

1.4 Overview of Dissertation Chapters

In my dissertation, I aimed to examine how host and environmental factors, such as host species and habitat, influence bacterial skin communities and how environmental temperatures can impact disease dynamics and the growth of the amphibian chytrid fungus. In chapter 2, I examined how host and environmental factors are associated with amphibian skin bacterial communities. Specifically, I conducted a field survey at Mianus River Gorge in Bedford, New York, USA, where I collected amphibian and environmental bacterial swabs. Using the swabs, I examined how infection patterns and bacterial communities differed between species and sampling sites Mianus River Gorge Preserve. I expected to find that infection patterns were uniform across sampling sites and amphibians species. Also, I expected that different adult amphibian species would have different skin bacterial communities. In Chapters 3 and 4, I focused on methods for predicting varying temperature impacts on the growth of the amphibian chytrid fungus from constant temperature data. Specifically, in Chapter 3, I examined Bd growth optical density patterns across several constant temperatures and tried to predict varying temperature optical density growth patterns with the constant temperature data and a Bayesian hierarchical logistic growth pattern. I expected that my hierarchical logistic growth model would accurately predict Bd varying temperature optical density growth. In Chapter 4, I fit the hierarchical logistic growth model, developed in Chapter 3, with new laboratory data. Additionally, I further developed the hierarchical model by making the delay period temperature-sensitive. I expected that the added temperature-dependent parameter and new optical density data would improve predictions. However, I noticed a disconnect between my model complexity and how informative my data was, therefore, I combined three types of Bd growth data to build a more detailed Bd growth model in Chapter 5. I used optical density, MTT assay results, and zoospore count data collected to fit the new model. I also examined the amount of zoospore count data needed

to fit this new Bd growth model. I predicted that the added data would improve model fits to Bd growth dynamics and would limit zoospore count data. Lastly, in chapter 6, I give some general conclusions based on my dissertation research and give some suggestions for future research in thermal ecology and amphibian microbial ecology.

Bibliography

[1] Abarca, J. G., Vargas, G., Zuniga, I., Whitfield, S. M., Woodhams, D. C., Kerby, J., McKenzie, V. J., Murillo-Cruz, C., and Pinto-Tomás, A. A. (2018). Assessment of bacterial communities associated with the skin of Costa Rican amphibians at La Selva Biological Station. *Frontiers in Microbiology*, 9:2001.

[2] Albecker, M. A., Belden, L. K., and McCoy, M. W. (2019). Comparative analysis of anuran amphibian skin microbiomes across inland and coastal wetlands. *Microbial Ecology*, 78(2):348–360.

[3] Angilletta Jr, M. J. (2006). Estimating and comparing thermal performance curves. *Journal of Thermal Biology*, 31(7):541–545.

[4] Becker, M. H., Brucker, R. M., Schwantes, C. R., Harris, R. N., and Minbiole, K. P. (2009). The bacterially produced metabolite violacein is associated with survival of amphibians infected with a lethal fungus. *Applied and Environmental Microbiology*, 75(21):6635–6638.

[5] Becker, M. H., Harris, R. N., Minbiole, K. P., Schwantes, C. R., Rollins-Smith, L. A., Reinert, L. K., Brucker, R. M., Domangue, R. J., and Gratwicke, B. (2011). Towards a better understanding of the use of probiotics for preventing chytridiomycosis in Panamanian golden frogs. *Ecohealth*, 8(4):501–506.

[6] Belden, L. K., Hughey, M. C., Rebollar, E. A., Umile, T. P., Loftus, S. C., Burzynski, E. A., Minbiole, K. P., House, L. L., Jensen, R. V., Becker, M. H., et al. (2015). Panamanian frog species host unique skin bacterial communities. *Frontiers in Microbiology*, 6:1171.

[7] Berger, L., Hyatt, A. D., Speare, R., and Longcore, J. E. (2005). Life cycle stages of the amphibian chytrid *Batrachochytrium dendrobatidis*. *Diseases of Aquatic Organisms*, 68:51–63.

[8] Berger, L., Speare, R., Hines, H., Marantelli, G., Hyatt, A., McDonald, K., Skerratt, L., Olsen, V., Clarke, J., Gillespie, G., et al. (2004). Effect of season and temperature on mortality in amphibians due to chytridiomycosis. *Australian Veterinary Journal*, 82(7):434–439.

[9] Bernhardt, J. R., Sunday, J. M., Thompson, P. L., and O'Connor, M. I. (2018). Nonlinear averaging of thermal experience predicts population growth rates in a thermally variable environment. *Proceedings of the Royal Society B: Biological Sciences*, 285(1886):20181076.

[10] Bird, A. K., Prado-Irwin, S. R., Vredenburg, V. T., and Zink, A. G. (2018). Skin microbiomes of California terrestrial salamanders are influenced by habitat more than host phylogeny. *Frontiers in Microbiology*, 9:442.

[11] Bletz, M. C., Archer, H., Harris, R. N., McKenzie, V. J., Rabemananjara, F. C., Rakotoarison, A., and Vences, M. (2017). Host ecology rather than host phylogeny drives amphibian skin microbial community structure in the biodiversity hotspot of Madagascar. *Frontiers in Microbiology*, 8:1530.

[12] Briere, J.-F., Pracros, P., Le Roux, A.-Y., and Pierre, J.-S. (1999). A novel rate model of temperature-dependent development for arthropods. *Environmental Entomology*, 28(1):22–29.

[13] Brucker, R. M., Baylor, C. M., Walters, R. L., Lauer, A., Harris, R. N., and Minbiole, K. P. (2008a). The identification of 2, 4-diacetylphloroglucinol as an antifungal metabolite produced by cutaneous bacteria of the salamander *Plethodon cinereus*. *Journal of Chemical Ecology*, 34(1):39–43.

[14] Brucker, R. M., Harris, R. N., Schwantes, C. R., Gallaher, T. N., Flaherty, D. C., Lam, B. A., and Minbiole, K. P. (2008b). Amphibian chemical defense: antifungal metabolites of the microsymbiont *Janthinobacterium lividum* on the salamander *Plethodon cinereus*. *Journal of Chemical Ecology*, 34(11):1422–1429.

[15] Buck, J. C., Truong, L., and Blaustein, A. R. (2011). Predation by zooplankton on *Batrachochytrium dendrobatidis*: biological control of the deadly amphibian chytrid fungus? *Biodiversity and Conservation*, 20(14):3549–3553.

[16] Burkart, D., Flechas, S., Vredenburg, V., and Catenazzi, A. (2017). Cutaneous bacteria, but not peptides, are associated with chytridiomycosis resistance in Peruvian marsupial frogs. *Animal Conservation*, 20(6):483–491.

[17] Carey, C. and Alexander, M. A. (2003). Climate change and amphibian declines: is there a link? *Diversity and Distributions*, 9(2):111–121.

[18] Cho, I. and Blaser, M. J. (2012). The human microbiome: at the interface of health and disease. *Nature Reviews Genetics*, 13(4):260–270.

[19] de Bruijn, I., Liu, Y., Wiegertjes, G. F., and Raaijmakers, J. M. (2018). Exploring fish microbial communities to mitigate emerging diseases in aquaculture. *Federation of European Microbiological Societies Microbiology Ecology*, 94(1):161.

[20] DuRant, S. E. and Hopkins, W. A. (2008). Amphibian predation on larval mosquitoes. *Canadian Journal of Zoology*, 86(10):1159–1164.

[21] Easterling, D. R., Meehl, G. A., Parmesan, C., Changnon, S. A., Karl, T. R., and Mearns, L. O. (2000). Climate extremes: observations, modeling, and impacts. *Science*, 289(5487):2068–2074.

[22] Ellison, S., Rovito, S., Parra-Olea, G., Vásquez-Almazán, C., Flechas, S. V., Bi, K., and Vredenburg, V. T. (2019). The influence of habitat and phylogeny on the skin microbiome of amphibians in Guatemala and Mexico. *Microbial Ecology*, 78(1):257–267.

[23] Estrada, A., Hughey, M. C., Medina, D., Rebollar, E. A., Walke, J. B., Harris, R. N., and Belden, L. K. (2019). Skin bacterial communities of neotropical treefrogs vary with local environmental conditions at the time of sampling. *PeerJ*, 7:e7044.

[24] Ferguson, L. V. and Sinclair, B. J. (2020). Thermal variability and plasticity drive the outcome of a host-pathogen interaction. *The American Naturalist*, 195(4):603–615.

[25] Fisher, M. C. and Garner, T. W. (2020). Chytrid fungi and global amphibian declines. *Nature Reviews Microbiology*, 18(6):332–343.

[26] Forrest, M. J. and Schlaepfer, M. A. (2011). Nothing a hot bath won't cure: infection rates of amphibian chytrid fungus correlate negatively with water temperature under natural field settings. *PLoS One*, 6(12):e28444.

[27] Garner, T., Garcia, G., Carroll, B., and Fisher, M. (2009). Using itraconazole to clear *Batrachochytrium dendrobatidis* infection, and subsequent depigmentation of *Alytes muletensis* tadpoles. *Diseases of Aquatic Organisms*, 83:257–260.

[28] Georoff, T. A., Moore, R. P., Rodriguez, C., Pessier, A. P., Newton, A. L., McAloose, D., and Calle, P. P. (2013). Efficacy of treatment and long-term follow-up of *Batrachochytrium dendrobatidis* PCR-positive anurans following itraconazole bath treatment. *Journal of Zoo and Wildlife Medicine*, 44(2):395–403.

[29] Greenspan, S. E., Bower, D. S., Webb, R. J., Roznik, E. A., Stevenson, L. A., Berger, L., Marantelli, G., Pike, D. A., Schwarzkopf, L., and Alford, R. A. (2017). Realistic heat pulses protect frogs from disease under simulated rainforest frog thermal regimes. *Functional Ecology*, 31(12):2274–2286.

[30] Haley, N. J. and Hoover, E. A. (2015). Chronic wasting disease of cervids: current knowledge and future perspectives. *Annual Review of Animal Biosciences*, 3(1):305–325.

[31] Harris, R. N., Brucker, R. M., Walke, J. B., Becker, M. H., Schwantes, C. R., Flaherty, D. C., Lam, B. A., Woodhams, D. C., Briggs, C. J., Vredenburg, V. T., et al. (2009a). Skin microbes on frogs prevent morbidity and mortality caused by a lethal skin fungus. *Multidisciplinary Journal of Microbial Ecology*, 3(7):818–824.

[32] Harris, R. N., Lauer, A., Simon, M. A., Banning, J. L., and Alford, R. A. (2009b). Addition of antifungal skin bacteria to salamanders ameliorates the effects of chytridiomycosis. *Diseases of Aquatic Organisms*, 83(1):11.

[33] Hocking, D. J. and Babbitt, K. J. (2014). Amphibian contributions to ecosystem services. *Herpetological Conservation and Biology*.

[34] Hoyt, J. R., Kilpatrick, A. M., and Langwig, K. E. (2021). Ecology and impacts of white-nose syndrome on bats. *Nature Reviews Microbiology*, pages 1–15.

[35] Hoyt, J. R., Langwig, K. E., White, J. P., Kaarakka, H. M., Redell, J. A., Parise, K. L., Frick, W. F., Foster, J. T., and Kilpatrick, A. M. (2019). Field trial of a probiotic bacteria to protect bats from white-nose syndrome. *Scientific Reports*, 9(1):1–9.

[36] Huey, R. B. and Kingsolver, J. G. (1989). Evolution of thermal sensitivity of ectotherm performance. *Trends in Ecology & Evolution*, 4(5):131–135.

[37] Hughey, M. C., Pena, J. A., Reyes, R., Medina, D., Belden, L. K., and Burrowes, P. A. (2017). Skin bacterial microbiome of a generalist Puerto Rican frog varies along elevation and land use gradients. *PeerJ*, 5:e3688.

[38] Ikemoto, T. (2005). Intrinsic optimum temperature for development of insects and mites. *Environmental Entomology*, 34(6):1377–1387.

[39] Jani, A. J. and Briggs, C. J. (2018). Host and aquatic environment shape the amphibian skin microbiome but effects on downstream resistance to the pathogen *Batrachochytrium dendrobatidis* are variable. *Frontiers in Microbiology*, 9:487.

[40] Johnson, M. L. and Speare, R. (2003). Survival of *Batrachochytrium dendrobatidis* in water: quarantine and disease control implications. *Emerging Infectious Diseases*, 9(8):922.

[41] Jones, K. R., Walke, J. B., Becker, M. H., Belden, L. K., and Hughey, M. C. (2021). Time in the Laboratory, but Not Exposure to a Chytrid Fungus, Results in Rapid Change in Spring Peeper (*Pseudacris crucifer*) Skin Bacterial Communities. *Ichthyology & Herpetology*, 109(1):75–83.

[42] Kingsolver, J. G., Higgins, J. K., and Augustine, K. E. (2015). Fluctuating temperatures and ectotherm growth: distinguishing non-linear and time-dependent effects. *Journal of Experimental Biology*, 218(14):2218–2225.

[43] Kontodimas, D. C., Eliopoulos, P. A., Stathas, G. J., and Economou, L. P. (2004). Comparative temperature-dependent development of *Nephus includens* (Kirsch) and *Nephus bisignatus* (Boheman)(Coleoptera: Coccinellidae) preying on *Planococcus citri* (Risso)(Homoptera: Pseudococcidae): evaluation of a linear and various nonlinear models using specific criteria. *Environmental Entomology*, 33(1):1–11.

[44] Krediet, C. J., Ritchie, K. B., Paul, V. J., and Teplitski, M. (2013). Coral-associated micro-organisms and their roles in promoting coral health and thwarting diseases. *Proceedings of the Royal Society B: Biological Sciences*, 280(1755):20122328.

[45] Kruger, A. (2020). Frog skin microbiota vary with host species and environment but not chytrid infection. *Frontiers in Microbiology*, 11:1330.

[46] Kueneman, J. G., Bletz, M. C., McKenzie, V. J., Becker, C. G., Joseph, M. B., Abarca, J. G., Archer, H., Arellano, A. L., Bataille, A., Becker, M., et al. (2019). Community richness of amphibian skin bacteria correlates with bioclimate at the global scale. *Nature Ecology & Evolution*, 3(3):381–389.

[47] Kueneman, J. G., Parfrey, L. W., Woodhams, D. C., Archer, H. M., Knight, R., and McKenzie, V. J. (2014). The amphibian skin-associated microbiome across species, space and life history stages. *Molecular Ecology*, 23(6):1238–1250.

[48] Lam, B. A., Walke, J. B., Vredenburg, V. T., and Harris, R. N. (2010). Proportion of individuals with anti-*Batrachochytrium dendrobatidis* skin bacteria is associated with population persistence in the frog *Rana muscosa*. *Biological Conservation*, 143(2):529–531.

[49] Lam, B. A., Walton, D. B., and Harris, R. N. (2011). Motile zoospores of *Batrachochytrium dendrobatidis* move away from antifungal metabolites produced by amphibian skin bacteria. *EcoHealth*, 8(1):36–45.

[50] Lindauer, A. L., Maier, P. A., and Voyles, J. (2020). Daily fluctuating temperatures decrease growth and reproduction rate of a lethal amphibian fungal pathogen in culture. *BMC ecology*, 20:1–9.

[51] Lips, K. R., Diffendorfer, J., Mendelson III, J. R., and Sears, M. W. (2008). Riding the wave: reconciling the roles of disease and climate change in amphibian declines. *PLoS Biology*, 6(3):e72.

[52] Liu, S.-S., Zhang, G.-M., and Zhu, J. (1995). Influence of temperature variations on rate of development in insects: analysis of case studies from entomological literature. *Annals of the Entomological Society of America*, 88(2):107–119.

[53] Logan, J., Wollkind, D., Hoyt, S., and Tanigoshi, L. (1976). An analytic model for description of temperature dependent rate phenomena in arthropods. *Environmental Entomology*, 5(6):1133–1140.

[54] Longo, A. V. and Zamudio, K. R. (2017a). Environmental fluctuations and host skin bacteria shift survival advantage between frogs and their fungal pathogen. *Multidisciplinary Journal of Microbial Ecology*, 11(2):349–361.

[55] Longo, A. V. and Zamudio, K. R. (2017b). Temperature variation, bacterial diversity and fungal infection dynamics in the amphibian skin. *Molecular Ecology*, 26(18):4787–4797.

[56] Lorch, J. M., Knowles, S., Lankton, J. S., Michell, K., Edwards, J. L., Kapfer, J. M., Staffen, R. A., Wild, E. R., Schmidt, K. Z., Ballmann, A. E., et al. (2016). Snake fungal disease: an emerging threat to wild snakes. *Philosophical Transactions of the Royal Society B: Biological Sciences*, 371(1709):20150457.

[57] McCallum, H., Tompkins, D. M., Jones, M., Lachish, S., Marvanek, S., Lazenby, B., Hocking, G., Wiersma, J., and Hawkins, C. E. (2007). Distribution and impacts of Tasmanian devil facial tumor disease. *EcoHealth*, 4(3):318–325.

[58] McMahon, T. A., Sears, B. F., Venesky, M. D., Bessler, S. M., Brown, J. M., Deutsch, K., Halstead, N. T., Lentz, G., Tenouri, N., Young, S., et al. (2014). Amphibians acquire resistance to live and dead fungus overcoming fungal immunosuppression. *Nature*, 511(7508):224–227.

[59] Muletz, C. R., Myers, J. M., Domangue, R. J., Herrick, J. B., and Harris, R. N. (2012). Soil bioaugmentation with amphibian cutaneous bacteria protects amphibian hosts from infection by *Batrachochytrium dendrobatidis*. *Biological Conservation*, 152:119–126.

[60] Niehaus, A. C., Angilletta, M. J., Sears, M. W., Franklin, C. E., and Wilson, R. S. (2012). Predicting the physiological performance of ectotherms in fluctuating thermal environments. *Journal of Experimental Biology*, 215(4):694–701.

[61] Piotrowski, J. S., Annis, S. L., and Longcore, J. E. (2004). Physiology of *Batrachochytrium dendrobatidis*, a chytrid pathogen of amphibians. *Mycologia*, 96(1):9–15.

[62] Pounds, J. A. (2001). Climate and amphibian declines. *Nature*, 410(6829):639–640.

[63] Prest, T. L., Kimball, A. K., Kueneman, J. G., and McKenzie, V. J. (2018). Host-associated bacterial community succession during amphibian development. *Molecular Ecology*, 27(8):1992–2006.

[64] Pullen, K. D., Best, A. M., and Ware, J. L. (2010). Amphibian pathogen *Batrachochytrium dendrobatidis* prevalence is correlated with season and not urbanization in central Virginia. *Diseases of Aquatic Organisms*, 91(1):9–16.

[65] Raffel, T. R., Halstead, N. T., McMahon, T. A., Davis, A. K., and Rohr, J. R. (2015). Temperature variability and moisture synergistically interact to exacerbate an epizootic disease. *Proceedings of the Royal Society B: Biological Sciences*, 282(1801):20142039.

[66] Ratkowsky, D., Lowry, R., McMeekin, T., Stokes, A., and Chandler, R. (1983). Model for bacterial culture growth rate throughout the entire biokinetic temperature range. *Journal of Bacteriology*, 154(3):1222–1226.

[67] Rebollar, E. A., Hughey, M. C., Medina, D., Harris, R. N., Ibáñez, R., and Belden, L. K. (2016). Skin bacterial diversity of Panamanian frogs is associated with host susceptibility and presence of *Batrachochytrium dendrobatidis*. *Multidisciplinary Journal of Microbial Ecology*, 10(7):1682–1695.

[68] Rebollar, E. A., Martínez-Ugalde, E., and Orta, A. H. (2020). The amphibian skin microbiome and its protective role against chytridiomycosis. *Herpetologica*, 76(2):167–177.

[69] Richardson, L. L. (2004). Black band disease. In *Coral Health and Disease*, pages 325–336. Springer.

[70] Rohr, J. R., Raffel, T. R., Romansic, J. M., McCallum, H., and Hudson, P. J. (2008). Evaluating the links between climate, disease spread, and amphibian declines. *Proceedings of the National Academy of Sciences*, 105(45):17436–17441.

[71] Scheele, B. C., Pasmans, F., Skerratt, L. F., Berger, L., Martel, A., Beukema, W., Acevedo, A. A., Burrowes, P. A., Carvalho, T., Catenazzi, A., et al. (2019). Amphibian fungal panzootic causes catastrophic and ongoing loss of biodiversity. *Science*, 363(6434):1459–1463.

[72] Schoolfield, R., Sharpe, P., and Magnuson, C. (1981). Non-linear regression of biological temperature-dependent rate models based on absolute reaction-rate theory. *Journal of Theoretical Biology*, 88(4):719–731.

[73] Searle, C. L., Mendelson, J. R., Green, L. E., and Duffy, M. A. (2013). Daphnia predation on the amphibian chytrid fungus and its impacts on disease risk in tadpoles. *Ecology and Evolution*, 3(12):4129–4138.

[74] Sharpe, P. J. and DeMichele, D. W. (1977). Reaction kinetics of poikilotherm development. *Journal of Theoretical Biology*, 64(4):649–670.

[75] Stevenson, L. A., Alford, R. A., Bell, S. C., Roznik, E. A., Berger, L., and Pike, D. A. (2013). Variation in thermal performance of a widespread pathogen, the amphibian chytrid fungus *Batrachochytrium dendrobatidis*. *PloS One*, 8(9):e73830.

[76] Stevenson, L. A., Roznik, E. A., Greenspan, S. E., Alford, R. A., and Pike, D. A. (2020). Host thermoregulatory constraints predict growth of an amphibian chytrid pathogen (*Batrachochytrium dendrobatidis*). *Journal of Thermal Biology*, 87:102472.

[77] Stice, M. J. and Briggs, C. J. (2010). Immunization is ineffective at preventing infection and mortality due to the amphibian chytrid fungus *Batrachochytrium dendrobatidis*. *Journal of Wildlife Diseases*, 46(1):70–77.

[78] Stinner, R., Gutierrez, A., and Butler, G. (1974). An Algorithm for Temperature-dependent Growth Rate Simulation 1,2. *The Canadian Entomologist*, 106(5):519–524.

[79] Trevelline, B. K., Fontaine, S. S., Hartup, B. K., and Kohl, K. D. (2019). Conservation biology needs a microbial renaissance: a call for the consideration of host-associated microbiota in wildlife management practices. *Proceedings of the Royal Society B: Biological Sciences*, 286(1895):20182448.

[80] Varela, B. J., Lesbarrères, D., Ibáñez, R., and Green, D. M. (2018). Environmental and host effects on skin bacterial community composition in Panamanian frogs. *Frontiers in Microbiology*, 9:298.

[81] Vasseur, D. A., DeLong, J. P., Gilbert, B., Greig, H. S., Harley, C. D., McCann, K. S., Savage, V., Tunney, T. D., and O'Connor, M. I. (2014). Increased temperature variation poses a greater risk to species than climate warming. *Proceedings of the Royal Society B: Biological Sciences*, 281(1779):2013–2612.

[82] Voyles, J., Berger, L., Young, S., Speare, R., Webb, R., Warner, J., Rudd, D., Campbell, R., and Skerratt, L. F. (2007). Electrolyte depletion and osmotic imbalance in amphibians with chytridiomycosis. *Diseases of Aquatic Organisms*, 77(2):113–118.

[83] Voyles, J., Johnson, L. R., Briggs, C. J., Cashins, S. D., Alford, R. A., Berger, L., Skerratt, L. F., Speare, R., and Rosenblum, E. B. (2012). Temperature alters reproductive life history patterns in *Batrachochytrium dendrobatidis*, a lethal pathogen associated with the global loss of amphibians. *Ecology and Evolution*, 2(9):2241–2249.

[84] Voyles, J., Johnson, L. R., Rohr, J., Kelly, R., Barron, C., Miller, D., Minster, J., and Rosenblum, E. B. (2017). Diversity in growth patterns among strains of the lethal fungal pathogen *Batrachochytrium dendrobatidis* across extended thermal optima. *Oecologia*, 184(2):363–373.

[85] Voyles, J., Young, S., Berger, L., Campbell, C., Voyles, W. F., Dinudom, A., Cook, D., Webb, R., Alford, R. A., Skerratt, L. F., et al. (2009). Pathogenesis of chytridiomycosis, a cause of catastrophic amphibian declines. *Science*, 326(5952):582–585.

[86] Walke, J. B., Becker, M. H., Loftus, S. C., House, L. L., Cormier, G., Jensen, R. V., and Belden, L. K. (2014). Amphibian skin may select for rare environmental microbes. *Multidisciplinary Journal of Microbial Ecology*.

[87] Walke, J. B., Becker, M. H., Loftus, S. C., House, L. L., Teotonio, T. L., Minbiole, K. P., and Belden, L. K. (2015). Community structure and function of amphibian skin microbes: an experiment with bullfrogs exposed to a chytrid fungus. *PloS One*, 10(10):e0139848.

[88] Woodhams, D. C., Alford, R. A., Antwis, R. E., Archer, H., Becker, M. H., Belden, L. K., Bell, S. C., Bletz, M., Daskin, J. H., Davis, L. R., et al. (2015). Antifungal isolates database of amphibian skin-associated bacteria and function against emerging fungal pathogens: Ecological Archives E096-059. *Ecology*, 96(2):595–595.

[89] Woodhams, D. C., Alford, R. A., and Marantelli, G. (2003). Emerging disease of amphibians cured by elevated body temperature. *Diseases of Aquatic Organisms*, 55(1):65–67.

[90] Woodhams, D. C., Vredenburg, V. T., Simon, M.-A., Billheimer, D., Shakhtour, B., Shyr, Y., Briggs, C. J., Rollins-Smith, L. A., and Harris, R. N. (2007). Symbiotic bacteria contribute to innate immune defenses of the threatened mountain yellow-legged frog, *Rana muscosa*. *Biological Conservation*, 138(3):390–398.

[91] Worner, S. P. (1992). Performance of phenological models under variable temperature regimes: consequences of the Kaufmann or rate summation effect. *Environmental Entomology*, 21(4):689–699.

[92] Yang, H., Li, J., Xiao, Y., Gu, Y., Liu, H., Liang, Y., Liu, X., Hu, J., Meng, D., and Yin, H. (2017). An integrated insight into the relationship between soil microbial community and tobacco bacterial wilt disease. *Frontiers in Microbiology*, 8:2179.

[93] Zipkin, E. F., DiRenzo, G. V., Ray, J. M., Rossman, S., and Lips, K. R. (2020). Tropical snake diversity collapses after widespread amphibian loss. *Science*, 367(6479):814–816.

Chapter 2

Amphibian skin bacterial community differences among three species of co-occurring Ranid frogs

Authors: Zachary Gajewski[1*], Leah R. Johnson[1,2], Daniel Medina[1], William Crainer[3], Trent Wascaser[4], Chris Nagy[5], Lisa K. Belden[1]

Affiliations: 1 Department of Biological Sciences, Virginia Tech, Blacksburg, VA, 24061

2 Department of Statistics, Virginia Tech, Blacksburg, VA, 24061

3 Hackley School, Tarrytown, NY, 10591

4 Putnam Valley High School, Putnam Valley, NY, 10579

5 Mianus River Gorge Preserve, Bedford, NY, 10506

* Corresponding Author: gzach93@vt.edu

2.1 Abstract

Skin microbial communities are an essential part of host health and can play a role in mitigating disease. Environmental and host factors can shape and alter host microbial communities, and therefore, we need to understand to what extent some of these factors shape microbial communities and how this influences disease dynamics. Microbial communities have been studied in amphibian systems due to skin microbial communities providing some resistance to the amphibian chytrid fungus, *Batrachochytrium dendrobatidis*. However, we are only starting to understand how host and environmental factors shape these communities. In this study, we examined whether amphibian skin bacterial communities differ among host species, host infection status, host development, and host habitat. To do this, we collected skin swabs from tadpoles and adults of three Ranid frog species (*Lithobates spp.*) at Mianus River Gorge Preserve in Bedford, New York, USA. With the skin swabs, bacterial community composition was determined using 16s rRNA gene amplicon sequencing. Overall, we found that adult *Lithobates spp.* did not have significantly different bacterial communities. Additionally, individuals infected with the amphibian chytrid fungus did not have different

skin bacterial communities from uninfected individuals. Bacterial communities on *Lithobates* tadpoles did significantly differ from adults. Across sampling sites, the adult *Lithobates* spp. bacterial communities were not different. These results suggest that amphibian species within the same genus that are close to each other may not have significantly different bacterial. However, amphibian skin bacterial communities do appear to change across host development. Some of our findings, such as tadpoles having different microbial communities than adults, have also been found in previous studies. However, the literature is mixed on some of our other results. For example, some studies, like ours, find that adult amphibians across different species had similar skin microbial communities and others do not. This highlights that we do not fully understand when or to what extent some of these host or environmental factors influence skin microbial communities. Surveying more amphibians species' skin microbial communities across a wider set of environments will help us to find broad patterns about which host and environmental factors are most important.

2.2 Introduction

The microbial communities that live on the skin of organisms are diverse and can serve a variety of important functions, including influencing host health [14, 47]. These communities can provide some resistance to invading pathogens in invertebrate, mammal, fish, and amphibian host systems [15, 21, 22, 23, 38, 42, 52]. Due to the protection that skin microbial communities can provide, there have been many studies examining the role of skin microbiomes and wildlife disease, including studies that examine the amphibian skin microbiome and chytridiomycosis [40].

Chytridiomycosis is caused by the fungal pathogen, *Batrachochytrium dendrobatidis* (Bd), and has been linked to significant amphibian population declines [8, 19, 44, 45]. Mobile aquatic Bd zoospores infect amphibians by encysting in their skin, where they develop into zoosporangia. Inside zoosporangia, more zoospores develop and are eventually released back into the water to reinfect the host or infect a new host [7]. At great enough infection intensity, skin infection can lead to death. Naturally occurring bacteria found on amphibian skin, such as *Janthinobacterium lividum*, offer some resistance to Bd through the production of antifungal metabolites [5, 20, 21].In the field, differences in skin bacterial communities have been associated with infection prevalence. For example, an amphibian or amphibian population with more Bd inhibitory bacteria has been found to have lower Bd infection [12, 29, 51].

Even with the increasing number of studies examining the amphibian skin microbiome, there are still many questions, such as how different are skin microbial communities of adult amphibians within the same genus or how do amphibian skin microbial communities differ across sampling sites within close proximity. By sampling wild amphibians we can answer questions centered around how and to what extent host, environmental, and pathogen factors influence the host microbiome, and how this could influence host susceptibility to disease. Studying factors that influence host microbial communities in amphibians allows us

to examine a wide set of host and environmental factors due to the diversity of amphibians. Amphibians are found around the world and can occupy different habitats, both terrestrial and aquatic [49]. Many species also go through a major developmental change from larval to adult forms. Due to their diversity and the large literature, amphibians provide a good opportunity to examine how environmental, pathogen, and host factors influence host skin microbial communities.

In this paper, we assessed Bd infection and the skin microbiome in a natural un-manipulated amphibian population through a survey of the skin microbiome and Bd infection status of amphibians at the Mianus River Gorge Preserve in Bedford, New York, USA. We collected skin bacterial community data from adults of three Ranid frog species (*Lithobates clamitans*, *Lithobates sylvaticus*, and *Lithobates palustris*) and from *Lithobates* tadpoles, to determine how bacterial communities might differ between life stages and across different environments. For all the species listed above, and for *Lithobates catesbeianus*, we also collected Bd infection data from three sites around the preserve to monitor Bd status. Due to the location of the preserve, we expected infection rates to be low and uniform across the sampled amphibian species, due to previous studies finding low infection prevalence in the Northeastern United States [41]. Based on previous work, we also expected to find species differences in skin bacterial communities and that the tadpole bacterial communities would be different than adult amphibians [1, 6, 28, 33].

2.3 Methods

2.3.1 Sample Collection

Field Site

We captured, swabbed, and released amphibians at three different sites on or near the Mianus River Gorge in Bedford, New York, USA, to collect samples of the skin bacterial communities and to detect Bd infection (Figure 2.1). The sampling took place in June 2017 and 2018. Site 1 consisted of a vernal pool in a forested area next to an open meadow. Next to the vernal pool was a small stream that feeds into a marshland. The stream and the vernal pool were the two areas at this site where amphibians were sampled in both 2017 and 2018. Site 2 was a marshland and had partial canopy cover. The marshland was fed by a privately-owned pond that had no canopy cover at the edge of a road. At the other end of the marshland was another pond on the preserve that was in a forested area. Both ponds and the marshland at site 2 were used to collect amphibian samples only in 2017. Lastly, Site 3 was along a stream that started in a forested area near two vernal pools and led into a thick marshland. Amphibians were collected near the marshland and at the vernal pools in 2018. Each site had subsites that were sampled, based on the difference in terrain. For example, site 1 had five subsites that included a vernal pool, streams, and marshlands.

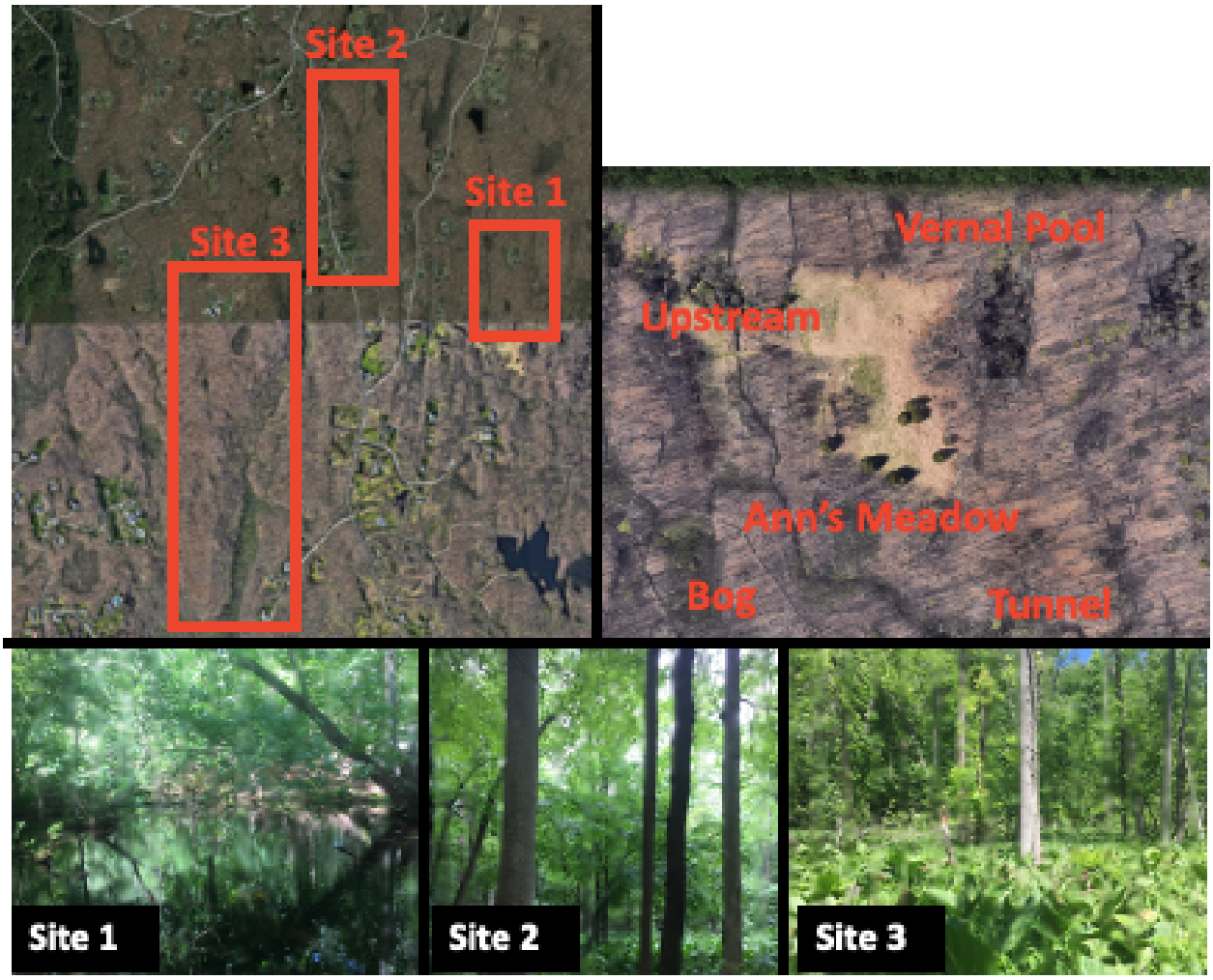

Figure 2.1: The map on the top left shows the main sites sampled at Mianus River Gorge Preserve. The map on the top right shows the subsites at site 1. The bottom row shows pictures of the sites amphibians were samples from. Site 1 consisted of a vernal pool and small nearby streams. Site 2 was a marshland covered mostly in skunk cabbage that had a pond on both sides. Lastly, site 3 was a marshland that was fed by larger streams. Site 1 was sampled in 2017 and 2018 while the other two sites were only sampled in one year; site 2 in 2017 and site 3 in 2018.

Amphibian Sampling

We collected skin swabs from *L. sylvaticus*, *L. clamitans*, *L. catesbeianus*, and *L. palustris*. At the three sites, we collected samples from *L. sylvaticus* and *L. clamitans*, while *L. catesbeianus* was only sampled at Site 2, and *L. palustris* was only found and sampled at site 1 and site 3 (Table 2.1). We also sampled tadpoles at site 1 in 2017 and 2018, at site 2 in 2017, and at site 3 in 2018 (Table 2.1). We sampled only one site and one species per day. Using dip nets, we caught amphibians, which were then placed individually into sterile Whirl-Pak bags until our sample size at the site was reached (Adults per site: 20 in 2017 and 25 in 2018; Tadpoles per site: 30 in 2017 and 20 in 2018) to avoid re-swabbing the same individual. For tadpoles, we included some water from the sample site in the bags. Once the sample size for that day was reached or it was noon, the amphibians were weighed in the Whirl-Pak bags using an Ohaus CS Series Compact Scale. Wearing sterile nitrile gloves, we then removed each amphibian from its bag and weighed the Whirl-Pak bag by itself, with amphibian mass as the difference. The amphibian was then rinsed with 50ml of autoclaved water to remove dirt and environmental bacteria. We then swabbed amphibians using a single sterile rayon swab (MW113, Medial Wire Equipment). Swabbing of adults consisted of 5 strokes in one direction on each of the hind feet and thighs, and 20 strokes on the ventral side (total strokes = 40), while for tadpoles, we swabbed around their mouth 25 times, an area commonly infected by Bd in tadpoles [32]. We then placed the swab in a sterile 1.5ml microcentrifuge tube and placed it on ice while in the field. Lastly, we measured the snout-vent length of the adult frogs and tail length, and the total length of tadpoles before they were released back in the site. Upon returning from the field (< 6 hours after sampling), we stored the microcentrifuge tubes containing swabs in a -20°C freezer.

Environmental Swab and Data Collection

At the start of June in both 2017 and 2018, we set up temperature probes (HOBO 8K Pendant Temperature/Alarm Data Logger UA-001-08) at various locations (in the water and air) that recorded a temperature measurement every 5 minutes. Temperatures were recorded at site 1 in both years, while site 2 temperatures were only recorded in 2017, and site 3 temperatures were only recorded in 2018. This corresponded to the sites that we sampled in 2017 and 2018.

We took environmental bacterial swabs at the site where amphibians were sampled each day. We took three swabs (sterile rayon swab, MW113, Medial Wire Equipment) at the location that we caught amphibians to collect environmental bacteria from the leaf litter, water, and muck. All environmental samples were taken after all amphibians were swabbed and released. Water environmental swabs consisted of dipping the swabs just under the surface of the water and circling the swab 25 times. Leaf litter bacterial samples were from dry leaves found on the edge of the water body and the swabs were run up and down 25 times on 1 leaf to collect the sample. Lastly, muck bacterial samples were from sediment

Amphibians Swabs	Sites	Infected		Not Infected		Total Caught	
		2017	2018	2017	2018	2017	2018
L. sylvaticus	Site 1	4 (**4**)	1	20 (**13**)	27	24 (**17**)	28
L. clamitans	Site 1	0	0	19 (**12**)	27	19 (**12**)	27
L. catebeianus	Site 1	0	0	0	0	0	0
L. palustris	Site 1	12 (**12**)	16	13 (**13**)	11	25 (**25**)	27
L. Tadpoles	Site 1	1	0	39 (**12**)	22	40 (**12**)	22
L. sylvaticus	Site 2	2	0	24	0	26	0
L. clamitans	Site 2	2	0	20	0	22	0
L. catebeianus	Site 2	1	0	11	0	12	0
L. palustris	Site 2	0	0	0	0	0	0
L. Tadpoles	Site 2	13	0	19	0	32	0
L. sylvaticus	Site 3	0	1	0	25	0	26
L. clamitans	Site 3	0	0	0	26	0	26
L. catebeianus	Site 3	0	0	0	0	0	0
L. palustris	Site 3	0	5	0	25	0	30
L. Tadpoles	Site 3	0	0	0	22	0	22
Total Amphibian Samples	-	35 (**16**)	23	165 (**47**)	185	200 (**66**)	208

Table 2.1: Species sampled at three field sites at Mianus River Gorge Preserve, Bedford, New York, USA. Listed in the table are how many individuals were sampled at each site and the number of individuals infected at the site broken down by species. Amphibian sample sizes for 16s rRNA gene amplicon sequencing are shown in parentheses in bold. Additionally, 15 environmental samples from site 1 (5 water, 5 leaf litter, and 5 muck swabs; 1 per subsite at site 1) were sequenced with the 66 amphibian samples.

from the bottom of the water body. These samples were collected using a sterile nitrile glove to scoop sediment up from the bottom of the water, and swabs were run gently back and forth 25 times over the sediment. The swabs were placed into 1.5ml microcentrifuge tubes and put on ice in the field until we stored them in a -20°C freezer at the end of the sampling period. We also took temperature and pH measurements (Oakton Waterproof pHTestr 30) at locations where amphibians were sampled each day.

2.3.2 Sample and Data Processing

Bacterial community data was obtained from the 2017 samples at site 1 and consisted of 66 swabs from three amphibian species; *L. sylvaticus*, *L. clamitans*, and *L. palustris*. We also sequenced 15 environmental samples, 1 set (water, leaf litter, and muck) of swabs for each of the 5 subsites at site 1.

Skin Bacterial Communities

The swabs were transported to Virginia Tech in Blacksburg, VA where they were all processed by a single individual (ZG). DNA was extracted from the amphibian and environmental swabs using a Qiagen DNeasy Blood and Tissue Kit (Qiagen Valencia CA, USA) with the lysozyme pre-treatment for gram-positive bacteria. We then stored the extracted DNA in 100 µl of molecular grade water in a -20°C freezer, and used it as template DNA for Bd PCR and assessing skin bacterial communities using 16S rRNA gene amplicon sequencing.

To assess the skin microbiome, we completed 16S rRNA gene amplicon sequencing of 81 samples collected in 2017 (17 *L. sylvaticus*, 25 *L. palustris*, 12 *L. clamitans*, 12 *Lithobates* tadpoles, and 15 environmental samples; 5 leaf litter, 5 water, and 5 muck). We amplified the V4 region of the 16S rRNA gene with 515F and 806R primers. The 806R primer contained a 12bp error-correcting Golay code to mark individual samples. Each 25 µl reaction contained 0.5 µl of both the 515F and 806R primers (at 10 µM concentration), along with 12 µl of ultra-clean PCR grade water, 10 µl of 5Prime hot master mix, and 2µl of the template DNA. Each 25 µL PCR reaction was run in triplicate, along with a negative control reaction that did not include any template DNA. The thermocycler conditions were: 94°C for 3mins to start, then 35 cycles of 94°C for 45seconds, 50°C for 1min, and 72°C for 1.5min, and a final 10 mins at 72°C. At the end of the PCR run, we combined each sample's triplicate PCR product into one microcentrifuge tube. We visualized the combined PCR product on a 1% TAE agarose gel, where the negative samples were checked for contamination and the sample wells were checked for amplification. The PCR products were quantified using a Qubit 2.0 fluorometer (Invitrogen, Carlsbad, California) with a dsDNA High Sensitivity assay kit. Using the DNA concentrations, we combined all the samples into a final pool with 200ng of DNA per sample (N=81). We then purified the pooled sample using the QIAquick PCR purification kit (Qiagen Valencia, CA) and sent it to the Genomics Center

at the Dana Farber Cancer Institute of Harvard University for 250bp single-end sequencing on an Illumina Mi-Seq instrument.

Sequence Processing

We processed the 250bp forward (single-end) reads using the QIIME2 pipeline [11]. We imported the raw reads and demultiplexed them. The reads were of consistently high quality across the full-length, so we did not need to trim them. We denoised the data using DADA2 [13], which included filtering out phiX and chimeric reads, as well as correcting amplicon errors. We used the recommended 'big data' parameters for DADA2, which included truncating reads with a quality score cut-off of 11. In addition, we only used 10000 reads to build the error distribution, which we have found is adequate for our high-quality data and significantly decreases the run time. The resulting amplicon sequence variants (ASV) table contained 45,080 ASVs. We then filtered out any ASVs that were present at less than 0.01% of the total read count. This left 1103 ASVs in the table. Taxonomy was assigned to these ASVs using the SILVA v132 database [37] and classifier with scikit-learn [35]. We then filtered out any ASVs that were assigned as chloroplasts, mitochondria, or were unassigned; this cut the number of ASVs to 1079. After visualizing the alpha rarefaction curve, the dataset was rarefied at 20000 reads, which resulted in the loss of 4 samples with lower read counts (3 *L. sylvaticus* and 1 *L. palustris*). The final table contained 77 samples (Table 2.1) and 1079 ASVs.

2.3.3 Bd detection

We screened all the amphibian swab samples collected (2017 and 2018, N= 408) for Bd using PCR [3]. Each 25 µl reaction, one per sample, contained: 0.5 µl of dNTPs, 0.2µl of Taq DNA Polymerase, 3.9µl of Taq Buffer with MgCl2, 2.5µl of ITS 1-3 primer, 2.5µl of 5.8S primer, 2µl of extracted sample DNA, and 13.4 µl of water. The thermocycler conditions were: 93°C for 10 mins to start, then 30 cycles of 93°C for 45seconds, 60°C for 45 seconds, and 72°C for 1min, and a final 10mins at 72°C. Every thermocycler run had a positive (extracted DNA from a Bd JEL 404 stock) and negative (molecular grade water) control. Each PCR product was run on a 1% TAE agarose gel. The gels were inspected to ensure the amplification in the positive sample and no amplification in the negative sample. We recorded a sample as Bd positive if a band was seen on the gel.

2.3.4 Statistical Methods

We calculated three metrics in QIIME2 [11] to estimate within sample diversity (alpha diversity): Shannon diversity, Faith's phylogenetic diversity, and ASV richness. Shannon diversity is a measurement that accounts for both richness and evenness of taxa. Faith's phylogenetic diversity is calculated using phylogenetic branch lengths. Lastly, ASV richness is the number of different ASVs in the sample. All data were exported from QIIME2 and analyzed in R v.4.0.0 [46]. All other analyses were completed using base R unless otherwise specified.

Differences in bacterial communities between amphibian groups and sampling subsites

To determine how bacterial communities differed across amphibian species and sampling sites, we used the amphibian skin bacterial samples and used multivariate methods along with generalized linear models (GLMs) to compare alpha diversity measures. To assess differences in the community structure of ASVs, the skin microbiome community data was visualized with non-metric multidimensional scaling (NMDS) plots using a Bray-Curtis dissimilarity index (Figure 3A) and Jaccard dissimilarity index (Figure 3B). The Bray-Curtis dissimilarity index uses relative abundance data and the Jaccard dissimilarity index uses presence and absence data. We used a permutational multivariate analysis of variance (PERMANOVA; `vegan`: `adonis`; [34]) to test if the multivariate means (centroids) and variances (dispersion) of the amphibian skin bacterial species samples were different. We also specifically tested if the dispersion between the species were different using a permutation test (`permutest`) in the vegan R package [34]. The permutation tests were run twice, once for each dissimilarity matrix, with 999 permutations for each test.

To determine how bacterial diversity measurements (Shannon diversity, ASV richness, and Faith's phylogenetic diversity) differed across amphibian groups and sampling sites, we used a series of generalized linear models (GLMs). For each alpha diversity measurement, we fit two models, one for sampling sites and one for amphibian groups. Shannon diversity and Faith's phylogenetic diversity GLM models were all fit using a Gamma distribution with an inverse link function and ASV richness GLM models were fit using a Negative Binomial distribution with a log link function. A Gamma distribution was chosen in this study for any data that was continuous and had to be positive. A Negative Binomial distribution was chosen for discrete data, and it was used over a Poisson distribution due to overdispersion. After fitting the models, we used `emmeans` to make contrasts, and uses the Tukey methods to adjust for multiple testing, between amphibian groups and sampling sites in the models.

Lastly, we used an indicator species analysis to determine which ASVs were significantly associated with bacterial community differences between tadpoles and adults. To do this, we used the `multipatt` function (func = IndVal.g, permutations = 999) in the `indicspecies`

package in R [16]. This analysis uses an ASV table to determine how strongly an ASV is associated with an amphibian group and computes a p-value.

Differences between bacterial communities in infected and non-infected *Lithobates palustris*

To compare bacterial communities between infected and non-infected amphibians, we only used *L. palustris* since this was the only species with enough samples of infected individuals (2017: N=12 infected, 13 uninfected) for a meaningful statistical comparison. Differences in bacterial communities between infected and non-infected *L. palustris* were compared using GLMs with alpha diversity measures set as predictor variables. The three models used a binomial distribution and a logit link function. Each alpha diversity measure addresses a different aspect of diversity and therefore only one was used in a model at a time. We also examined the bacterial community structure between infected and non-infected individuals using a PERMANOVA and permutation test, as described above.

Differences in pH, temperature, and amphibian bacterial communities across subsampling sites

The 2017 pH readings among sampling sites at site 1, were compared using a GLM with a Gamma distribution with an inverse link function and the `emmeans` package in R [30] was used to make contrasts between these locations. The 2017 temperature among sampling sites at site 1, were compared using a linear model and contrasts again were made using `emmeans`. We then compared amphibian skin bacterial diversity measurements (Shannon diversity, ASV richness, and Faith's phylogenetic diversity) across subsites at site 1. To do this we used GLMs, as described above. We then used `emmeans` with the GLMs to make contrasts, with a Bonferroni correction, between sampling sites and determine which subsites at site 1 had significantly different bacterial diversity measurements.

2.4 Results

We identified a total of 1079 unique ASVs. There were 946 ASVs from *L. clamitans*, 893 ASVs from *L. palustris*, 811 ASVs from *Lithobates* tadpoles, 769 ASVs from *L. sylvaticus*, and 879 ASVs from the environmental samples. The phyla Proteobacteria dominated most of the amphibian and environmental bacterial samples, with 596 and 60% of the total relative abundance in all environmental and amphibian samples. Bacterioidetes was another dominant phyla in tadpoles, *L. sylvaticus*, and a stream subsite with 126 ASVs and $>$ 12% relative abundance in these groups, however, this phyla was low in the rest of the amphibian and environmental samples with $<$ 5% relative abundance. Common bacterial

families included Burkholderiaceae, Enterobacteriaceae, and Beijerinckiaceae with a mean relative abundance of over 10% in multiple amphibian groups and environmental samples (Figure 2.2).

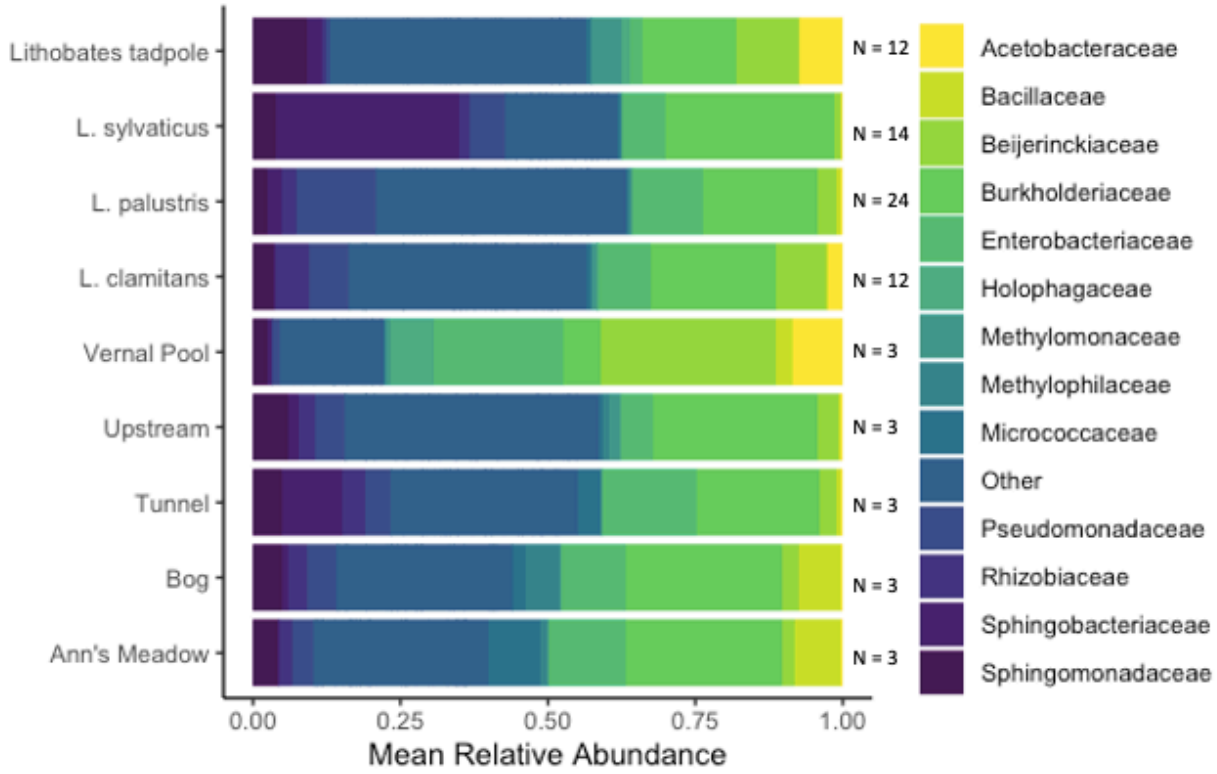

Figure 2.2: The mean relative abundance of bacterial families found on amphibian and environmental bacterial swabs. Families that had less than 5% mean relative abundance were grouped into the other category. The sample size used to create the mean relative abundance bars for each group is shown at the end of each bar.

Differences in bacterial communities between amphibian groups

Adult amphibians had similar Faith's phylogenetic diversity (all `emmeans` contrasts p-values > 0.05) and ASV richness (all `emmeans` contrasts p-values > 0.05). We found that there was a significant difference in Shannon diversity (Figure 2.3) between *L. clamitans* and *L. sylvaticus* (p-value $= 0.018$), but both species had similar Shannon diversity compared to *L. palustris* (all contrasts p-values > 0.05). Lastly, when we compared bacterial communities of adults to tadpoles, we found that tadpoles had a higher Faith's phylogenetic diversity (Figure 2.3) than all adult species (tadpoles-*L. palustris* p-value <0.0001; tadpoles-*L. sylvaticus*, p-value <0.0001; tadpoles-*L. clamitans*, p-value $= 0.001$), a higher ASV richness diversity than two of the adult species (tadpoles-*L. palustris* p-value $= 0.0212$; tadpoles-*L. sylvaticus*, p-value $= 0.0319$; other p-value > 0.05), and a higher Shannon diversity than one adult species

(tadpoles-*L. sylvaticus*, p-value = 0.0003; all other p-value > 0.05).

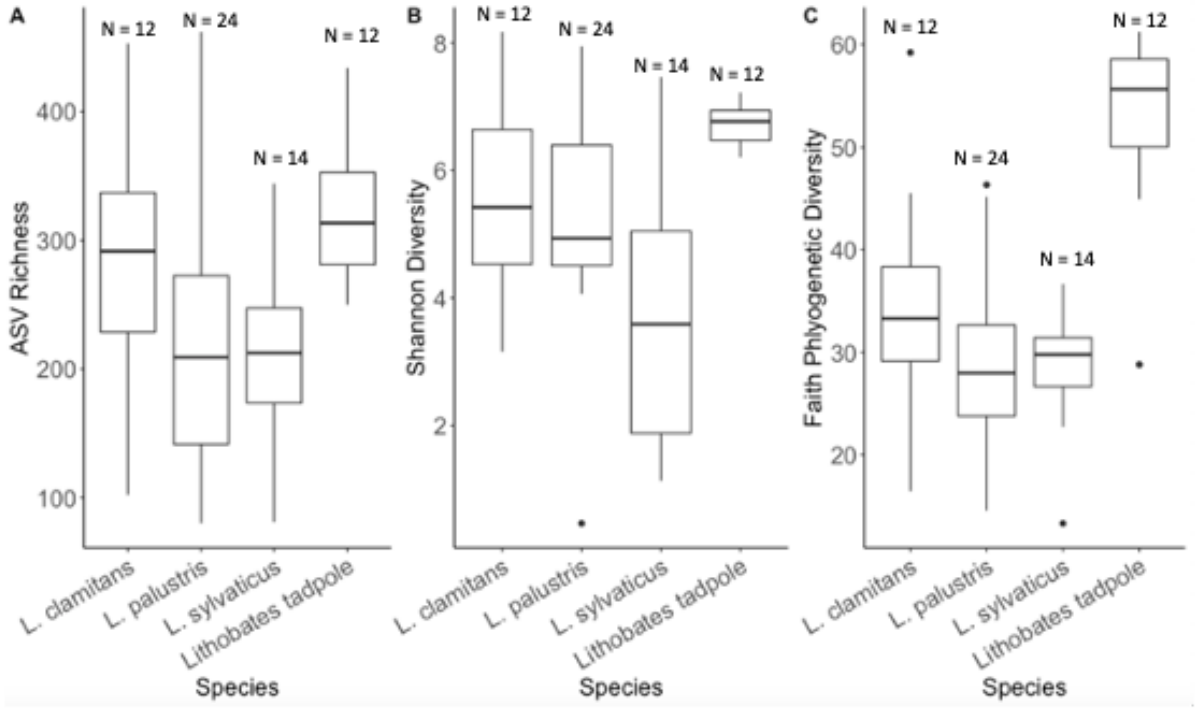

Figure 2.3: Three alpha diversity measurements, A) ASV richness, B) Shannon Diversity, and C) Faith's Phylogenetic Diversity, of amphibian bacterial samples grouped by developmental stage and species. Show on top of each boxplot are the sample size for each group plotted.

We found differences in bacterial community structure by life stage, with tadpoles grouping by themselves (PERMANOVA Bray-Curtis: $F_{(3,58)} = 4.8837$, $R^2 = 0.202$, p-value = 0.001; Jaccard: $F_{(3,58)} = 4.488$, $R^2 = 0.188$, p-value = 0.001). Further, we found that dispersion was significantly different among species (`permutest` Bray-Curtis: $F_{(3,58)} = 7.305$, p-value = 0.001; Jaccard: $F_{(3,58)} = 7.305$, p-value = 0.001). Visually, the tadpoles group by themselves to the right of the adult amphibians, which all grouped together(Figure 2.4). Some adult amphibians were grouped near the tadpole group, however, most of these samples were *L. clamitans* and found at the vernal pool where the tadpoles were collected from. Additionally, there was one tadpole sample that grouped with the adult amphibians.

Lastly, based on the indicator species analysis, we found that 250 ASVs were significantly associated with *Lithobates* tadpoles. From these 250 ASVs, the majority belonged to phyla Proteobacteria (99), Bacteroidetes (53), and Firmicutes (40). There was a lot more diversity in bacterial families, but some of the common families of the 250 ASVs were Ruminococcaceae (27), Burkholderiaceae (23), Acidobacteriaceae (17), and Acetobacteraceae (17).

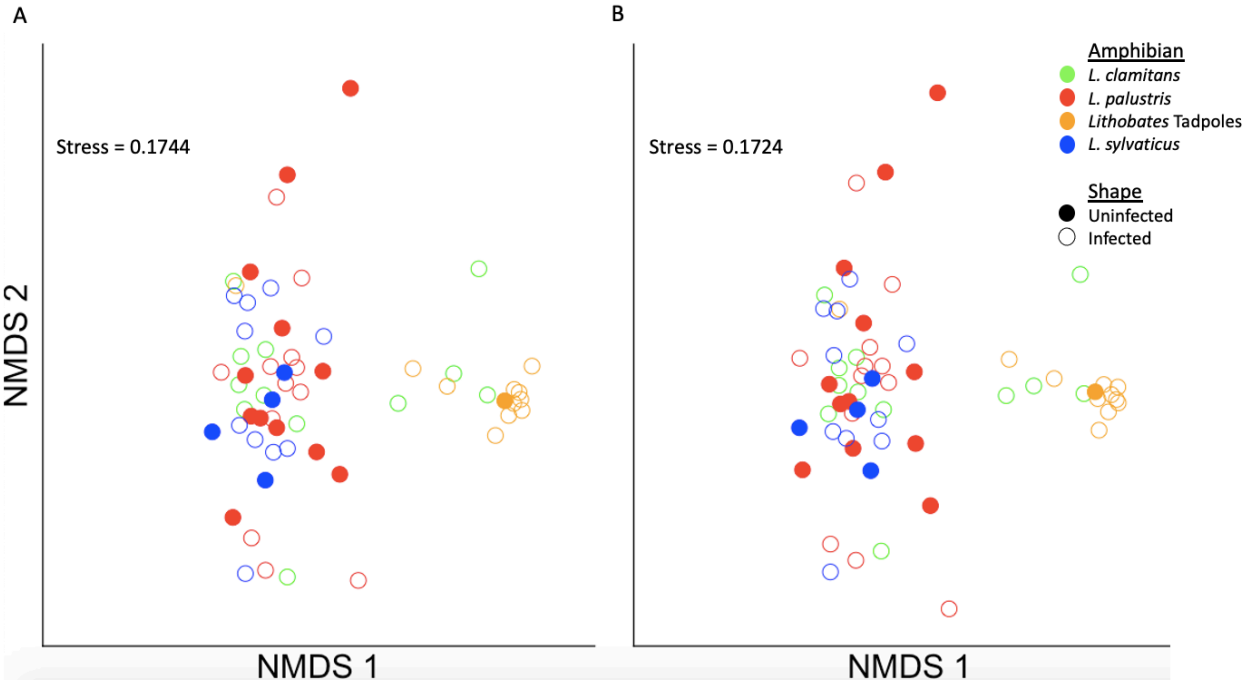

Figure 2.4: The bacterial data was plotted twice with non-metric multidimensional scaling (NMDS) plots. The plots show all amphibian bacterial samples plotted with an A) Bray-Curtis dissimilarity matrix and B) Jaccard dissimilarity matrix. Amphibian samples were colored by adult *Lithobates* species and *Lithobates* tadpoles. Also plotted is the amphibian's infection status shown by filled circles (infected) and empty circles (uninfected)

Differences between bacterial communities in infected and non-infected *Lithobates palustris*

Infection prevalence was greatest in *L. palustris* at site 1, with 48% infected in 2017 and 59% infected in 2018. Other species all had infection prevalence below 17%, and at site 3 only 17% of *L. palustris* were infected (Table 2.1). A comparison between the infected and non-infected *L. palustris* bacterial communities suggested no differences in any of the alpha diversity measurements (Shannon diversity: glm, b = 0.2032, SE = 0.2854, Z = 0.712, p-value = 0.467; Faith's phylogenetic diversity: glm, b = 0.0001, SE = 0.0482, Z = 0.003, p-value = 0.997; ASV richness: glm, b = -0.0005, SE = 0.0041, Z = -0.122, p-value = 0.903). We also did not find any differences in bacterial community structure (Figure 2.4) between infected and non-infected *L. palustris* (PERMANOVA Bray-Curtis: $F_{(1,22)} = 0.717$, $R^2 = 0.032$, p-value = 0.871; PERMANOVA Jaccard: $F_{(1,22)} = 0.832$, $R^2 = 0.0362$, p-value = 0.873 ; `permutest` Bray-Curtis: $F_{(1,22)} = 0.2792$, p-value = 0.569; `permutest` Jaccard: $F_{(3,58)} = 0.1282$, p-value =0.727).

Differences in pH and temperature between subsampling sites

The vernal pool site was the only sampling site that had a significantly different pH from other sampling sites (`emmeans` contrasts: Vernal Pool-Ann's Meadow p-value <0.001; Vernal Pool-Bog p-value <0.001; Vernal Pool-Tunnel p-value <0.001; Vernal Pool-Upstream p-value <0.001; All other contrasts p-value > 0.05). All sampling sites had similar temperatures (all `emmeans` contrasts p-value >0.05).

Differences between amphibian bacterial communities across sampling sites

We found that amphibians at different subsites (Figure 2.5) had similar skin bacterial ASV richness (all `emmeans` contrast p-values > 0.05). The vernal pool had a higher Faith's phylogenetic diversity measurement (Figure 2.6) compared to the rest of the subsites, which were all similar (Ann's Meadow-Vernal Pool p-value = 0.001, Bog-Vernal Pool p-value = 0.0437, Tunnel-Vernal Pool p-value = 0.0136, Upstream-Vernal Pool p-value < 0.001, all other contrasts p-value > 0.05). Shannon diversity of amphibians skin bacterial communities was similar across all subsites (Figure 2.6) except for between upstream and vernal pool site (`emmeans` contrast p-value = 0.0223).

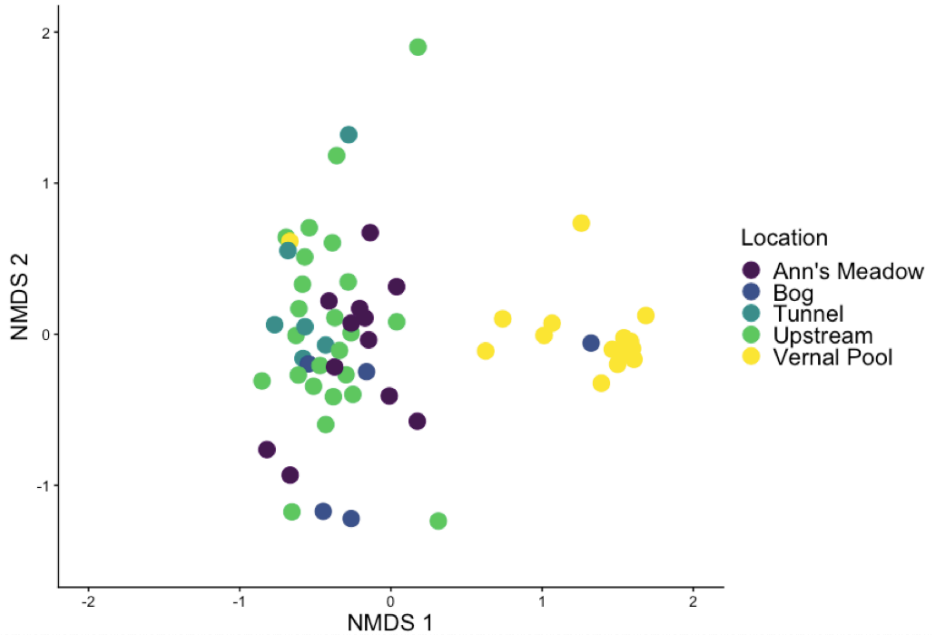

Figure 2.5: All amphibian bacterial samples are shown plotted with an NMDS using a Bray-Curtis distance matrix. All samples are colored based on where the sample was collected from at site 1. The stress value is 0.1744.

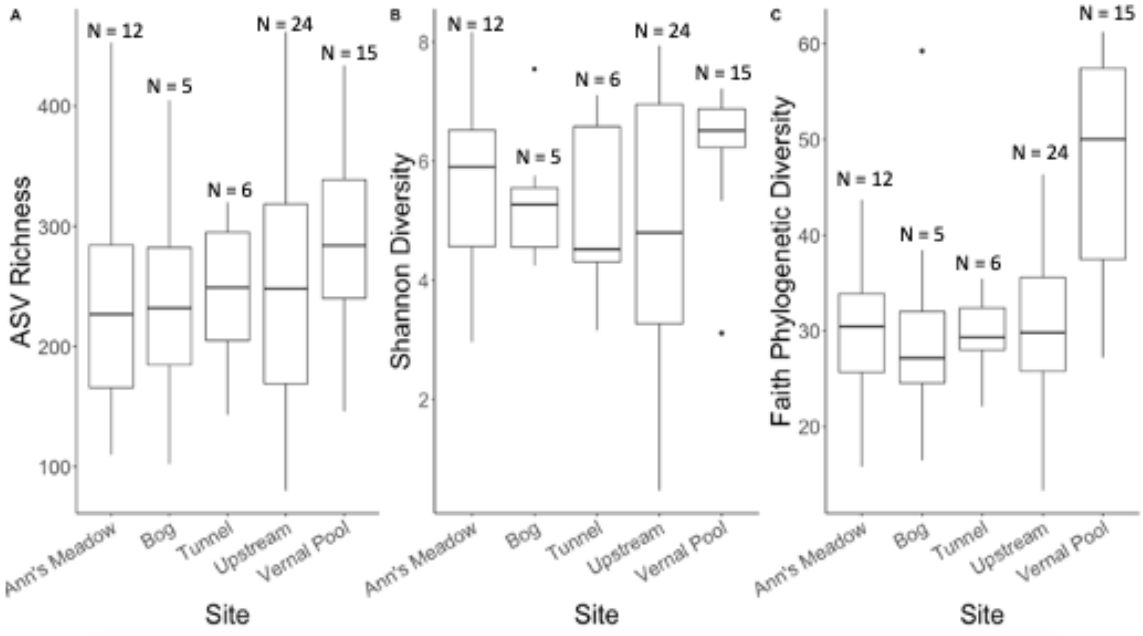

Figure 2.6: Three alpha diversity measurements, A) ASV richness, B) Shannon Diversity, and C) Faith's Phylogenetic Diversity, of amphibian bacterial samples grouped by sampling site. Show above the boxplots are the sample sizes for each group.

2.5 Discussion

For this study, we examined how skin bacterial communities and Bd infection prevalence varied across Ranid frog species at the Mianus River Gorge Preserve in Bedford, New York, USA. We expected to find low infection prevalence throughout the preserve and for infections to be uniform across all sampled species. However, we found that *L. palustris* had a higher infection prevalence than other species at one of the sites sampled. Additionally, we found that when we sampled *L. palustris* at this site the next year, infection prevalence remained higher compared to other sites and other amphibians species. A similar result was found in amphibians surveyed in the southeastern United States, where *L. palustris* had a higher infection prevalence than other amphibians surveyed [43]. A survey in Connecticut, close to our sampling sites, found that infection prevalence in *L. palustris* was similar to *L. clamitans*, although there were only 18 *L. palustris* samples compared to the 266 *L. clamitans* samples [41]. Our results, along with results from the literature, show how variable Bd infection can be across different sampling sites, even sampling sites that might be right next to each other. This result indicates the importance of sampling over a wide set of sites in an area to determine Bd dynamics and how threatened amphibians in the area might be.

We also predicted that infected individuals would have different bacterial communities than non-infected individuals, but we did not find significant differences in bacterial communities between infected and non-infected *L. palustris*. Experimental trials have shown that skin microbial communities change with Bd infection and, in field studies, skin bacterial diversity differs between Bd positive and negative sites [25, 39]. However, other studies do not show differences in skin bacterial communities and Bd infection status [6, 27]. We only used one amphibian species to compare bacterial communities due to low infection prevalence across all other species, and Bd might impact host skin microbial communities differently. Additionally, we did not test for infection intensity, and the severity of Bd infection can affect bacterial communities [26]. Therefore, if infected individuals in our study had low infection intensity there might have been no impact on bacterial communities or the impact on bacterial communities with our sample size might be too small to find. With field studies, we also do not know about previous infections and whether some of our uninfected individuals may have already been infected and cleared it. Those individuals might have similar microbial communities to individuals currently infected.

We did not find evidence of differences in bacterial communities among adults of different amphibian species. Previous studies, however, have found species that coexist at the same site had different skin bacterial communities, suggesting that there might be some host-specific factors that influence what bacteria are becoming members of the skin bacterial community instead of passively collecting bacteria from their environment [1, 6, 28, 33, 50]. However, all of the amphibian species that we compared were Ranids, and specifically from the genus *Lithobates*, while these other studies had a more diverse set of amphibian species they were comparing [6, 28, 33, 50]. Other studies have found that host phylogeny is associated with differences in skin bacterial communities, but these differences are weaker

at lower taxonomic groupings (i.e., genus and species). Habitat, along with host life history, may be a better predictor of bacterial community differences [9, 10, 17]. Due to the species in our study all being within the same genus, and within a similar habitat, there might not be large differences in bacterial communities. However, even though this finding is supported in the literature, we had a small sample size and subsequent studies should check our results with a larger sample size and determine if this result is similar in other amphibians genera.

We found bacterial community differences between tadpoles and adult frogs. There were differences in both alpha and beta diversity measurements between adults and tadpoles, but no differences in Shannon diversity measurements between most adult species and tadpoles. This result suggests that bacterial communities change due to metamorphosis, which has also been found in previous studies [28, 36]. Even though we found these differences between tadpoles and adult amphibians, we swabbed different parts of the amphibians, mouthparts for tadpoles and whole body for adult amphibians. Amphibian skin microbial communities have been found to differ across body regions of the amphibian [4], and this might contribute to some of the differences between adult and tadpoles' microbial communities. Future studies should swab the whole tadpole when comparing them to adult amphibians. All collected tadpoles were from the vernal pool, which had a lower pH than the surrounding wetlands. This environmental difference could have led to some of the differences in the bacterial communities we saw between tadpoles and adults. Environmental factors, such as temperature, salinity, elevation, precipitation, and pH, can shape bacterial communities [2, 18, 24, 31, 48].

Our results highlight potential developmental and environmental factors that could influence host bacterial communities and that Bd infection varied among species and sites. Collecting more data on a variety of amphibian hosts in different environments will help determine how environmental, host, and pathogen characteristics can influence the amphibian skin microbiome. This data will allow us to determine when certain factors might influence host microbial communities and to what extent. Host microbiomes can be critically important to their disease susceptibility and understanding what characteristics shape microbiomes could provide insights into conservation efforts by allowing a successful probiotic to be applied to mitigate diseases. This research into host and environmental characteristics that influence amphibian skin bacterial communities can also help lead research in other systems where the host microbiome is trying to be understood.

Bibliography

[1] Abarca, J. G., Vargas, G., Zuniga, I., Whitfield, S. M., Woodhams, D. C., Kerby, J., McKenzie, V. J., Murillo-Cruz, C., and Pinto-Tomás, A. A. (2018). Assessment of bacterial communities associated with the skin of Costa Rican amphibians at La Selva Biological Station. *Frontiers in Microbiology*, 9:2001.

[2] Albecker, M. A., Belden, L. K., and McCoy, M. W. (2019). Comparative analysis of anuran amphibian skin microbiomes across inland and coastal wetlands. *Microbial Ecology*, 78(2):348–360.

[3] Annis, S. L., Dastoor, F. P., Ziel, H., Daszak, P., and Longcore, J. E. (2004). A DNA-based assay identifies *Batrachochytrium dendrobatidis* in amphibians. *Journal of Wildlife Diseases*, 40(3):420–428.

[4] Bataille, A., Lee-Cruz, L., Tripathi, B., Kim, H., and Waldman, B. (2016). Microbiome variation across amphibian skin regions: implications for chytridiomycosis mitigation efforts. *Microbial Ecology*, 71(1):221–232.

[5] Becker, M. H., Brucker, R. M., Schwantes, C. R., Harris, R. N., and Minbiole, K. P. (2009). The bacterially produced metabolite violacein is associated with survival of amphibians infected with a lethal fungus. *Applied and Environmental Microbiology*, 75(21):6635–6638.

[6] Belden, L. K., Hughey, M. C., Rebollar, E. A., Umile, T. P., Loftus, S. C., Burzynski, E. A., Minbiole, K. P., House, L. L., Jensen, R. V., Becker, M. H., et al. (2015). Panamanian frog species host unique skin bacterial communities. *Frontiers in Microbiology*, 6:1171.

[7] Berger, L., Hyatt, A. D., Speare, R., and Longcore, J. E. (2005). Life cycle stages of the amphibian chytrid *Batrachochytrium dendrobatidis*. *Diseases of Aquatic Organisms*, 68(1):51–63.

[8] Berger, L., Speare, R., Daszak, P., Green, D. E., Cunningham, A. A., Goggin, C. L., Slocombe, R., Ragan, M. A., Hyatt, A. D., McDonald, K. R., et al. (1998). Chytridiomycosis causes amphibian mortality associated with population declines in the rain forests of Australia and Central America. *Proceedings of the National Academy of Sciences*, 95(15):9031–9036.

[9] Bird, A. K., Prado-Irwin, S. R., Vredenburg, V. T., and Zink, A. G. (2018). Skin microbiomes of California terrestrial salamanders are influenced by habitat more than host phylogeny. *Frontiers in Microbiology*, 9:442.

[10] Bletz, M. C., Archer, H., Harris, R. N., McKenzie, V. J., Rabemananjara, F. C., Rakotoarison, A., and Vences, M. (2017). Host ecology rather than host phylogeny drives amphibian skin microbial community structure in the biodiversity hotspot of Madagascar. *Frontiers in Microbiology*, 8:1530.

[11] Bolyen, E., Rideout, J. R., Dillon, M. R., Bokulich, N. A., Abnet, C., Al-Ghalith, G. A., Alexander, H., Alm, E. J., Arumugam, M., Asnicar, F., et al. (2018). QIIME 2: Reproducible, interactive, scalable, and extensible microbiome data science. Technical report, PeerJ Preprints.

[12] Burkart, D., Flechas, S., Vredenburg, V., and Catenazzi, A. (2017). Cutaneous bacteria, but not peptides, are associated with chytridiomycosis resistance in Peruvian marsupial frogs. *Animal Conservation*, 20(6):483–491.

[13] Callahan, B. J., McMurdie, P. J., Rosen, M. J., Han, A. W., Johnson, A. J. A., and Holmes, S. P. (2016). DADA2: high-resolution sample inference from Illumina amplicon data. *Nature methods*, 13(7):581–583.

[14] Cho, I. and Blaser, M. J. (2012). The human microbiome: at the interface of health and disease. *Nature Reviews Genetics*, 13(4):260–270.

[15] de Bruijn, I., Liu, Y., Wiegertjes, G. F., and Raaijmakers, J. M. (2018). Exploring fish microbial communities to mitigate emerging diseases in aquaculture. *Federation of European Microbiological Societies Microbiology Ecology*, 94(1):fix161.

[16] De Cáceres, M. (2013). How to use the indicspecies package (ver. 1.7. 1). *R Project*, 29.

[17] Ellison, S., Rovito, S., Parra-Olea, G., Vásquez-Almazán, C., Flechas, S. V., Bi, K., and Vredenburg, V. T. (2019). The influence of habitat and phylogeny on the skin microbiome of amphibians in Guatemala and Mexico. *Microbial Ecology*, 78(1):257–267.

[18] Estrada, A., Hughey, M. C., Medina, D., Rebollar, E. A., Walke, J. B., Harris, R. N., and Belden, L. K. (2019). Skin bacterial communities of neotropical treefrogs vary with local environmental conditions at the time of sampling. *PeerJ*, 7:e7044.

[19] Fisher, M. C., Garner, T. W., and Walker, S. F. (2009). Global emergence of *Batrachochytrium dendrobatidis* and amphibian chytridiomycosis in space, time, and host. *Annual Review of Microbiology*, 63:291–310.

[20] Harris, R. N., Brucker, R. M., Walke, J. B., Becker, M. H., Schwantes, C. R., Flaherty, D. C., Lam, B. A., Woodhams, D. C., Briggs, C. J., Vredenburg, V. T., et al. (2009a). Skin microbes on frogs prevent morbidity and mortality caused by a lethal skin fungus. *Multidisciplinary Journal of Microbial Ecology*, 3(7):818–824.

[21] Harris, R. N., Lauer, A., Simon, M. A., Banning, J. L., and Alford, R. A. (2009b). Addition of antifungal skin bacteria to salamanders ameliorates the effects of chytridiomycosis. *Diseases of Aquatic Organisms*, 83(1):11–16.

[22] Hoyt, J. R., Cheng, T. L., Langwig, K. E., Hee, M. M., Frick, W. F., and Kilpatrick, A. M. (2015). Bacteria isolated from bats inhibit the growth of *Pseudogymnoascus destructans*, the causative agent of white-nose syndrome. *PLoS One*, 10(4):e0121329.

[23] Hoyt, J. R., Langwig, K. E., White, J. P., Kaarakka, H. M., Redell, J. A., Parise, K. L., Frick, W. F., Foster, J. T., and Kilpatrick, A. M. (2019). Field trial of a probiotic bacteria to protect bats from white-nose syndrome. *Scientific Reports*, 9(1):1–9.

[24] Hughey, M. C., Pena, J. A., Reyes, R., Medina, D., Belden, L. K., and Burrowes, P. A. (2017). Skin bacterial microbiome of a generalist Puerto Rican frog varies along elevation and land use gradients. *PeerJ*, 5:e3688.

[25] Jani, A. J. and Briggs, C. J. (2014). The pathogen *Batrachochytrium dendrobatidis* disturbs the frog skin microbiome during a natural epidemic and experimental infection. *Proceedings of the National Academy of Sciences*, 111(47):E5049–E5058.

[26] Jani, A. J. and Briggs, C. J. (2018). Host and aquatic environment shape the amphibian skin microbiome but effects on downstream resistance to the pathogen *Batrachochytrium dendrobatidis* are variable. *Frontiers in Microbiology*, 9:487.

[27] Kruger, A. (2020). Frog skin microbiota vary with host species and environment but not chytrid infection. *Frontiers in Microbiology*, 11:1330.

[28] Kueneman, J. G., Parfrey, L. W., Woodhams, D. C., Archer, H. M., Knight, R., and McKenzie, V. J. (2014). The amphibian skin-associated microbiome across species, space and life history stages. *Molecular Ecology*, 23(6):1238–1250.

[29] Lam, B. A., Walke, J. B., Vredenburg, V. T., and Harris, R. N. (2010). Proportion of individuals with anti-*Batrachochytrium dendrobatidis* skin bacteria is associated with population persistence in the frog *Rana muscosa*. *Biological Conservation*, 143(2):529–531.

[30] Lenth, R., Singmann, H., Love, J., Buerkner, P., and Herve, M. (2018). `Emmeans`: Estimated marginal means, aka least-squares means. *R package Version*, 1(1):3.

[31] Longo, A. V. and Zamudio, K. R. (2017). Temperature variation, bacterial diversity and fungal infection dynamics in the amphibian skin. *Molecular Ecology*, 26(18):4787–4797.

[32] Marantelli, G., Berger, L., Speare, R., and Keegan, L. (2004). Distribution of the amphibian chytrid *Batrachochytrium dendrobatidis* and keratin during tadpole development. *Pacific Conservation Biology*, 10(3):173–179.

[33] McKenzie, V. J., Bowers, R. M., Fierer, N., Knight, R., and Lauber, C. L. (2012). Co-habiting amphibian species harbor unique skin bacterial communities in wild populations. *Multidisciplinary Journal of Microbial Ecology*, 6(3):588–596.

[34] Oksanen, J., Blanchet, F. G., Kindt, R., Legendre, P., Minchin, P. R., O'hara, R., Simpson, G. L., Solymos, P., Stevens, M. H. H., Wagner, H., et al. (2013). Package '`vegan`'. *Community Ecology Package, Version*, 2(9):1–295.

[35] Pedregosa, F., Varoquaux, G., Gramfort, A., Michel, V., Thirion, B., Grisel, O., Blondel, M., Prettenhofer, P., Weiss, R., Dubourg, V., et al. (2011). Scikit-learn: Machine learning in Python. *The Journal of Machine Learning Research*, 12:2825–2830.

[36] Prest, T. L., Kimball, A. K., Kueneman, J. G., and McKenzie, V. J. (2018). Host-associated bacterial community succession during amphibian development. *Molecular Ecology*, 27(8):1992–2006.

[37] Quast, C., Pruesse, E., Yilmaz, P., Gerken, J., Schweer, T., Yarza, P., Peplies, J., and Glöckner, F. O. (2012). The SILVA ribosomal RNA gene database project: improved data processing and web-based tools. *Nucleic Acids Research*, 41(D1):D590–D596.

[38] Ramsey, J. P., Mercurio, A., Holland, J. A., Harris, R. N., and Minbiole, K. P. (2015). The cutaneous bacterium *Janthinobacterium lividum* inhibits the growth of *Trichophyton rubrum* in vitro. *International Journal of Dermatology*, 54(2):156–159.

[39] Rebollar, E. A., Hughey, M. C., Medina, D., Harris, R. N., Ibáñez, R., and Belden, L. K. (2016). Skin bacterial diversity of Panamanian frogs is associated with host susceptibility and presence of *Batrachochytrium dendrobatidis*. *Multidisciplinary Journal of Microbial Ecology*, 10(7):1682–1695.

[40] Rebollar, E. A., Martínez-Ugalde, E., and Orta, A. H. (2020). The amphibian skin microbiome and its protective role against chytridiomycosis. *Herpetologica*, 76(2):167–177.

[41] Richards-Hrdlicka, K. L., Richardson, J. L., and Mohabir, L. (2013). First survey for the amphibian chytrid fungus *Batrachochytrium dendrobatidis* in Connecticut (USA) finds widespread prevalence. *Diseases of Aquatic Organisms*, 102(3):169–180.

[42] Ritchie, K. B. (2006). Regulation of microbial populations by coral surface mucus and mucus-associated bacteria. *Marine Ecology Progress Series*, 322:1–14.

[43] Rothermel, B. B., Walls, S. C., Mitchell, J. C., Dodd Jr, C. K., Irwin, L. K., Green, D. E., Vazquez, V. M., Petranka, J. W., and Stevenson, D. J. (2008). Widespread occurrence of the amphibian chytrid fungus *Batrachochytrium dendrobatidis* in the southeastern USA. *Diseases of Aquatic Organisms*, 82(1):3–18.

[44] Scheele, B. C., Pasmans, F., Skerratt, L. F., Berger, L., Martel, A., Beukema, W., Acevedo, A. A., Burrowes, P. A., Carvalho, T., Catenazzi, A., et al. (2019). Amphibian fungal panzootic causes catastrophic and ongoing loss of biodiversity. *Science*, 363(6434):1459–1463.

[45] Stuart, S. N., Chanson, J. S., Cox, N. A., Young, B. E., Rodrigues, A. S., Fischman, D. L., and Waller, R. W. (2004). Status and trends of amphibian declines and extinctions worldwide. *Science*, 306(5702):1783–1786.

[46] Team, R. C. et al. (2013). R: A language and environment for statistical computing.

[47] Trevelline, B. K., Fontaine, S. S., Hartup, B. K., and Kohl, K. D. (2019). Conservation biology needs a microbial renaissance: a call for the consideration of host-associated microbiota in wildlife management practices. *Proceedings of the Royal Society B: Biological Science*, 286(1895):20182448.

[48] Varela, B. J., Lesbarrères, D., Ibáñez, R., and Green, D. M. (2018). Environmental and host effects on skin bacterial community composition in Panamanian frogs. *Frontiers in Microbiology*, 9:298.

[49] Vences, M. and Köhler, J. (2007). Global diversity of amphibians (Amphibia) in freshwater. In *Freshwater Animal Diversity Assessment*, pages 569–580. Springer.

[50] Walke, J. B., Becker, M. H., Loftus, S. C., House, L. L., Cormier, G., Jensen, R. V., and Belden, L. K. (2014). Amphibian skin may select for rare environmental microbes. *Multidisciplinary Journal of Microbial Ecology*, 8(11):2207–2217.

[51] Woodhams, D. C., Vredenburg, V. T., Simon, M.-A., Billheimer, D., Shakhtour, B., Shyr, Y., Briggs, C. J., Rollins-Smith, L. A., and Harris, R. N. (2007). Symbiotic bacteria contribute to innate immune defenses of the threatened mountain yellow-legged frog, *Rana muscosa*. *Biological Conservation*, 138(3-4):390–398.

[52] Yang, H., Li, J., Xiao, Y., Gu, Y., Liu, H., Liang, Y., Liu, X., Hu, J., Meng, D., and Yin, H. (2017). An integrated insight into the relationship between soil microbial community and tobacco bacterial wilt disease. *Frontiers in Microbiology*, 8:2179.

Chapter 3

Predicting the Growth of the Amphibian Chytrid Fungus in Varying Temperature Environments

Zachary Gajewski[1,2,*], Lisa Stevenson[3], David Pike[3], Elizabeth A. Roznik[3,4], Ross A. Alford[3], Leah R. Johnson[1,2]

1. Department of Biological Science, Virginia Tech, Blacksburg, VA, 24061

2. Department of Statistics, Virginia Tech, Blacksburg, VA, 24061

3. College of Science and Engineering, James Cook University, Townsville, Queensland, 4810, Australia

4. North Carolina Zoo, Asheboro NC, 27205

∗ Corresponding author; e-mail: gzach93@vt.edu.

3.1 Abstract

Environmental temperature influences the success of ectothermic organisms, including hosts and pathogens in disease systems. One example is the amphibian chytrid fungus, *Batrachochytrium dendrobatidis* (Bd), which has led to widespread amphibian population declines. Understanding its thermal ecology is essential to effectively predict outbreaks. Studies that examine the impact of temperature on hosts and pathogens often do so in controlled constant temperatures. Although varying temperature experiments are becoming increasingly common, it is unrealistic to test every temperature scenario. Thus, reliable methods that use constant temperature data to predict performance in varying temperatures are needed. We tested a Bayesian hierarchical modeling approach to try to improve varying temperature performance predictions from constant temperature data using Bd laboratory experiments as a test case. We fit Bd growth data using a modified logistic growth function with the logistic growth rate constrained by five different thermal performance curves (TPCs). Although all TPCs over-predicted Bd growth in the varying temperature regimes some functional forms performed better than others. Varying temperature impacts on disease systems are still not

well understood and improving our understanding and methodologies to predict these effects could provide insights into disease systems and help conservation efforts.

3.2 Introduction

Temperature is often a key factor in determining if an ectothermic organism can succeed in a particular environment. Temperature affects multiple characteristics and traits of ectotherms, such as development rates, reproduction, and behavior, that impact the success of individuals or populations in an environment [9, 27, 33, 42]. Therefore, it is not surprising that temperature effects on organisms have been studied in many different systems.

Studies that examine temperature effects on organisms often do so in the lab under highly controlled conditions where temperature is set to one or multiple constant levels for the duration of an experiment. Many of these studies examine an organism's performance at several temperatures and compare the results at different conditions [1, 7, 12, 17, 57, 65]. Such studies have been used to answer questions about temperatures that optimize performance/traits, the thermal ranges of traits, and thermal adaptation of traits.

One way that the results of these thermal experiments are compared or summarized is by fitting a thermal performance curve (TPC) to the performance data across temperature treatments. TPCs are mathematical functions that are used to describe how an organism performs over a range of temperatures [25]. Most of these functions are assumed to be unimodal, meaning that they exhibit an optimal temperature (T_{opt}) where the trait being described is maximized. These functions also typically include maximum and minimum temperature thresholds denoted as T_{max} and T_{min}, respectively, where the trait being measured approaches, or is equal to, zero [2, 24]. TPCs have been fit for numerous species across a variety of traits using constant temperature data [14, 41, 57, 65]. These functions describe how performance changes over constant temperatures and can be used to infer performance at temperature not directly measured [25].

TPCs can be applied to microscopic organisms, including pathogens [47, 63, 65]. Thus, TPCs are often used in disease studies to quantify how environmental temperatures may regulate disease dynamics. Temperatures can influence both pathogens and hosts and their relationship [11, 20, 31, 35]. Pathogenic characteristics such as their distributions, growth rates, and survival rates, can be affected by environmental temperatures [22, 32, 57].

The effects of temperature on disease have often been studied in controlled constant temperature environments [1, 57, 63, 65]. These data can be used to predict how an organism will perform in more natural thermal conditions because experiments using more complex, fluctuating temperatures are often rare [21]. However, extrapolating from these constant temperature experiments and TPCs to varying temperature regimes (as are experienced in almost all natural thermal conditions) is difficult and the accuracy of doing so is still debated [6, 36, 41]. It is important to improve methods to generalize from constant temperature experiments to more natural varying temperature environments due to the numerous host and pathogen characteristics that temperature can influence [1, 3, 57, 66].

The amphibian chytrid fungus, *Batrachochytrium dendrobatidis* (Bd), is a fungal pathogen that causes chytridiomycosis [4, 18]. This disease has been linked to amphibian population declines worldwide [53]. Field studies have found that Bd infections are strongly affected by temperatures. For example, infection prevalence and intensity tend to be lower in warmer seasons, lower elevations, and in warmer aquatic and terrestrial habitats [5, 19, 52]. Lab studies have shown that Bd growth and survival are limited at temperatures over 30°C and optimal growth occurs at temperatures between 17 °C and 25 °C [43, 57, 67]. Bd can grow at temperatures as low as 4 °C, although growth at this temperature is slow [43, 64]. Recently research has also shown how temperature fluctuations can impact Bd's growth rate [34, 58]. Fluctuating temperatures and heat pulses can reduce mortality and morbidity in amphibian hosts [21, 46, 68].

In this study, we assessed the capability of a hierarchical model fit to constant temperature data to predict measurements taken under known fluctuating temperature regimes, using Bd grown *in vitro* as our study system. We used data collected by [57, 58] and previously modeled in a different manner by [21]. They grew Bd at constant and varying temperatures and took optical density readings over time to measure fungal growth. We fitted the hierarchical logistic growth model and constrained the shape of the logistic growth parameter (r) with one of five TPCs that have previously been proposed. This allowed us to examine how changing the shape of the assumed TPC impacted model predictions. We then use the fitted models to predict growth under known fluctuation temperatures and compare model performance.

Given previous work [30, 38, 61] we expected that generalizing from constant to time-varying temperatures would perform least well for varying temperatures near the TPC peak, due to non-linearity. We also expected that the generalization would perform best under the varying temperature regime with the smallest daily fluctuations. Lastly, we expected that the TPCs that had a typical left-skewed shape would make more accurate predictions due to their common use and model comparisons in the literature [24, 48, 54].

3.3 Methods

3.3.1 Bd Cultures

The Bd strain Paluma-Lgenimaculata #2-2001-CO was used for the temperature trials in this study. This strain was isolated from a green-eyed tree frog tadpole (*Litoria serrata*) near Paluma, Queensland, Australia, using the protocol described in [57]. The strain was cultured in TGhL broth (8g Tryptone, 1g gelatin hydrolysate, and 2 g lactose in 1 L of distilled water) and passaged 24 times before the constant temperature experiments and 12 times for the varying temperature experiments.

3.3.2 Constant Temperature Experiments

Here we briefly review the protocols used by [57] to collect constant temperature optical density growth measurements. Bd grew the strain on TGhL agar plates prior to the study. They allowed the Bd to grow for three days, on these plates, before flooding the plates with TGhL broth. The TGhL broth used to flood the plates was recollected, and filtered to remove zoosporangia. Zoospores in the filtered solution were quantified with a hemocytometer. The zoospore concentration in the filtered solution was found to be 5.75×10^7 zoospores per ml. The zoospores solution was then used to inoculate 96 well plates used in the constant temperature growth experiments.

Each 96 well plate consisted of: 18 positive wells (100 µL of the filtered zoospore solution), 6 negative wells (100 µL of heat-killed Bd, 60°C for 45 mins), and 24 wells containing 100 µL of TGhL. The plates were randomly assigned to 1 of 10 constant temperature treatment (13°C, 15°C, 17°C, 19°C, 21°C, 23°C, 25°C, 26°C, 27°C, and 28°C).

For each of the plates, [57] measured optical density of Bd growth in each well every day from day 0 to day 14. Optical density was measured using a Multiskan Ascent 96/384 Plate Reader (MTX Lab Systems Incorporated, Virginia, USA) at 492nm. Plates were checked daily for contamination, usually seen by high optical density readings and/or discoloration in the well. Contaminated wells were not included in the final analysis. All optical density readings were adjusted by subtracting out the mean of the negative control wells (heat-killed Bd wells).

3.3.3 Bd Optical Density Logistic Growth Model

We assumed that the Bd optical density growth pattern could be described by a logistic growth model that had a delay period before Bd's exponential growth (Fig. 3.1). Specifically, we used the following equation:

$$Y(T_i) = Y_0 \ \mathbb{1}_{(t_i<d)} + \frac{KY_0}{Y_0 + (K - Y_0)e^{-r_T(t_i-d)}} \mathbb{1}_{(t_i \geq d)} \tag{3.1}$$

to fit Bd optical density growth patterns, where $Y(t_i)$ is the initial optical density measurement, d is the delay period, K is the maximum optical density, Y_0 is the initial optical density, r_T is the logistic growth rate, and t_i is the ith time. This logistic growth model was first described in [65] and used to fit Bd optical growth patterns (Fig. 3.1). The logistic growth equation (Eq. 3.1), was modified to add a delay period due to the time it takes zoospores to settle in the well and develop into zoosporangia. This phase is known as the delay phase and lasts for d amount of time. Next, wells enter the exponential phase where zoosporangia release new zoospores, and those new zoospores settle and develop into zoosporangia. The rate at which this happens is controlled by r_T; the higher the value of r_T, the faster the growth and development of Bd. Lastly, there is the stationary phase when optical density is not increasing anymore due to new zoosporangia not releasing new zoospores into

the wells.

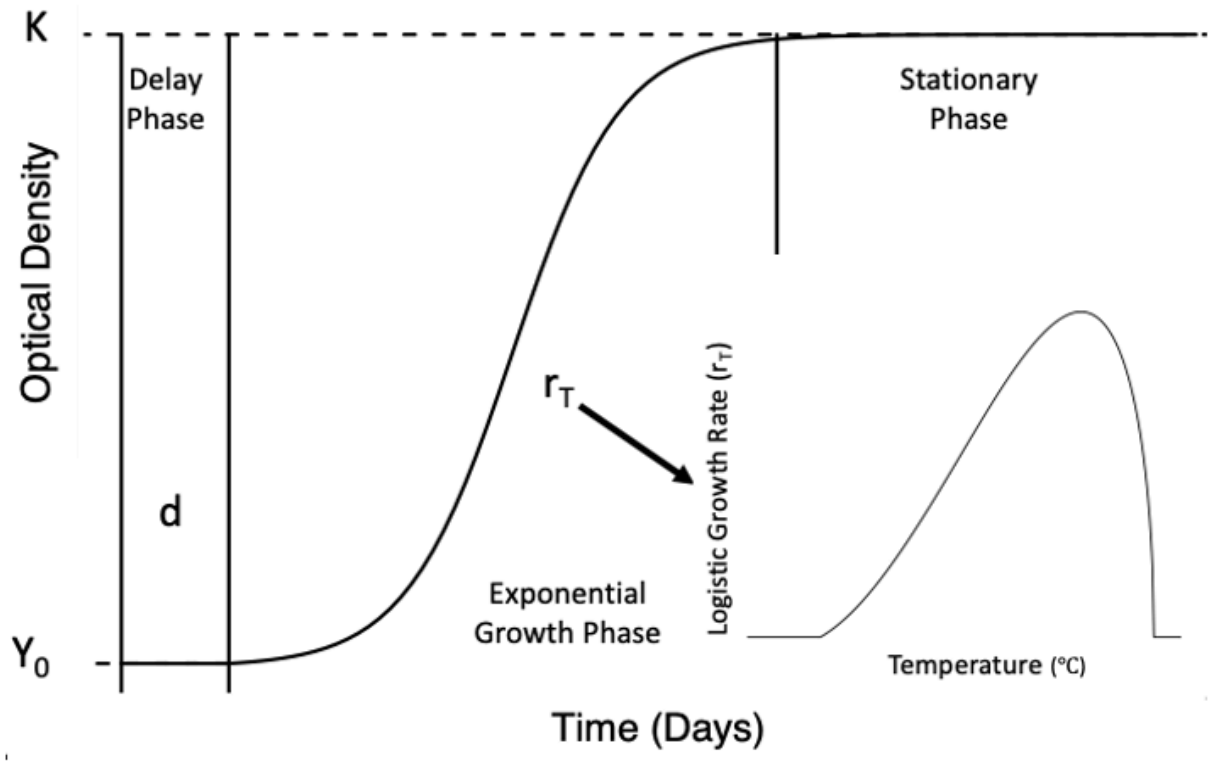

Figure 3.1: The figure shows a graphical representation of Eq. 3.1 used to fit the Bd optical density data and also shows the three phase of the model. The model starts out at time 0 and Y_0 and enters the delay phases. The length of the delay phase is controlled by d. The steepness of the exponential growth phase is controlled by r_T and the stationary phase is reached once the optical density value is equal to K. The logistic growth rate, r_T, is temperature sensitive is regulated by a thermal performance curve (shown in the bottom right corner).

3.3.4 Thermal Performance Curves

We found several thermal performance curves (TPCs) in the literature. The TPCs found varied in functional form and were developed for a wide range of organisms. Most of the TPCs found were phenomenological models, but some were mechanistic models based on enzyme kinetics. We chose five TPCs from the literature that varied in function and purpose for development. The models we selected were: Briere 2 [8], Ratkowsky [47], Ikemoto [26], Logan 10 [37], and Stinner [59]. The TPCs selected were used to explore how different TPC shapes and mathematical functions could affect predictions made about Bd growth in a varying temperature environment. All parameter definitions for the chosen TPCs can be found in the supplemental material.

The five TPCs chosen ranged in the number of parameters (4 – 8). The five functions also varied in whether they included critical thermal parameters such as, T_{min}, T_{opt}, and T_{max}.

Briere 2, Logan 10, and Ratkowsky each have two critical thermal parameters while Ikemoto and Stinner each have only one [8, 26, 37, 47, 59]. Most functions came from the entomology literature, with Logan 10 being one of the most popular. Ratkowsky is an outlier in the TPCs we consider, coming from the microbial literature. The Stinner model, the oldest model that we included, has a distinct tabletop shape that differed from the other TPCs. Lastly, some of the TPCs chosen do not have true T_{min} or T_{max} values because they asymptotically approach zero. Thus for these functions, the logistic growth rate (r_T) will never be exactly zero. In order to allow comparisons between all models, we define effective T_{min} and T_{max} for each TPC, which are the lower and upper temperatures where the logistic growth rate (defined by the TPC) becomes ≤ 0.01.

3.3.5 Fitting the Logistic Growth Model

We fit Eq. 3.1 to the constant temperature Bd optical density growth data using a hierarchical Bayesian approach. That is, we fit all the constant temperature optical density data simultaneously using one logistic growth model (Eq. 3.1). However, instead of placing a simple prior on the logistic growth rate (r_T), we constrained the shape of the growth rate to conform to one of the five TPCs functional forms as presented in the previous section. Each of the five was fit in turn and the predictions of the fitted models were compared. Mathematically, the hierarchical model is given by:

$$
\begin{aligned}
Y(T_i) &\sim \log\mathcal{N}(\mu_i, \tau_i) \\
\mu(T_i) &= Y_0 \mathbb{1}_{(t_i<d)} + \frac{KY_0}{Y_0 + (K - Y_0)e^{-r_T(t_i-d)}} \mathbb{1}_{(t_i \geq d)} \\
r_T &= f(T, \theta) \\
\theta &\sim g(\ominus) \\
\tau_i &= 1/\sigma_i^2 \\
\sigma &\sim \text{Exp}(.001) \\
Y_0 &\sim \text{U}(.001, .01) \\
d &\sim \text{Exp}(2) \\
K &\sim \text{U}(0.1, 0.6)
\end{aligned}
$$

This is the general formulation of the model where $f(T, \theta)$ denotes the functional form of a chosen TPC with parameter set θ and the priors distributions of the parameters determining the shape of the TPC is denoted by $g(\ominus)$.Logistic growth parameters priors were based on [65] priors. Priors for the parameters in each of the TPC were based on values found in previous publications, which are given in `devRate` [48]. TPC priors are shown in the supplemental material.

Parameters from the model were estimated via MCMC using the `rjags` package [45] in R [60]. For each fitted model, 5 chains were run for 20,000 iterations and the first 10,000 samples were discarded for burn-in for a total of 50,000 MCMC samples from the posterior

distribution for each model. Trace plots of the MCMC chains were checked visually for convergence. We also checked chains for autocorrelation. Two of the hierarchical models exhibited high autocorrelation. In these cases, the number of iterations was increased from 10,000 to 100,000 then thinned (keeping every 100th sample) to maintain the same number of posterior samples.

To compare the different hierarchical model fits to the constant temperature optical density data we used deviance information criterion (DIC), which is defined by:

$$DIC = \bar{D} + pD \tag{3.2}$$

where $\bar{D}$ is the expected deviance and is added to (pD), effective number of parameters [56]. The pD was defined as the one proposed by [44]. We used DIC for model comparison due to its use for Bayesian model comparison by taking into account the fit (expected deviance) and complexity (effective number of parameters) of the model [56]. The DIC calculations for each hierarchical model were done in `rjags` using the `dic.sample` function [45]. The DIC values were compared and the model with the lowest DIC value was considered the best fit to the constant temperature data (Table. 3.1).

TPC Function	Adjusted T_{min}	Adjusted T_{max}	Maximum r_T	Pen. Dev.	Δ DIC
Stinner	10.95	27.52	0.813	-31269	0
	(10.86, 11.04)	(27.44, 27.58)	(0.789, 0.839)		
Logan 10	-0.03	26.98	0.852	-30369	900
	(-0.15, 0.06)	(26.98, 26.98)	(0.826, 0.881)		
Briere 2	7.33	27.92	1.070	-28076	3193
	(6.01, 8.39)	(27.78, 27.99)	(1.015, 1.128)		
Ratkowsky	3.07	28.31	1.166	-28055	3214
	(1.45, 4.60)	(28.22, 28.40)	(1.106, 1.238)		
Ikemoto	2.93	40.35	1.010	-28014	3255
	(2.64, 3.18)	(40.30, 40.42)	(0.991, 1.021)		

Table 3.1: The adjusted T_{min}, adjusted T_{max}, maximum r_T, penalized deviance values, and Δ DIC, for each thermal performance curve used in the hierarchical models. The $Tmin$, T_{max}, and r_T columns show the posterior mean and the 95% highest posterior density interval in parentheses. Adjusted T_{min} and T_{max} are defined at the temperatures at which the posterior medians of the logistic growth rate reaches 0.01. Maximum r_T is the temperature at which the logistic growth rate is maximized. Penalized Deviance column shows the values calculated by `rjags` using the `dic.sample` function. Lastly, the Δ DIC, is defined by $\Delta DIC = DIC_i - DICmin$. The DIC indicates that the Stinner model is the best fit to the constant temperature data.

3.3.6 Varying Temperature Experiments

We validated our predictions made from the constant temperature hierarchical models with varying temperature Bd optical density data [58]. The varying temperature regimes were realistic simulations of regimes experienced by amphibians based on temperature loggers

placed in the environment. Thermal regimes were recorded during the wet summer season and dry winter season, at low and high elevations, and in the water, air, or in a frog model (made from agar, using models with both perfect and zero resistance to evaporative water loss; [50, 51]). The agar frog models were placed in daytime and nighttime locations used by tracked frogs [51]. The incubator temperature regimes were created by taking the logged temperature information and averaging it (separately for daytime and nighttime locations) and splitting it into 4 hour intervals. A temperature logger was placed in each incubator to record the temperature during the experiments (Figure 3.2).

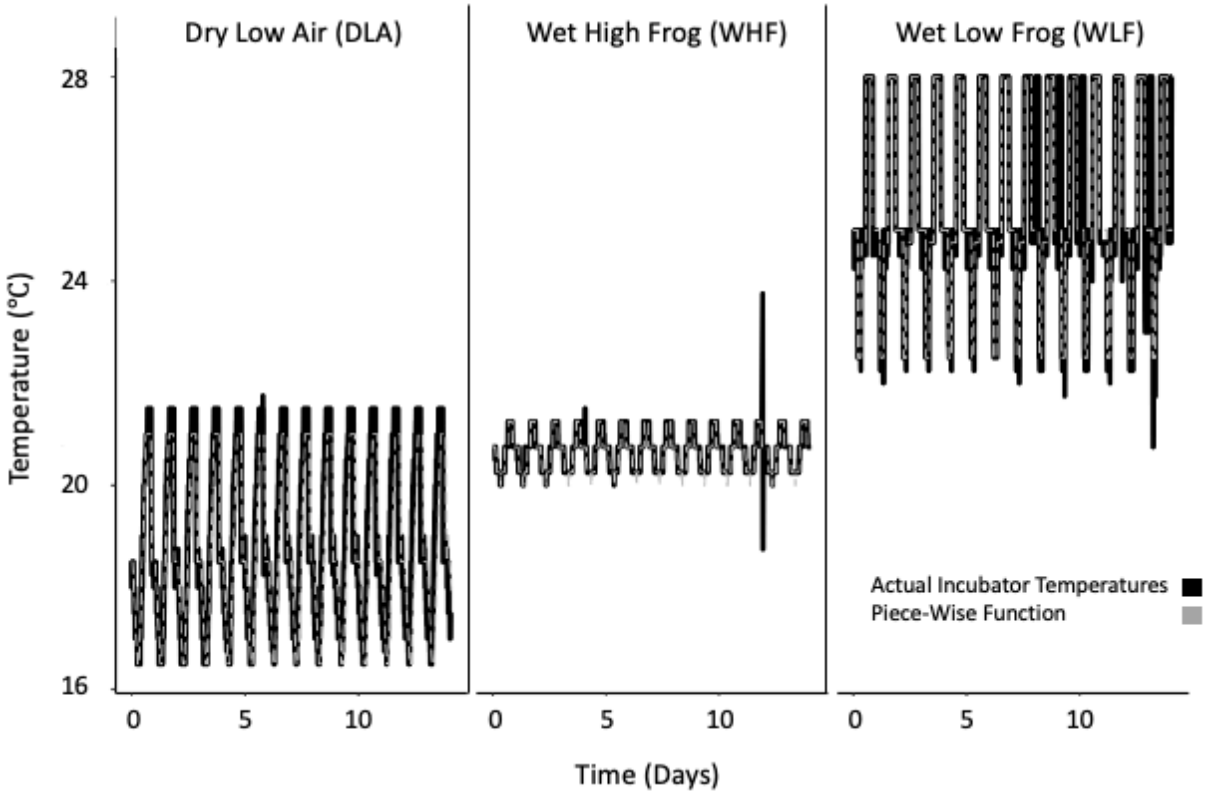

Figure 3.2: Plotted are the varying temperature regimes that were used to grow Bd in incubators. The three regimes are based on temperatures recorded in either low or high altitude, wet or dry seasons, and air or on a frog. Black lines are temperatures recorded in the incubator over time, while the dashed grey lines represent the piece-wise functions fit to the incubator temperatures. There were some inconsistencies in the thermal data, as seen in the spike in the wet high frog regime and when the wet low frog cycle went out of sync. The dry low air also had tiny spikes that the piece-wise function did not take into account due to the short time frame of the spikes.

We only used data from 3 out of the 12 varying temperature regimes (all reported in [58]) because of natural weather fluctuations in the other 9 datasets made it difficult to evaluate consistency in thermal regimes across days. This constraint highlights that our method and other methods using integration [69] are essentially unable to evaluate 75% of our data, which was collected under natural weather conditions. We used 3 varying temperature regimes

(shown in Figure 3.2) in our analyses because they had the most consistent temperature fluctuations over time (across days), whereas the other temperature regimes varied much more widely and unpredictably in their fluctuations over time, which is representative of the weather conditions and thermoregulatory behavior of the animals studied at that time (Figure 3.2).

The experimental setup for the varying temperature 96 well plates was the same as for the constant temperature experiments. After the 96 well plates were inoculated, they were placed in varying temperature incubators that used one of three varying temperature treatments (Dry Low Air, Wet High Frog, or Wet Low Frog). Optical density Bd growth measurements were taken daily, for each well and plate, for 12 days using the same protocol as the constant temperature treatments.

3.3.7 Predicting Bd Performance in Varying Temperature Regimes

To make predictions about how Bd grew in the three varying temperature regimes we used the following logistic growth function:

$$\frac{dx}{dt} = r_T x \left(\frac{1-x}{K}\right) \mathbb{1}(t > d) \tag{3.3}$$

where x is optical density, r_T is the temperature-dependent logistic growth rate, and K is the maximum optical density. With this model, we were able to integrate over time and use a time-varying temperature regime to inform the logistic growth rate (r_t) value. The logistic growth rate (r_t) was solved for from one of the five TPCs. To determine what the time-varying temperature should be at each time point we fit three piece-wise functions, one to each of the varying temperature regimes, and used these to solve for the temperature at time i. Parameters for both the thermal performance curve and logistic growth model were from 1000 samples taken from the posterior distribution of each hierarchical model (from the fits utilizing each of the 5 TPCs).

We then integrated the logistic growth model (Eq. 3.3) over 16 days by intervals of 0.001 to predict Bd's growth in each of the varying thermal regimes for each of the 5 hierarchical models. Integration was done using `deSolve` and the default `lsoda` integrator [55]. Time was linked to temperature by the piece-wise function fit to the incubator temperature data (Figure 3.2). We made 1000 predictions, based on the 1000 parameter values sampled from the posterior distributions. We calculated the median prediction and the 95% highest posterior density interval for both the optical density growth prediction and the TPCs.

We wanted to compare predictions about the parameters in the logistic growth model, so we refit Eq. 3.1, once per varying temperature regime (n=3), without constraining the logistic growth rate by a TPC. This model was fit with `rjags` and used similar priors to the hierarchical model and r_T had a prior this time (Gamma$(1, 1)$). We also assigned Y_i a Normal distribution due to negative optical density values in the varying temperature treatments. We ran the model for the same number of iterations and removed the same burnin. We then

compared our predicted parameter values to these parameter values, found by just fitting a non-temperature-dependent logistic growth model.

3.4 Results

3.4.1 Thermal Performance Curve Models:

The relationships between the logistic growth rate (r_T) and temperature in the hierarchical models were constrained by the thermal performance curves (TPC) used. The structure of the Briere 2, Logan 10, and Ratkowsky models results in similar relationships between Bd growth rate and temperature – that is, these three models have a left-skewed shape. In contrast, the Ikemoto model is more symmetrical (Figure 3.3). The Stinner model is also symmetrical, but is nearly constant at intermediate temperatures.

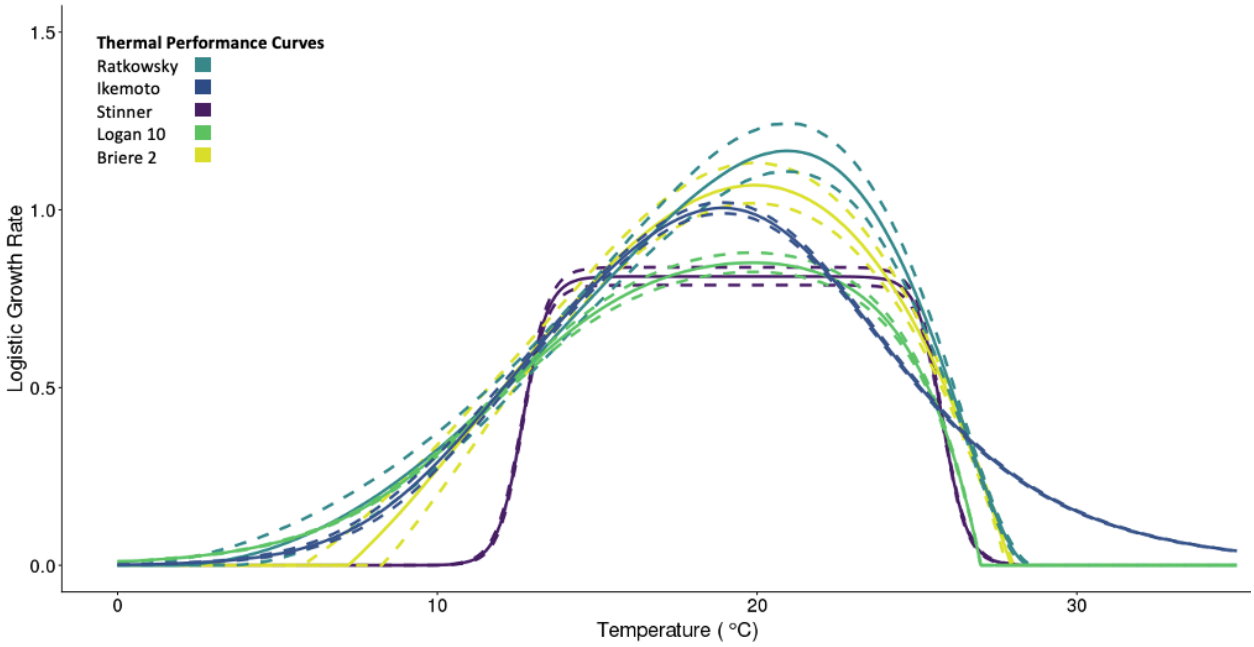

Figure 3.3: Thermal performance curves were created from 1000 samples from the posterior distribution of each of the hierarchical models. The output from five thermal performance curves used to constrain the logistic growth rate. Dashed lines represent 95% credible intervals and solid lines represent medians.

We compare predictions of key thermal parameters such as T_{min}, T_{opt}, and T_{max} which differed due to using different TPCs to constrain the shape of the logistic growth rate over temperature. At lower temperatures, the predicted logistic growth rates (r_T) patterns were similar in the Logan 10, Ikemoto, and Ratkowsky models. These three models have a less drastic reduction in r_T as temperature decreases compared to the other two models. The Briere 2 and Stinner models had higher adjusted T_{min} and a more distinctive decrease in r_T as temperatures become cooler. The Stinner model had the highest median adjusted T_{min} at 10.95°C (Table 3.1). There were similar patterns at the upper end of the TPCs. All models

except the Ikemoto model predicted a sharp drop in r_T at temperatures over the predicted thermal optimums (Figure 3.3). The Ikemoto model also had a much higher $Tmax$ than the other 4 models (Table 3.1).

Hierarchical models assuming the Logan 10 and Briere 2 TPCs were the only ones that predicted similar temperatures for their thermal optimums, with median values of 19.86°C and 19.92°C respectively (Table 3.2). The lowest optimal temperature predicted was 18.92°C from the Logan 10 model, while the highest optimal temperature was 20.94°C predicted from the Rakowsky model. At the TPCs' optimal temperatures, we found that the predicted maximal logistic growth rate for each TPC varied considerably. The Ratkowsky and Briere 2 models had the two highest maximal logistic growth rates (r_T). The Ikemoto had the third highest r_T and was not significantly different than the Briere 2 r_T value (Table 3.1). The last two models, Stinner and Logan 10, had significantly lower (but similar) maximal r_T values compared to the other three models.

Param	Briere 2	Ratkowsky	Ikemoto	Logan 10	Stinner
d	1.026 (0.985, 1.114)	1.065 (.993, 1.186)	0.007 (0.001, .033)	0.220 (0.055, 0.381)	0.356 (0.191, 0.539)
K	0.122 (0.113, 0.131)	0.119 (0.110, 0.128)	0.135 (0.133, 0.136)	0.134 (0.133, 0.136)	0.134 (0.133, 0.136)
T_{min}	7.214 (5.949, 8.403)	274.6 (272.9, 276.5)	NA NA	NA NA	NA NA
T_{opt}	19.92 (19.74, 20.11)	20.94 (20.68, 21.19)	18.92 (18.87, 18.97)	19.86 (19.80, 19.93)	19.23 (19.22, 19.25)
T_{max}	27.95 (27.806, 28.040)	301.6 (301.4, 301.7)	NA NA	27.001 (27.000, 27.005)	NA NA

Table 3.2: Comparison of estimated logistic model parameters (excluding $r(T)$) obtained under the 5 assumed thermal performance curve functions. For each model we report the posterior median values and 95% highest posterior density intervals values calculated from samples from the posterior distributions (N= 1000). Medians and highest posterior density intervals are also shown for the critical thermal values (T_{min}, T_{opt}, and T_{max}) if these were estimated parameters in the given model (adjusted T_{min} and T_{max} are shown in the supplemental material. All median values for Y_0 are 1×10^{-3} and have all models have an interval that falls between $(1 \times 10^{-3}, 1.04 \times 10^{-3})$.

Given the differences in patterns caused by the various TPCs, we sought to evaluate which of these was most consistent with the data used for fitting. We compared the deviance information criteria (DICs) from the 5 hierarchical model fits to the constant temperature data. Surprisingly, the Stinner model has the lowest DIC value, indicating that this model fit the constant temperature optical density data the best (Table 3.1). The Logan 10 model was the second best fit having a ΔDIC value of 900 (Table 3.1), indicating that even this second model performed significantly more poorly fitting these data. The other models performed even more poorly. This indicates that the models with similar intermediate temperature logistic growth rates and lower maximal logistic growth rates did a better job of fitting the constant temperature data.

3.4.2 Hierarchical Model Parameters

Along with the TPC parameters, the hierarchical models also had differences in the logistic growth model parameters, specifically the carrying capacity, K, and the length of the delay period, d. The delay parameter ranged from 1.065 in the Ratkowsky model to 0.007 in the Ikemoto model. The Briere 2 model had a similar delay to the Ratkowsky model. While the Logan 10 and Stinner d values were similar. The 5 different maximum optical density parameter values, K, fell into two significantly different groups. Briere 2 and Ratkowsky had lower K values predicted, while the Ikemoto, Logan 10, and Stinner models predicted a significantly higher K value (Table 3.2). In contrast, the estimated initial optical density, Y_0, was the same across all models.

3.4.3 Predicting Optical Density Under Varying Temperature Conditions

We attempted to use the fitted models from the previous sections to predict optical density measurements under 3 time-varying temperature regimes (predictions shown in Figure. 3.4) and compared their performance to a simple logistic model fit directly to the time-varying data. All models over-predicted optical density growth at the low and intermediate, Dry Low Air (DLA) and Wet High Frog (WHF), temperature regimes. However, the Ikemoto model which performed the worst at predicting optical density growth in the DLA and WHF temperature regimes, did the best at predicting growth at the highest temperature regime. While the Stinner model was the closest to accurately predicting optical density growth in the DLA and WHF temperature regimes, it resulted in the worst prediction at the highest temperature regime, Wet Low Frog (WLF).

The Wet High Frog (WHF) regime exhibits the least amount of variation between maximum and minimum temperatures. Again, the Stinner model performed the best and had a closer average logistic growth rate to the logistic growth rate predicted at that temperature regime (see supplemental material for values). The Ikemoto, again, was the worst at predicting Bd growth at the WHF temperature regime. However, at the WHF temperature regime, the Ikemoto model made a better prediction compared to the DLA prediction and was closer to predictions made by the other 4 models. The other models, Briere 2, Ratkowsky, and Logan 10, were all similar but overlapped less with each other.

Lastly, the Wet Low Frog (WLF) temperature regime had the highest mean and maximum temperature, with a range that spans most of the thermal maxima estimated by the hierarchical models. The Stinner model, which had the best Bd growth predictions in the other two varying temperatures, made the worst prediction at this temperature regime. The Ikemoto model, which had the worst predictions in the other two temperature regimes made the best prediction in the WLF temperature regime. The Logan 10 and Ratkowsky models, which made similar predictions, did over-predict Bd growth but not by a significant amount. Briere 2 again over-predicted Bd growth at this temperature regime but made a

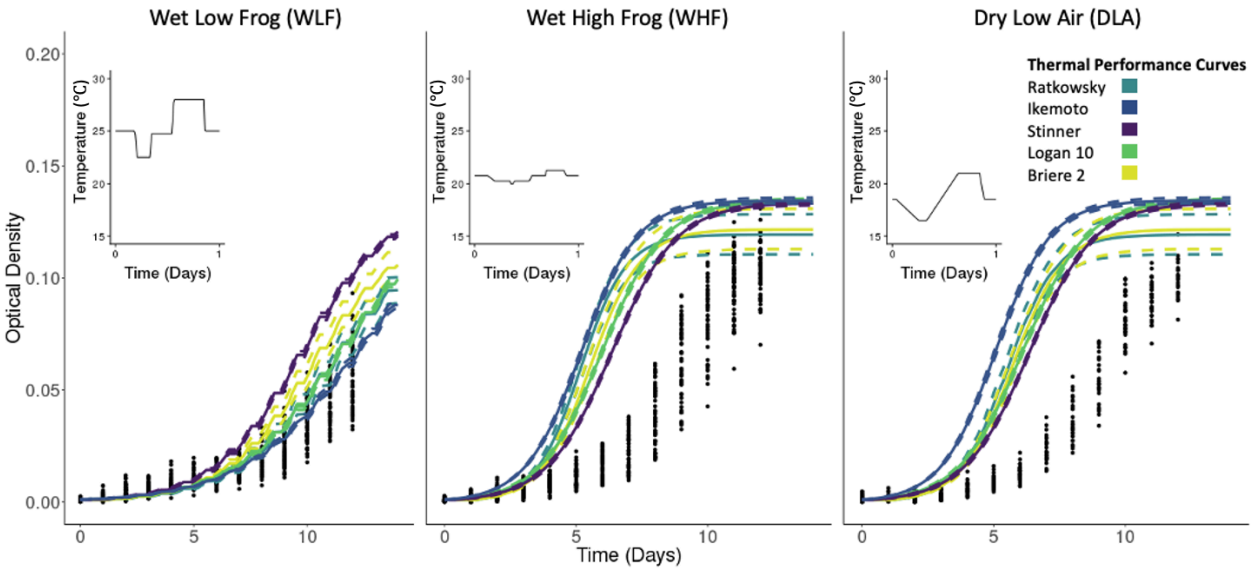

Figure 3.4: Varying temperature predictions at three different temperature regimes; A) Wet Low Frog (WLF), B) Wet High Frog (WHF), and C) Dry Low Air (DLA). Each panel shows predictions made from five different thermal hierarchical models. Dashed lines represent the 95% credible interval, while the solid lines represent median predictions from 1000 samples. The points in each panel represent optical density measurements taken under the specified temperature regimes. Above each prediction plot shows what the corresponding fluctuating temperature regime looks like for 24 hours.

more accurate prediction at this temperature regime when compared to the WHF and DLA temperature regime predictions.

3.5 Discussion

In this study, we explored the extent to which thermal performance curves (TPCs) estimated under multiple constant temperatures can be generalized to make predictions of growth of a fungal pathogen, Bd, under varying temperature regimes. We also explored how changing the assumed form of the TPC used to constrain the logistic growth rate (r_T) in the hierarchical model affected predictions. Surprisingly, we found that our method did not make the most accurate predictions with the temperature regime that had the smallest fluctuations or with temperature regimes with more intermediate temperatures. We also found that the TPC used in the hierarchical model made a difference, and that the more typical left-skewed TPCs, like Briere 2, did not make the best predictions. This reinforces the inadequacy of current methods for predicting thermal performance under time-varying temperature conditions, even for these small organisms, from measurements taken at constant temperatures.

All the hierarchical models generally over-predicted the growth of Bd in the three different varying temperature regimes. However, which ones performed best or worst were often

surprising. For example, the Ikemoto model (with the highest thermal maximum) made the most accurate prediction for the warmest varying temperature regime (WLF), but the worst predictions for the other two varying temperature regimes. The Stinner model was the reverse, performing the best for the intermediate and lower temperature regimes but making the worst prediction for the highest temperature. By examining these best and worst fitting models, we may be able to parse out what features of the TPCs are improving or hampering predictions. For example, the Ikemoto curve does not have a drastic drop off in growth rate after the thermal optimum, which may have allowed improved prediction in the high temperature regime. Another example is the Stinner model's predictions at intermediate temperatures, which were predicted to all be very similar. These factors and how the TPCs influence the logistic growth parameters, such as the delay rate (d) (which was lower than expected in the Ikemoto model), highlight the need to take the function and shape of the TPC into account and consider what they might say about the biology of the trait.

Some predictions that our hierarchical models made about Bd optical density growth are inconsistent with the known biology of Bd. The fitted Stinner model predicts little to no growth at lower temperatures (< 10°C), while the Logan 10 model predicted growth at close to 0°C. The Ikemoto model predicted Bd to continue growing at temperature > 40°C. Based on other laboratory studies we know that the Bd does not grow at temperatures > 40°C and can grow at temperatures < 10°C [43, 57, 65]. Although both the Stinner model and Ikemoto model make better predictions in different varying temperature regimes than the other models, they make predictions that are not consistent with known Bd critical thermal values.

The TPC fits can be improved by incorporating more data into the models. For example, more data from constant temperatures below 13 °C could shift the thermal minimum to more reasonable values and refine the shape of the TPCs at low and intermediate temperatures. Similarly, constant temperature data above 28 °C, which would show little to no growth of Bd, could restrain TPCs predicting thermal maximums above this temperature. This could remove error due to extrapolating into temperatures for which we don't have data. This emphasizes the need to collect data over a range of temperatures to provide enough information to the model to make accurate predictions.

The impact of temperature variability on the performance of organisms is being explored in the literature and more studies are trying to predict performance in varying environments [6, 13, 16, 28, 29, 41]. The accuracy of methods such as rate summation, which integrates over time-varying temperature to determine growth or trait performance at a given time, are still under debate [6, 36, 41]. Most of these studies, similar to ours, deal with regular fluctuating temperature regime and do not make predictions on more irregular temperature regimes that might be caused by a weather event or thermoregulatory behavior. Current methods that integrate over time-varying temperature regimes make it difficult to make predictions over irregular temperature regimes and test the accuracy of current methods. Integrating across time-varying temperature requires temperature needed at every time point. We used a piece-wise function on three repetitive temperature regimes in this study for this reason. However,

more complex sporadic temperature regimes, like the 9 temperature regimes in [58] that were not used in this study, would require long piece-wise function. A better understanding of the limitations of predicting varying temperature performance from constant temperature data and easier methods to make prediction on irregular temperature regimes are needed.

Thermal regimes are changing around the world [15]. Many publications ([10, 23, 39, 40]) have suggested that if the thermal envelopes of areas shift beyond the tolerances of the organisms inhabiting them, those organisms will either die out, emigrate, or perhaps adapt. Changing temperatures could accentuate mismatches between host and pathogen performance curves and produce large changes in interactions [11]. However, this may underestimate the effects of the changing climate by not considering variation in temperature. Previous research has shown that temperature variation can affect species' biology and interspecific interactions such as disease [21, 34, 62, 68]. However, for most species our understanding of the effects of temperature variation is poor and it is possible that changes in thermal regimes that do not overstep simple critical tolerances may still cause profound effects on species and species interactions, such as disease. Although some lab studies might help us determine how these temperatures might affect disease dynamics or organisms in certain locations, it would be time consuming and resource intensive to try to determine how an organism might perform in numerous varying temperature scenarios. However, if we improve our understanding of how an organism's performance in constant temperatures relates to their performance in varying temperatures, we would only need to measure a trait across several constant temperatures. This would require more constant temperature experiments with the pathogen and potentially a more holistic approach that examines both pathogen and host together. However, the current literature has a lot of constant temperate data (examples can be found in [1, 14, 57, 65]) that can be used to refine techniques and guide further work.

We were unable to accurately predict an organism's performance in a varying temperature environment from constant temperature data even with different TPCs and a hierarchical modeling approach that allows us to account for more uncertainty. This highlights a gap in our current models for understanding how organisms, even simple organisms, react in varying temperature environments. Trying to make predictions with larger organisms we assumed that methods would need to be improved; however, we showed that even when trying to make predictions on smaller simple organisms, there is still a knowledge gap. Building off current methods, future studies could take some of these phenomenological functions and build more mechanistic functions explaining how an organism performance in varying temperature environments. With these models, we can start to determine what factors affect varying temperature performance and when current methods, like our hierarchical modeling approach, might be sufficient. For example, including an acclimation period for larger organisms might be needed instead of allowing the performance or a trait rate to immediately adjust based on the new temperature [49]. When temperatures exceed or drop below the thermal maximum and minimum, the organism could also accumulate damage and need to recover from that when temperatures are more optimal, further slowing the

performance of a certain trait. Models will also have to make predictions with more irregular and sporadic temperature regimes; caused by weather events or thermoregulatory behavior. Building these new models will not only help improve our predictions of how organisms perform in varying temperature environments, but also improve our understanding of how temperature impacts organisms.

Bibliography

[1] Adamo, S. A. and Lovett, M. M. (2011). Some like it hot: the effects of climate change on reproduction, immune function and disease resistance in the cricket *Gryllus texensis*. *Journal of Experimental Biology*, 214(12):1997–2004.

[2] Angilletta Jr, M. J. (2006). Estimating and comparing thermal performance curves. *Journal of Thermal Biology*, 31(7):541–545.

[3] Bailey, C., Segner, H., Casanova-Nakayama, A., and Wahli, T. (2017). Who needs the hotspot? The effect of temperature on the fish host immune response to *Tetracapsuloides bryosalmonae* the causative agent of proliferative kidney disease. *Fish & Shellfish Immunology*, 63:424–437.

[4] Berger, L., Speare, R., Daszak, P., Green, D. E., Cunningham, A. A., Goggin, C. L., Slocombe, R., Ragan, M. A., Hyatt, A. D., McDonald, K. R., et al. (1998). Chytridiomycosis causes amphibian mortality associated with population declines in the rain forests of Australia and Central America. *Proceedings of the National Academy of Sciences*, 95(15):9031–9036.

[5] Berger, L., Speare, R., Hines, H., Marantelli, G., Hyatt, A., McDonald, K., Skerratt, L., Olsen, V., Clarke, J., Gillespie, G., et al. (2004). Effect of season and temperature on mortality in amphibians due to chytridiomycosis. *Australian Veterinary Journal*, 82(7):434–439.

[6] Bernhardt, J. R., Sunday, J. M., Thompson, P. L., and O'Connor, M. I. (2018). Nonlinear averaging of thermal experience predicts population growth rates in a thermally variable environment. *Proceedings of the Royal Society B: Biological Sciences*, 285(1886):20181076.

[7] Bieri, M., Baumgartner, J., Bianchi, G., Delucchi, V., Arx, R. v., et al. (1983). Development and fecundity of pea aphid (*Acyrthosiphon pisum Harris*) as affected by constant temperatures and by pea varieties. *Mitteilungen der Schweizerischen Entomologischen Gesellschaft*, 56(1/2):163–171.

[8] Briere, J.-F., Pracros, P., Le Roux, A.-Y., and Pierre, J.-S. (1999). A novel rate model of temperature-dependent development for arthropods. *Environmental Entomology*, 28(1):22–29.

[9] Cator, L., Johnson, L. R., Mordecai, E. A., El Moustaid, F., Smallwood, T. R., LaDeau, S. L., Johansson, M. A., Hudson, P. J., Boots, M., Thomas, M. B., et al. (2020). The role of vector trait variation in vector-borne disease dynamics. *Frontiers in Ecology and Evolution*.

[10] Chen, I.-C., Hill, J. K., Ohlemüller, R., Roy, D. B., and Thomas, C. D. (2011). Rapid range shifts of species associated with high levels of climate warming. *Science*, 333(6045):1024–1026.

[11] Cohen, J. M., Venesky, M. D., Sauer, E. L., Civitello, D. J., McMahon, T. A., Roznik, E. A., and Rohr, J. R. (2017). The thermal mismatch hypothesis explains host susceptibility to an emerging infectious disease. *Ecology Letters*, 20(2):184–193.

[12] Damos, P. and Savopoulou-Soultani, M. (2008). Temperature-dependent bionomics and modeling of *Anarsia lineatella* (Lepidoptera: Gelechiidae) in the laboratory. *Journal of Economic Entomology*, 101(5):1557–1567.

[13] Denny, M. (2019). Performance in a variable world: using Jensen's inequality to scale up from individuals to populations. *Conservation Physiology*, 7(1):coz053.

[14] Deutsch, C. A., Tewksbury, J. J., Huey, R. B., Sheldon, K. S., Ghalambor, C. K., Haak, D. C., and Martin, P. R. (2008). Impacts of climate warming on terrestrial ectotherms across latitude. *Proceedings of the National Academy of Sciences*, 105(18):6668–6672.

[15] Easterling, D. R., Meehl, G. A., Parmesan, C., Changnon, S. A., Karl, T. R., and Mearns, L. O. (2000). Climate extremes: observations, modeling, and impacts. *Science*, 289(5487):2068–2074.

[16] Ferguson, L. V. and Sinclair, B. J. (2020). Thermal variability and plasticity drive the outcome of a host-pathogen interaction. *The American Naturalist*, 195(4):603–615.

[17] Fielding, D. J. and Ruesink, W. G. (1988). Prediction of egg and nymphal developmental times of the squash bug (Hemiptera: *Coreidae*) in the field. *Journal of Economic Entomology*, 81(5):1377–1382.

[18] Fisher, M. C., Garner, T. W., and Walker, S. F. (2009). Global emergence of *Batrachochytrium dendrobatidis* and amphibian chytridiomycosis in space, time, and host. *Annual Review of Microbiology*, 63:291–310.

[19] Forrest, M. J. and Schlaepfer, M. A. (2011). Nothing a hot bath won't cure: infection rates of amphibian chytrid fungus correlate negatively with water temperature under natural field settings. *PLoS One*, 6(12):e28444.

[20] Gehman, A.-L. M., Hall, R. J., and Byers, J. E. (2018). Host and parasite thermal ecology jointly determine the effect of climate warming on epidemic dynamics. *Proceedings of the National Academy of Sciences*, 115(4):744–749.

[21] Greenspan, S. E., Bower, D. S., Webb, R. J., Roznik, E. A., Stevenson, L. A., Berger, L., Marantelli, G., Pike, D. A., Schwarzkopf, L., and Alford, R. A. (2017). Realistic heat pulses protect frogs from disease under simulated rainforest frog thermal regimes. *Functional Ecology*, 31(12):2274–2286.

[22] Harvell, C. D., Mitchell, C. E., Ward, J. R., Altizer, S., Dobson, A. P., Ostfeld, R. S., and Samuel, M. D. (2002). Climate warming and disease risks for terrestrial and marine biota. *Science*, 296(5576):2158–2162.

[23] Hinder, S. L., Gravenor, M. B., Edwards, M., Ostle, C., Bodger, O. G., Lee, P. L., Walne, A. W., and Hays, G. C. (2014). Multi-decadal range changes vs. thermal adaptation for north east Atlantic oceanic copepods in the face of climate change. *Global Change Biology*, 20(1):140–146.

[24] Huey, R. B. and Kingsolver, J. G. (1989). Evolution of thermal sensitivity of ectotherm performance. *Trends in Ecology & Evolution*, 4(5):131–135.

[25] Huey, R. B. and Stevenson, R. (1979). Integrating thermal physiology and ecology of ectotherms: a discussion of approaches. *American Zoologist*, 19(1):357–366.

[26] Ikemoto, T. (2005). Intrinsic optimum temperature for development of insects and mites. *Environmental Entomology*, 34(6):1377–1387.

[27] Johnson, C. A., Coutinho, R. M., Berlin, E., Dolphin, K. E., Heyer, J., Kim, B., Leung, A., Sabellon, J. L., and Amarasekare, P. (2016). Effects of temperature and resource variation on insect population dynamics: the bordered plant bug as a case study. *Functional Ecology*, 30(7):1122–1131.

[28] Khelifa, R., Blanckenhorn, W. U., Roy, J., Rohner, P. T., and Mahdjoub, H. (2019). Usefulness and limitations of thermal performance curves in predicting ectotherm development under climatic variability. *Journal of Animal Ecology*, 88(12):1901–1912.

[29] Kingsolver, J. G., Higgins, J. K., and Augustine, K. E. (2015). Fluctuating temperatures and ectotherm growth: distinguishing non-linear and time-dependent effects. *Journal of Experimental Biology*, 218(14):2218–2225.

[30] Kingsolver, J. G. and Woods, H. A. (2016). Beyond thermal performance curves: modeling time-dependent effects of thermal stress on ectotherm growth rates. *The American Naturalist*, 187(3):283–294.

[31] Kirk, N. L., Ward, J. R., and Coffroth, M. A. (2005). Stable Symbiodinium composition in the sea fan *Gorgonia ventalina* during temperature and disease stress. *The Biological Bulletin*, 209(3):227–234.

[32] Lafferty, K. D. (2009). The ecology of climate change and infectious diseases. *Ecology*, 90(4):888–900.

[33] Lemoine, N. P., Drews, W. A., Burkepile, D. E., and Parker, J. D. (2013). Increased temperature alters feeding behavior of a generalist herbivore. *Oikos*, 122(12):1669–1678.

[34] Lindauer, A. L., Maier, P. A., and Voyles, J. (2020). Daily fluctuating temperatures decrease growth and reproduction rate of a lethal amphibian fungal pathogen in culture. *BMC ecology*, 20:1–9.

[35] Linder, J. E., Owers, K. A., and Promislow, D. E. (2008). The effects of temperature on host–pathogen interactions in *D. melanogaster*: Who benefits? *Journal of Insect Physiology*, 54(1):297–308.

[36] Liu, S.-S., Zhang, G.-M., and Zhu, J. (1995). Influence of temperature variations on rate of development in insects: analysis of case studies from entomological literature. *Annals of the Entomological Society of America*, 88(2):107–119.

[37] Logan, J., Wollkind, D., Hoyt, S., and Tanigoshi, L. (1976). An analytic model for description of temperature dependent rate phenomena in arthropods. *Environmental Entomology*, 5(6):1133–1140.

[38] Ma, G., Hoffmann, A. A., and Ma, C.-S. (2015). Daily temperature extremes play an important role in predicting thermal effects. *Journal of Experimental Biology*, 218(14):2289–2296.

[39] Marshall, D. J., McQuaid, C. D., and Williams, G. A. (2010). Non-climatic thermal adaptation: implications for species' responses to climate warming. *Biology Letters*, 6(5):669–673.

[40] Narum, S. R., Campbell, N. R., Meyer, K. A., Miller, M. R., and Hardy, R. W. (2013). Thermal adaptation and acclimation of ectotherms from differing aquatic climates. *Molecular Ecology*, 22(11):3090–3097.

[41] Niehaus, A. C., Angilletta, M. J., Sears, M. W., Franklin, C. E., and Wilson, R. S. (2012). Predicting the physiological performance of ectotherms in fluctuating thermal environments. *Journal of Experimental Biology*, 215(4):694–701.

[42] Nielsen, M. E. and Papaj, D. R. (2015). Effects of developmental change in body size on ectotherm body temperature and behavioral thermoregulation: caterpillars in a heat-stressed environment. *Oecologia*, 177(1):171–179.

[43] Piotrowski, J. S., Annis, S. L., and Longcore, J. E. (2004). Physiology of *Batrachochytrium dendrobatidis*, a chytrid pathogen of amphibians. *Mycologia*, 96(1):9–15.

[44] Plummer, M. (2002). Discussion of the paper by Spiegelhalter et al. *Journal of the Royal Statistical Society Series B*, 64:620.

[45] Plummer, M. et al. (2003). `JAGS`: A program for analysis of Bayesian graphical models using Gibbs sampling. In *Proceedings of the 3rd international workshop on distributed statistical computing*, volume 124, page 125. Vienna.

[46] Raffel, T. R., Halstead, N. T., McMahon, T. A., Davis, A. K., and Rohr, J. R. (2015). Temperature variability and moisture synergistically interact to exacerbate an epizootic disease. *Proceedings of the Royal Society B: Biological Sciences*, 282(1801):20142039.

[47] Ratkowsky, D., Lowry, R., McMeekin, T., Stokes, A., and Chandler, R. (1983). Model for bacterial culture growth rate throughout the entire biokinetic temperature range. *Journal of Bacteriology*, 154(3):1222–1226.

[48] Rebaudo, F., Struelens, Q., and Dangles, O. (2018). Modelling temperature-dependent development rate and phenology in arthropods: The `devRate` package for R. *Methods in Ecology and Evolution*, 9(4):1144–1150.

[49] Rohr, J. R., Civitello, D. J., Cohen, J. M., Roznik, E. A., Sinervo, B., and Dell, A. I. (2018). The complex drivers of thermal acclimation and breadth in ectotherms. *Ecology Letters*, 21(9):1425–1439.

[50] Roznik, E. A. and Alford, R. A. (2014). Using pairs of physiological models to estimate temporal variation in amphibian body temperature. *Journal of Thermal Biology*, 45:22–29.

[51] Roznik, E. A. and Alford, R. A. (2015). Seasonal ecology and behavior of an endangered rainforest frog (*Litoria rheocola*) threatened by disease. *PLoS One*, 10(5):e0127851.

[52] Roznik, E. A., Sapsford, S. J., Pike, D. A., Schwarzkopf, L., and Alford, R. A. (2015). Natural disturbance reduces disease risk in endangered rainforest frog populations. *Scientific Reports*, 5:13472.

[53] Scheele, B. C., Pasmans, F., Skerratt, L. F., Berger, L., Martel, A., Beukema, W., Acevedo, A. A., Burrowes, P. A., Carvalho, T., Catenazzi, A., et al. (2019). Amphibian fungal panzootic causes catastrophic and ongoing loss of biodiversity. *Science*, 363(6434):1459–1463.

[54] Shi, P. and Ge, F. (2010). A comparison of different thermal performance functions describing temperature-dependent development rates. *Journal of Thermal Biology*, 35(5):225–231.

[55] Soetaert, K. E., Petzoldt, T., and Setzer, R. W. (2010). Solving differential equations in R: package `deSolve`. *Journal of Statistical Software*, 33.

[56] Spiegelhalter, D. J., Best, N. G., Carlin, B. P., and Van Der Linde, A. (2002). Bayesian measures of model complexity and fit. *Journal of the Royal Statistical Society Series B*, 64(4):583–639.

[57] Stevenson, L. A., Alford, R. A., Bell, S. C., Roznik, E. A., Berger, L., and Pike, D. A. (2013). Variation in thermal performance of a widespread pathogen, the amphibian chytrid fungus *Batrachochytrium dendrobatidis*. *PloS One*, 8(9):e73830.

[58] Stevenson, L. A., Roznik, E. A., Greenspan, S. E., Alford, R. A., and Pike, D. A. (2020). Host thermoregulatory constraints predict growth of an amphibian chytrid pathogen (*Batrachochytrium dendrobatidis*). *Journal of Thermal Biology*, 87:102472.

[59] Stinner, R., Gutierrez, A., and Butler, G. (1974). An Algorithm for Temperature-dependent Growth Rate Simulation 1,2. *The Canadian Entomologist*, 106(5):519–524.

[60] Team, R. C. et al. (2013). R: A language and environment for statistical computing.

[61] Tomanek, L. (2010). Variation in the heat shock response and its implication for predicting the effect of global climate change on species' biogeographical distribution ranges and metabolic costs. *Journal of Experimental Biology*, 213(6):971–979.

[62] Vasseur, D. A., DeLong, J. P., Gilbert, B., Greig, H. S., Harley, C. D., McCann, K. S., Savage, V., Tunney, T. D., and O'Connor, M. I. (2014). Increased temperature variation poses a greater risk to species than climate warming. *Proceedings of the Royal Society B: Biological Sciences*, 281(1779):2013–2612.

[63] Verant, M. L., Boyles, J. G., Waldrep Jr, W., Wibbelt, G., and Blehert, D. S. (2012). Temperature-dependent growth of *Geomyces destructans*, the fungus that causes bat white-nose syndrome. *PloS One*, 7(9):e46280.

[64] Voyles, J., Johnson, L. R., Briggs, C. J., Cashins, S. D., Alford, R. A., Berger, L., Skerratt, L. F., Speare, R., and Rosenblum, E. B. (2012). Temperature alters reproductive life history patterns in *Batrachochytrium dendrobatidis*, a lethal pathogen associated with the global loss of amphibians. *Ecology and Evolution*, 2(9):2241–2249.

[65] Voyles, J., Johnson, L. R., Rohr, J., Kelly, R., Barron, C., Miller, D., Minster, J., and Rosenblum, E. B. (2017). Diversity in growth patterns among strains of the lethal fungal pathogen *Batrachochytrium dendrobatidis* across extended thermal optima. *Oecologia*, 184(2):363–373.

[66] Ward, J. R., Kim, K., and Harvell, C. D. (2007). Temperature affects coral disease resistance and pathogen growth. *Marine Ecology Progress Series*, 329:115–121.

[67] Woodhams, D. C., Alford, R. A., Briggs, C. J., Johnson, M., and Rollins-Smith, L. A. (2008). Life-history trade-offs influence disease in changing climates: strategies of an amphibian pathogen. *Ecology*, 89(6):1627–1639.

[68] Woodhams, D. C., Alford, R. A., and Marantelli, G. (2003). Emerging disease of amphibians cured by elevated body temperature. *Diseases of Aquatic Organisms*, 55(1):65–67.

[69] Worner, S. P. (1992). Performance of phenological models under variable temperature regimes: consequences of the Kaufmann or rate summation effect. *Environmental Entomology*, 21(4):689–699.

Chapter 4

Revisiting a Bayesian hierarchical modeling approach to predict performance in varying temperature environments

Zachary Gajewski[1*], Jamie Voyles[2], Cierra Sheets[2], Leah R. Johnson[1,3]

1. Department of Biological Science, Virginia Tech, Blacksburg, VA, 24061
2. Department of Biology, University of Nevada Reno, Reno, NV 89557
3. Department of Statistics, Virginia Tech, Blacksburg, VA, 24061

∗ Corresponding author; e-mail: gzach93@vt.edu.

4.1 Abstract

Natural temperature regimes can vary significantly over time, and these variations have an impact on organisms' performance or trait rates. However, currently, most temperature studies measure performance or trait rates in constant temperature environments. There has been a push to use these constant temperature experiments to predict how organisms perform in varying temperature environments, but current predictive methods can not accurately use constant temperature data and predict how an organism will perform in varying temperature environments. In this study, we revisit a hierarchical logistic growth model, fit constant temperature data, that made inaccurate predictions about the amphibian chytrid fungus, *Batrachochytrium dendrobatidis* (Bd), in varying temperature environments, and attempt to improve the accuracy of the predictions. Disease dynamics in the amphibian chytrid fungus system are strongly influenced by environmental temperatures, with lower infection prevalence at warmer temperatures. In this study, we collected Bd growth data using optical density at eight constant temperatures. Using these constant temperature data, we fit a logistic growth model to each treatment's optical density data. We then compared the logistic growth parameters across the eight constant temperatures. We found that the logistic growth parameters d had a clear exponential relationship with temperature and r exhibit a

clear unimodal pattern across temperatures. Due to the relationship between temperature and the delay period (d), we revisited the hierarchical logistic growth model and expanded it by changing the delay period (d) to be temperature-dependent, in addition to keeping the logistic growth rate temperature-dependent. However, when adding a temperature-dependent delay period to the hierarchical model, we found that the model parameters become unidentifiable. With this hierarchical model, one temperature-dependent parameter was not enough and two temperature-dependent parameters in the model were too much. This highlights the difficulty in trying to predict varying temperature performance from constant temperature data. Additionally, these results highlight the need to ensure that the appropriate data are matched to the complexity of a model. To accurately predict Bd growth in varying temperatures a new growth model that is not reliant only on optical density data should be identified.

4.2 Introduction

Temperature is a critical factor in ectothermic organisms and can strongly influence many biotic interactions, such as disease outcomes [5, 19, 30, 37]. The impact of temperature has been studied in numerous systems [1, 8, 17, 22, 30, 35]. However, the effects of temperature on an organism are usually studied in the lab under constant and controlled conditions [1, 6, 30, 37]. The temperatures that organisms would normally experience, however, can significantly vary across days, seasons, and years.

Temperature fluctuations can significantly impact an organism's performance [13, 20, 31, 33, 34]. The importance of variation in temperature indicates that prediction about an organism's performance based solely on constant temperatures could be missing an important element. The effect of different varying temperature regimes can be tested in the lab. However, the different temperature regimes that organisms can experience are too numerous to investigate individually. Therefore, there is interest in predicting varying temperature performance from constant temperature data [3, 18, 20].

Methods that use constant temperatures to predict performance in varying temperature environments often use a thermal performance curve and then integrate performance across the time-varying temperatures to determine net performance [18, 40]. Some studies find that these methods can accurately predict performance in varying temperatures, while others find that these methods make inaccurate predictions [3, 18, 20]. However, with the importance of temperature on many systems, it is critical to determine when and why these methods work and to develop new methods for when current methods can not accurately predict performance.

Here, we use as a case study the amphibian chytrid fungus system, *Batrachochytrium dendrobatidis* (Bd), for which the importance of temperature has been well established [2, 11, 27]. This fungal pathogen has been linked to amphibian population declines around the world

[10, 28]. In warmer seasons and environments, Bd infection prevalence is lower [11, 27]. In the lab, the growth of Bd is limited at 27°C, but it grows at temperatures as low as 4°C [23, 30, 36, 39]. Depending on the strain of Bd, the growth of the pathogen is optimized at around 21°C [23, 30]. Additionally, the importance of temperature variation has also been studied in this system [13, 16, 25, 31]. Temperature variation can impact the growth rate of Bd, and fluctuating temperatures and heat pulses influence disease in amphibians [13, 15].

In Chapter 3, we developed a Bayesian hierarchical model to predict Bd growth in varying temperature environments from constant temperature optical density data. This model that only considered the logistic growth rate to be temperature-dependent could not accurately predict Bd growth. However, other parameters in our logistic growth model, such as the delay period, probably are also temperature-dependent. In this study, we determine which logistic growth parameters are temperature sensitive. We then revisited the Bayesian hierarchical logistic growth model and expanded the model to include a temperature-dependent delay period. Using simulated data, we tested whether our hierarchical model can accurately identify parameter values before using it to predict Bd growth in varying temperatures.

4.3 Methods

We first used optical density to quantify Bd from 8 constant temperatures. We then used the optical density to fit eight logistic growth models, one per temperature treatment. The logistic growth parameters, maximum optical density K, logistic growth rate r, and delay period d, from the eight constant temperatures models, were then compared across temperature treatments to determine temperature sensitivity. Lastly, we revisited the hierarchical Bayesian model constructed in Chapter 3 and expanded the model to include a temperature-dependent delay period. To ensure that our model could correctly identify parameter values, we simulated data and fit the expanded hierarchical model.

4.3.1 Bd Optical Density Growth Data

We collected Bd optical density growth data at eight constant temperature treatments (4°C, 12°C, 17°C, 19°C, 21°C, 24°C, 26°C, and 28°C). We set up the temperature treatments with a cryopreserved Bd strain CJB, originally from *Rana muscosa* in the Serra Nevada Mountains, CA. Before the study, Bd was grown in TGhL nutrient media at 21°C to create a stock. At peak zoospore density (5 days) zoospores were harvested by passing the Bd solution through sterile filter paper to remove zoosporangia. We collected the filtered zoospore solution, and using a hemocytometer we determined the concentration of zoospores in the solution. Starting concentrations for all temperature treatments are given in Table 4.1.

Using the filtered zoospore solution, we set up three 96 well plates per temperature treatment. The plate's perimeter wells were filled with 100 µl of TGhL broth to reduce evaporation in

the experimental wells. The rest of the wells were split in half for positive and negative treatments. The positive wells were filled with 50 µl of the filtered zoospore solution and 50µl of TGhL broth. The negative wells were filled with 50µl of TGhL and 50µl of heat-killed Bd (filtered zoospore solution that was placed in 80°C water for 10mins). The plate was then wrapped with parafilm and placed in the incubator of the assigned temperature treatment. Using a plate reader, we took optical density measurements daily at 490nm for all temperature treatments. We took optical density readings daily until optical density readings (Figure 4.1) stopped increasing. All wells were checked for contamination or low TGhL volume, and these wells were excluded from the analysis.

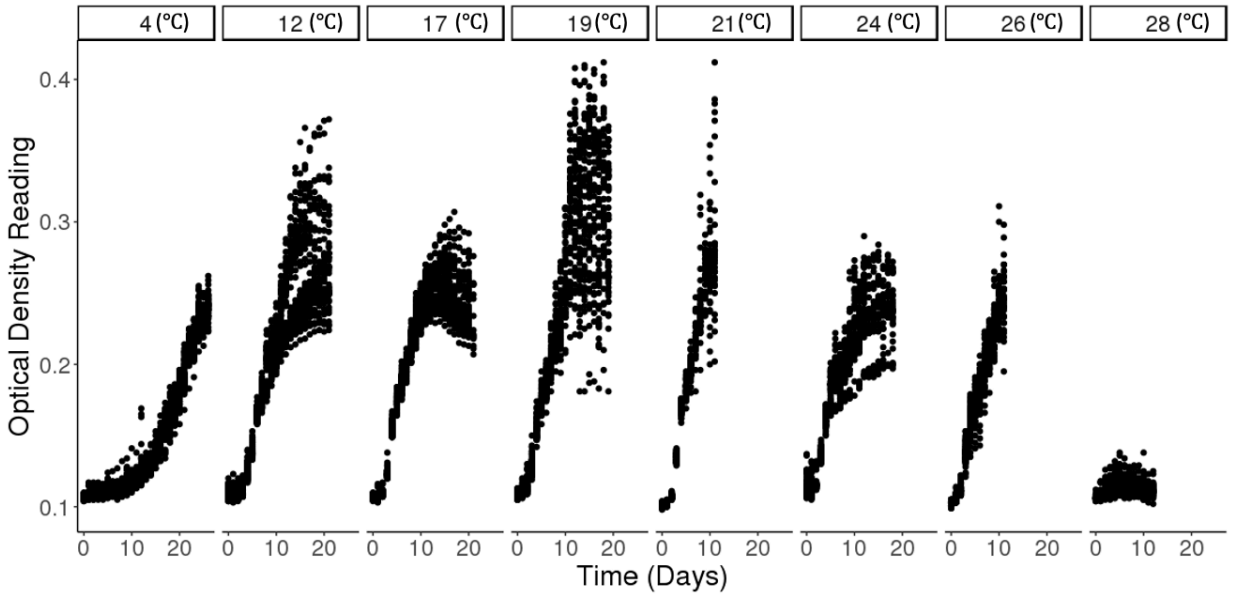

Figure 4.1: Optical density is plotted across time for 8 constant temperature treatments.

Temperature treatments were not all started together due to the limited amount of zoospores produced by the Bd stock. Therefore, we kept a stock of Bd growing at 21°C to harvest zoospores every week to set up new temperature treatments. All temperature treatments were set up with the methods described above. Starting dates for all temperature treatments are in Table 4.1.

Temperature Treatments	Zoospore Starting Conc.	Treatment Start Date
4°C, 12°C, and 17°C	75×10^4	March 28^{th}, 2019
21°C and 26°C	82×10^4	April 4^{th}, 2019
19°C and 28°C	70×10^4	April 25^{th}, 2019
24°C	67×10^4	May 7^{th}, 2019

Table 4.1: All the optical density constant temperature treatments are all listed, along with the starting zoospore concentration and the treatments start dates.

4.3.2 Logistic Growth Models with Bd Optical Density Data

We fit the following deterministic logistic growth model to each temperature treatment's optical density data:

$$Y(t_i) = Y_0 \mathbb{1}_{(t_i<d)} + \frac{KY_0}{Y_0 + (K - Y_0)e^{-r(t_i-d)}} \mathbb{1}_{(t_i \geq d)}. \tag{4.1}$$

The model contains five parameters: an initial optical density reading (Y_0), a delay period (d), a maximum optical density reading (K), a logistic growth rate (r), and observation time (t_i). The model starts with having an optical density value of Y_0 and optical density readings remain at this value until t_i is greater than the delay period d. After the delay is over, the optical density readings increase at a rate r until the maximum optical density level, K, is reached. Once K is reached, all optical density readings after that are equal to K. Overlaid on this model is observational noise. We assume that the noise is log-normal with the mean of the distribution centered at the function $Y(t_i)$. That is, the likelihood of the data conditional on the model and parameters is given by:

$$\begin{aligned} Y_i &\sim \log\mathcal{N}(\mu_i, \tau_i) \\ \mu_i &= Y_0 \mathbb{1}_{(t_i<d)} + \frac{KY_0}{Y_0 + (K - Y_0)e^{-r(t_i-d)}} \mathbb{1}_{(t_i \geq d)}. \end{aligned} \tag{4.2}$$

We fit this model eight separate times with the constant temperature optical density data using Bayesian methods. All temperature treatments used the same prior distribution for Y_0, K, r, and d. Priors were based on those used in Chapter 3 and [37]. Thus the full fitted model and priors are:

$$\begin{aligned} Y_i &\sim \log\mathcal{N}(\mu_i, \tau_i) \\ \mu_i &= Y_0 \mathbb{1}_{(t_i<d)} + \frac{KY_0}{Y_0 + (K - Y_0)e^{-r(t_i-d)}} \mathbb{1}_{(t_i \geq d)} \\ r &\sim \text{Gamma}(0.6, 1) \\ d &\sim \text{U}(0, 20) \\ Y_0 &\sim \text{U}(0.001, 0.2) \\ K &\sim \text{U}(0.21, 0.6) \\ \tau_i &= 1/\sigma_i^2 \\ \sigma &\sim \text{Exp}(.001) \end{aligned}$$

Using `rjags` [24] in R [32], we estimated the parameters using MCMC. The fitted models all had five chains, each run for 30,000 iterations. The first 5,000 iterations were removed for burnin, leaving 25000 iterations per chain for each model. We visually checked the MCMC chains with trace plots to make sure convergence was reached. Lastly, we checked to ensure that no MCMC had a high autocorrelation using ACF.

The parameters r, d, and K were compared across temperature treatments by taking a thinned (every 50th) sample from the posterior distribution to allow easier visualization. This left us with 2500 samples for each r, d, and K per temperature treatment. We then plotted the posterior samples across temperatures and visually inspected the plots for temperature patterns.

4.3.3 Expanding the Hierarchical Logistic Growth Model

In Chapter 3, we constructed a hierarchical logistic growth model. That model included one temperature-dependent parameter, the logistic growth rate, r_T. However, with that model, we could not accurately predict Bd growth in varying temperature environments. Based on the constant temperature logistic parameters, described above, we identified that the delay period, d, is also temperature-sensitive. We wanted to determine if accounting for this second temperature-sensitive parameter would improve Bd varying temperature growth predictions. We did this by expanding the logistic growth model to include a temperature-dependent delay parameter, d_T:

$$Y(T_i) = Y_0 \mathbb{1}_{(t_i < d_T)} + \frac{KY_0}{Y_0 + (K - Y_0)e^{-r_T(t_i - d_T)}} \mathbb{1}_{(t_i \geq d_T)}, \tag{4.3}$$

where other parameters remain as in Equation 4.1.

Similar to the hierarchical model in Chapter 3, we set the logistic growth rate to be temperature-dependent. The relationship between logistic growth rate and temperature is described with the Briere 1 [4] thermal performance curve across temperatures:

$$r_T = c(T_i - T_{min})(T_{max} - T_i)^{1/2}. \tag{4.4}$$

The logistic growth rate becomes 0 when temperatures exceed the thermal maximum (T_{max}) or drop below the thermal minimum (T_{min}). The last parameter in the model, c, is an empirical constant that, with the other parameters, determines the height and curvature of the curve.

In this expanded model, we also made the delay period temperature-dependent. The delay period in the model was made temperature-dependent by assuming that it takes a certain amount of accumulated development, T_{Dev}, before the optical density can start increasing. The rate that development accumulates, Dev, depends on temperature. More specifically, we define the rate that development accumulates with the logistic function:

$$Dev = \frac{K_d}{1 + e^{-(a + b \times T_i)}}. \tag{4.5}$$

This function is a modified Davidson thermal performance curve, where the maximum development is K_d, a modifies the position of the curve, T_i is the temperature at the i^{th} time

point, and b describes the rate of increase from low development rate to a higher development rate at warmer temperatures [7]. This model assumes that development accumulates slowly at cooler temperatures and faster at warmer temperatures. The model also assumes that development is always accumulating at warmer temperatures, and there is no drop-off in development accumulation at hot temperatures.

We assume that development accumulates linearly with the function:

$$\frac{dD}{dt} = Dev(T), \tag{4.6}$$

which has a temperature-dependent development rate, Dev. Rearranging this linear relationship, we can integrate over time to a set total development T_{dev}, assuming constant temperature. The rearranged function can be written as:

$$d_T = \frac{T_{dev}}{Dev}, \tag{4.7}$$

where Dev is the rate of development and is a constant when working with constant temperature data, and T_{dev} is total development threshold. In our model, development accumulation must pass the threshold before Bd can grow. The time it takes constant temperatures to surpass the development threshold is d_T

4.3.4 Simulated Data

To ensure that parameters in the expanded hierarchical model can be correctly identified (Eq. 4.3), we simulated Bd optical density data from the logistic model with delay as described above. We set values for each parameter (Table 4.2 in the logistic growth model (Eq. 4.3), Briere 1 function (Eq. 4.4), and development rate function (Eq. 4.5; Figure 4.2).

We then solved for optical density every day for 30 days, at seven different constant temperature treatments. The solved optical density values were used as the mean optical density value at that time point for that temperature treatment (Figure 4.3). At each time point, 50 random deviates were taken from a log-normal distribution, where the log mean was set to the deterministic value of the optical density and the log standard deviation was log(1.01). This gave us a total of 1,500 simulated data points per temperature treatment.

4.3.5 Hierarchical Model Fitting

All optical density data, from the simulated data, was fit with one logistic growth model (Eq. 4.3). Using a Bayesian approach, we fit the logistic growth model hierarchically. That is, both the delay period and logistic growth rate were temperature-dependent and each were

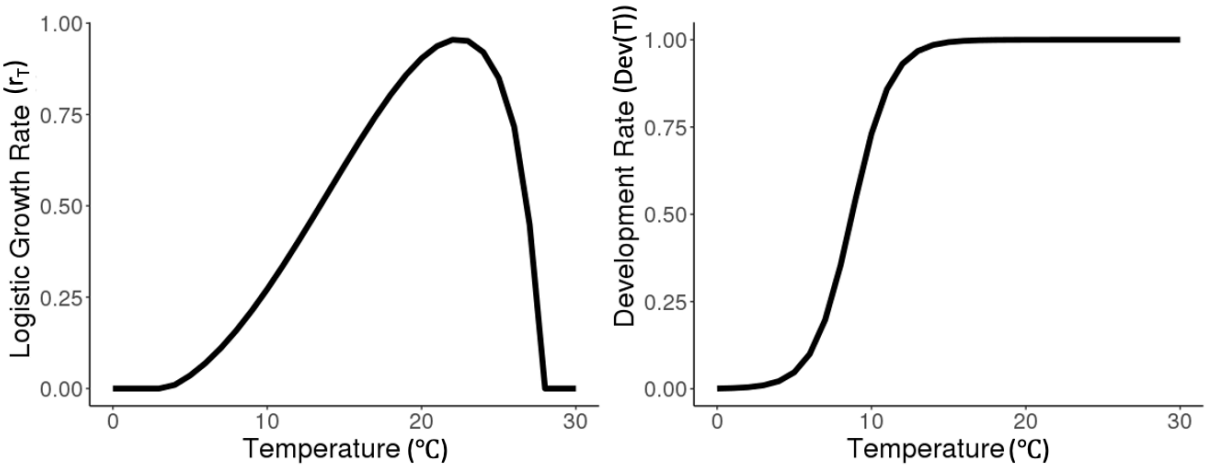

Figure 4.2: The thermal performance curves for the development rate (left) and logistic growth rate (right) are shown above. These curves were made based on parameters values used to simulate the optical density data.

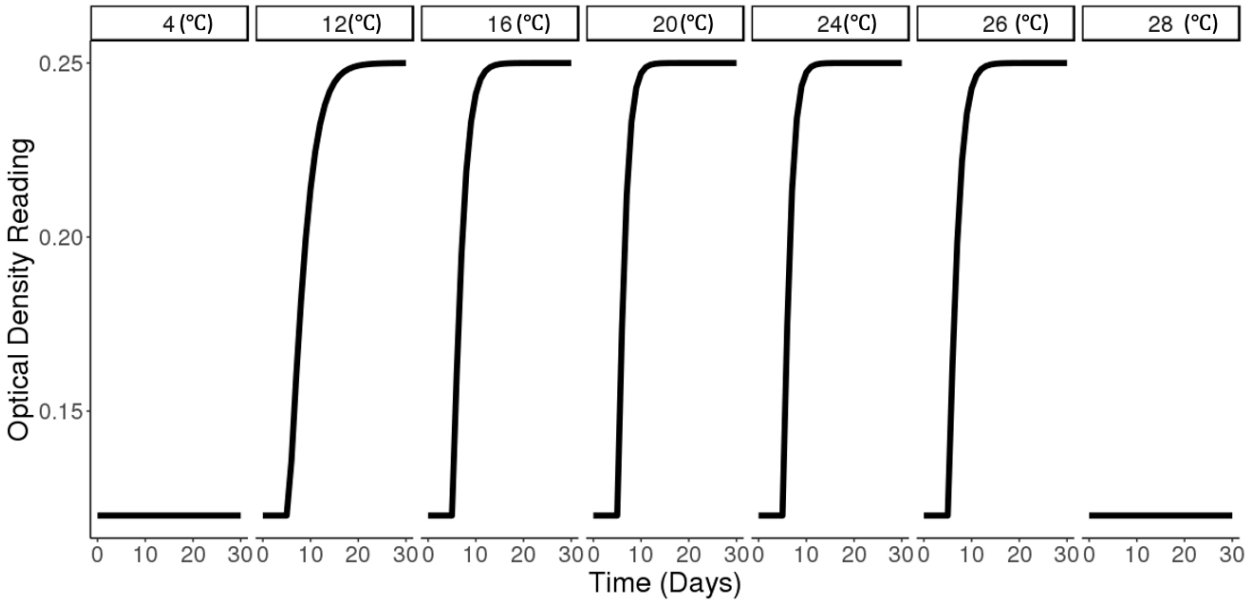

Figure 4.3: Using set parameter values, shown in Table 4.2, we solved for optical density at 7 different temperatures. We used these solutions to simulate optical density data to test the hierarchical logistic growth model.

Parameters	Definition	Prior Distribution	Simulation Value
$Y0$	Initial Optical Density	Exp(0.001)	0.12
K	Maximum Optical Density	U$(0.16, 0.5)$	.25
c	Constant	Gamma$(1, 1)$	0.001
T_{min}	Thermal Minimum	U$(0, 4)$	3.5
T_{max}	Thermal Maximum	$\mathcal{N}(32, 0.5)$	27.5
T_{Dev}	Development Threshold	Gamma$(1, 1)$	5
K_d	Maximum Development Rate	Fixed(1)	1
a	Relative Position of the Curve	$\mathcal{N}(10, 0.25)$	-7
b	Development Logistic Growth Rate	Gamma$(1, 1)$	.8

Table 4.2: Parameters from the hierarchical logistic growth model are shown along with the parameter definitions, prior distributions, and parameter values for the simulated data. All normal distributions are given as $N(\mu, \tau)$, where $\tau = \frac{1}{\sigma^2}$.

described by the functions listed, not fit with a prior directly; instead, priors were placed on the parameters for each function. The hierarchical model is given as:

$$
\begin{aligned}
Y(T_i) &\sim \log\mathcal{N}(\mu_i, \tau_i) \\
\mu(T_i) &= Y_0 \mathbb{1}_{(t_i < d_T)} + \frac{KY_0}{Y_0 + (K - Y_0)e^{-r_T(t_i - d_T)}} \mathbb{1}_{(t_i \geq d_T)} \\
r_T &= c(T_i - T_{min})(T_{max} - T_i)^{1/2} \\
Dev &= \frac{K2}{1 + e^{-(a + b \times T_i)}} \\
d_T &= T_{Dev}/Dev \\
K2 &= 1 \\
a &\sim \mathcal{N}(10, 0.25) \\
b &\sim \text{Gamma}(1, 1) \\
c &\sim \text{Gamma}(1, 1) \\
T_{min} &\sim \text{U}m(0, 4) \\
T_{max} &\sim \mathcal{N}(32, 0.5) \\
\tau_i &= 1/\sigma_i^2 \\
\sigma &\sim \text{Exp}(.001) \\
Y_0 &\sim \text{U}(0.0001, 0.14) \\
K &\sim \text{U}(0.16, 0.5)
\end{aligned}
$$

The logistic growth parameters received priors based on the model in Chapter 3. All parameters in the two thermal performance curves (Briere 1 and the logistic function) received priors based on Chapter 3 for Briere 1 and parameter values found in `devrate` [26].

The model was fit to the simulated data and all parameters were estimated via MCMC in the

`rjags` package [24] in R [32]. The model was run with 5 chains each with 50,000 iterations, of which 10,000 were removed due to burnin. The MCMC traceplots were visually inspected for convergence and checked for autocorrelation using ACF. We also compared all posterior distributions to prior distributions to assess whether data were informative for parameters. Using the true parameter values (Table 4.2), we could ensure whether our fitting procedure was able to accurately estimate the true parameter values.

4.4 Results

4.4.1 Optical Density Logistic Growth Models

Examining the relationship between r, d, and K from Eq. 4.1, visually in Figure 4.4, there are patterns associated with the plotted posterior samples of r and d across temperature. The logistic growth rate, r, shows a clear unimodal relationship with temperature, where the rate is maximized at some intermediate temperature and decreases as the temperature warms or cools. The delay period, d, exhibits an exponential decrease (presumably to some minimum value that is greater than zero) as temperature increases. The maximum optical density, K, does not have a clear relationship with temperature.

The model predicts a much higher maximum optical density at 4°C due to the optical density data at this temperature not having more optical density data after the maximum optical density reading is reached. However, in Figure 4.1, it appears that the 4°C treatment is starting to level off near the other treatments' maximum optical density. Lastly, the 28°C maximum optical density value is not fit well with this model, and is just sampling the parameters given the prior distribution.

4.4.2 Expanded Hierarchical Logistic Growth Model

In Figure 4.5, we can see that posterior distributions for the majority of the parameters were not different from the prior distributions. Only posterior distributions for Y_0 and c were different from their prior distributions. However, the posterior distributions for Y_0 and c did not include the true parameter value. This indicates that adding the additional complexity of a temperature-dependent delay here makes the model parameters unidentifiable with the optical density data.

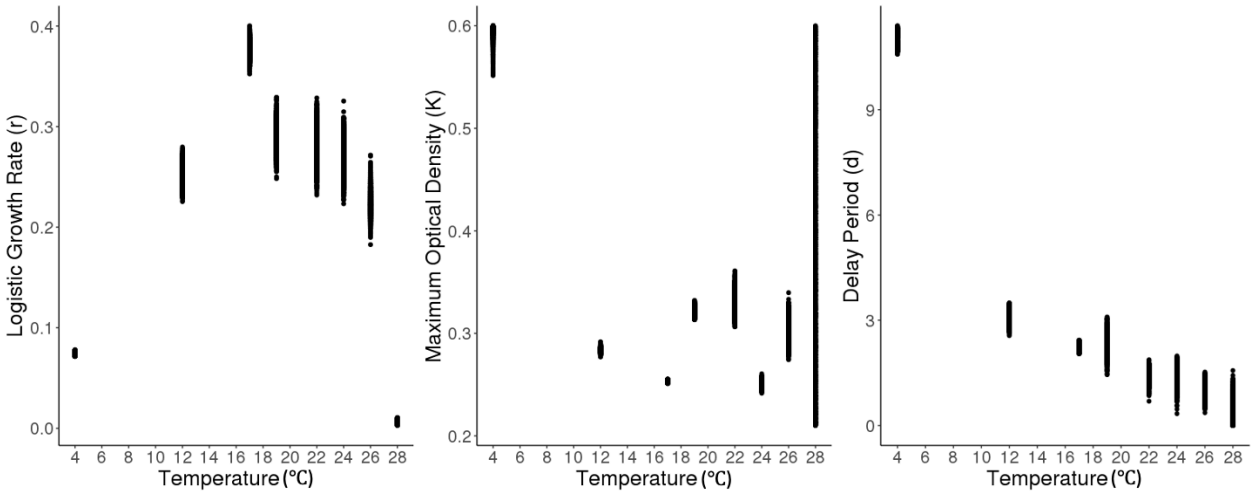

Figure 4.4: From the 8 logistic growth models, posterior samples (n = 2500 per temperature) from the logistic growth rate r (left), maximum optical density K (middle), and delay period d (right) are plotted across temperature.

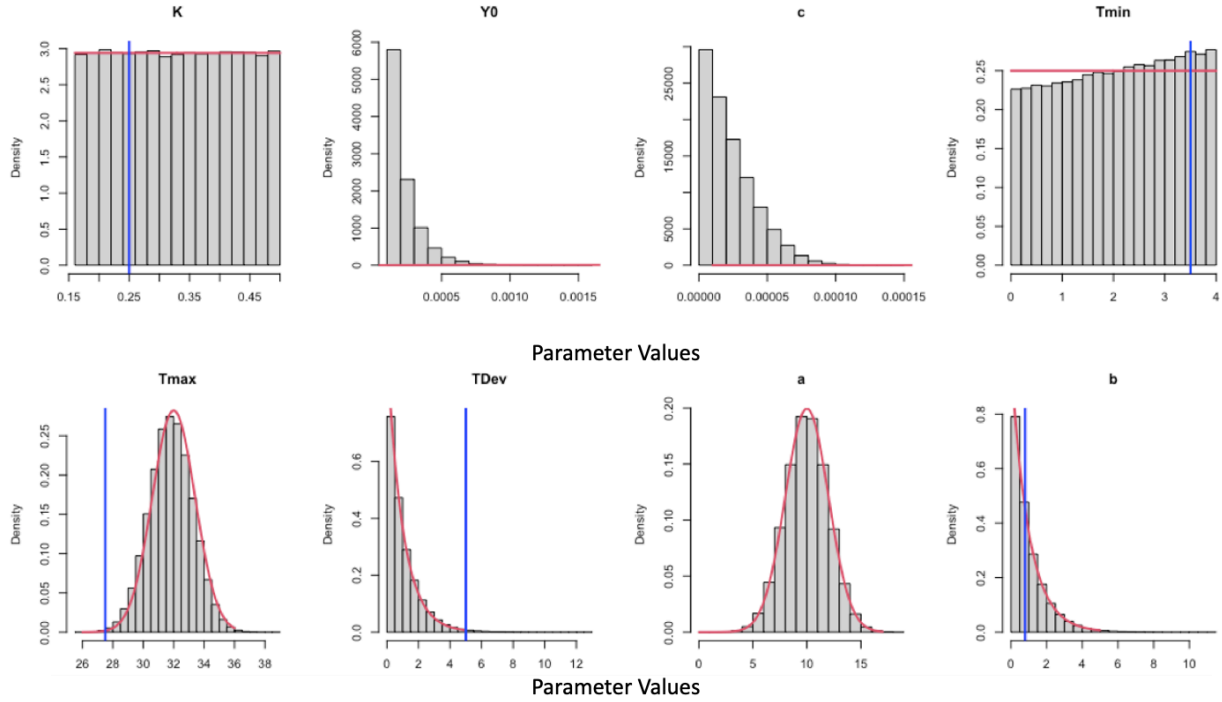

Figure 4.5: For each parameter in the hierarchical logistic growth model, the posterior distribution (shown as a histogram) and prior distribution (shown as a red line) are shown. The true parameter values are also shown with a vertical blue line. True parameter values are not given on the Y_0, c, and a due to the true value being far outside the x axis limits ($Y_0 = 0.12$, $c = 0.001$, a = -7). All true parameter values are given in Table 4.2

4.5 Discussion

In Chapter 3, we used constant temperature data to fit a hierarchical logistic growth model and used it to predict Bd growth in varying temperature environments. However, that model made inaccurate predictions about Bd growth in three different varying temperature environments. Here, we reexamined assumptions about which logistic growth parameters were temperature-sensitive. We fit eight logistic growth models to data collected at eight different constant temperatures. Using the information about which logistic growth parameters were temperature-sensitive, we modified the hierarchical logistic growth model to include a temperature-dependent delay period. We predicted that adding in a second temperature-dependent parameter would improve the accuracy of our growth predictions in varying temperatures. However, this added temperature-dependent model component made the model unidentifiable when fit with the optical density data only, and therefore, we were unable to make any varying temperature predictions with this model.

This modeling exercise seems to indicate that predicting varying temperature optical density patterns with a relatively simple model like this one, fit with only with constant temperature from optical density measurements, will generally be problematic. Although Chapter 3 uses a simpler model, it made inaccurate predictions. While the expanded model in this study only makes the simple addition of the temperature-dependent delay period, the available data are not sufficient to identify the parameters' true values, even in a simulation. This highlights the difficulty, also observed in the literature, with determining and predicting the effects of varying temperatures using constant temperature data [14, 20].

This study also shows that although some biological processes might need more complex models to understand a pattern, the appropriate type and amount of data is needed to fit these models. However, determining the correct type and amount of data can be difficult [9, 12]. We can see that to predict important population processes (like those that result in the delay of the increase in optical density after inoculation) requires different data than optical density data. Future studies should consider using other data that reflects key biological processes in this system, such as zoospore count data, to try to predict varying temperature growth patterns.

Phenomenological models, such as the hierarchical logistic growth model, are useful for describing temperature patterns [21, 36, 38]. However, they do not allow us to test specific mechanistic assumptions about how temperature affects an organism's performance. Mechanistic models can test different hypotheses about how temperature influences performance [29, 38]. With mechanistic models, we can examine the temperature sensitivity of Bd growth factors, such as zoospore settlement rates, zoosporangia developmental rates, or maximum zoospore production.

Bibliography

[1] Adamo, S. A. and Lovett, M. M. (2011). Some like it hot: the effects of climate change on reproduction, immune function and disease resistance in the cricket *Gryllus texensis*. *Journal of Experimental Biology*, 214(12):1997–2004.

[2] Berger, L., Speare, R., Hines, H., Marantelli, G., Hyatt, A., McDonald, K., Skerratt, L., Olsen, V., Clarke, J., Gillespie, G., et al. (2004). Effect of season and temperature on mortality in amphibians due to chytridiomycosis. *Australian Veterinary Journal*, 82(7):434–439.

[3] Bernhardt, J. R., Sunday, J. M., Thompson, P. L., and O'Connor, M. I. (2018). Nonlinear averaging of thermal experience predicts population growth rates in a thermally variable environment. *Proceedings of the Royal Society B: Biological Sciences*, 285(1886):20181076.

[4] Briere, J.-F., Pracros, P., Le Roux, A.-Y., and Pierre, J.-S. (1999). A novel rate model of temperature-dependent development for arthropods. *Environmental Entomology*, 28(1):22–29.

[5] Cohen, J. M., Venesky, M. D., Sauer, E. L., Civitello, D. J., McMahon, T. A., Roznik, E. A., and Rohr, J. R. (2017). The thermal mismatch hypothesis explains host susceptibility to an emerging infectious disease. *Ecology letters*, 20(2):184–193.

[6] Damos, P. and Savopoulou-Soultani, M. (2008). Temperature-dependent bionomics and modeling of *Anarsia lineatella* (Lepidoptera: Gelechiidae) in the laboratory. *Journal of economic entomology*, 101(5):1557–1567.

[7] Davidson, J. (1944). On the relationship between temperature and rate of development of insects at constant temperatures. *The Journal of Animal Ecology*, pages 26–38.

[8] Deutsch, C. A., Tewksbury, J. J., Huey, R. B., Sheldon, K. S., Ghalambor, C. K., Haak, D. C., and Martin, P. R. (2008). Impacts of climate warming on terrestrial ectotherms across latitude. *Proceedings of the National Academy of Sciences*, 105(18):6668–6672.

[9] Drew, K., Cieri, M., Schueller, A. M., Buchheister, A., Chagaris, D., Nesslage, G., McNamee, J. E., and Uphoff Jr, J. H. (2021). Balancing model complexity, data requirements, and management objectives in developing ecological reference points for Atlantic Menhaden. *Frontiers in Marine Science*, 8:53.

[10] Fisher, M. C. and Garner, T. W. (2020). Chytrid fungi and global amphibian declines. *Nature Reviews Microbiology*, 18(6):332–343.

[11] Forrest, M. J. and Schlaepfer, M. A. (2011). Nothing a hot bath won't cure: infection rates of amphibian chytrid fungus correlate negatively with water temperature under natural field settings. *PLoS One*, 6(12):e28444.

[12] Getz, W. M., Marshall, C. R., Carlson, C. J., Giuggioli, L., Ryan, S. J., Romañach, S. S., Boettiger, C., Chamberlain, S. D., Larsen, L., D'Odorico, P., et al. (2018). Making ecological models adequate. *Ecology letters*, 21(2):153–166.

[13] Greenspan, S. E., Bower, D. S., Webb, R. J., Roznik, E. A., Stevenson, L. A., Berger, L., Marantelli, G., Pike, D. A., Schwarzkopf, L., and Alford, R. A. (2017). Realistic heat pulses protect frogs from disease under simulated rainforest frog thermal regimes. *Functional Ecology*, 31(12):2274–2286.

[14] Kingsolver, J. G., Higgins, J. K., and Augustine, K. E. (2015). Fluctuating temperatures and ectotherm growth: distinguishing non-linear and time-dependent effects. *Journal of Experimental Biology*, 218(14):2218–2225.

[15] Lindauer, A., May, T., Rios-Sotelo, G., Sheets, C., and Voyles, J. (2019). Quantifying Batrachochytrium dendrobatidis and Batrachochytrium salamandrivorans viability. *EcoHealth*, 16(2):346–350.

[16] Lindauer, A. L., Maier, P. A., and Voyles, J. (2020). Daily fluctuating temperatures decrease growth and reproduction rate of a lethal amphibian fungal pathogen in culture. *BMC ecology*, 20:1–9.

[17] Linder, J. E., Owers, K. A., and Promislow, D. E. (2008). The effects of temperature on host–pathogen interactions in *D. melanogaster*: Who benefits? *Journal of insect physiology*, 54(1):297–308.

[18] Liu, S.-S., Zhang, G.-M., and Zhu, J. (1995). Influence of temperature variations on rate of development in insects: analysis of case studies from entomological literature. *Annals of the Entomological Society of America*, 88(2):107–119.

[19] Mordecai, E. A., Cohen, J. M., Evans, M. V., Gudapati, P., Johnson, L. R., Lippi, C. A., Miazgowicz, K., Murdock, C. C., Rohr, J. R., Ryan, S. J., et al. (2017). Detecting the impact of temperature on transmission of Zika, dengue, and chikungunya using mechanistic models. *PLoS neglected tropical diseases*, 11(4):e0005568.

[20] Niehaus, A. C., Angilletta, M. J., Sears, M. W., Franklin, C. E., and Wilson, R. S. (2012). Predicting the physiological performance of ectotherms in fluctuating thermal environments. *Journal of Experimental Biology*, 215(4):694–701.

[21] Pell, B., Kuang, Y., Viboud, C., and Chowell, G. (2018). Using phenomenological models for forecasting the 2015 Ebola challenge. *Epidemics*, 22:62–70.

[22] Petton, B., Pernet, F., Robert, R., and Boudry, P. (2013). Temperature influence on pathogen transmission and subsequent mortalities in juvenile Pacific oysters *Crassostrea gigas*. *Aquaculture environment interactions*, 3(3):257–273.

[23] Piotrowski, J. S., Annis, S. L., and Longcore, J. E. (2004). Physiology of *Batrachochytrium dendrobatidis*, a chytrid pathogen of amphibians. *Mycologia*, 96(1):9–15.

[24] Plummer, M. et al. (2003). JAGS: A program for analysis of Bayesian graphical models using Gibbs sampling. In *Proceedings of the 3rd international workshop on distributed statistical computing*, volume 124, page 125. Vienna.

[25] Raffel, T. R., Halstead, N. T., McMahon, T. A., Davis, A. K., and Rohr, J. R. (2015). Temperature variability and moisture synergistically interact to exacerbate an epizootic disease. *Proceedings of the Royal Society B: Biological Sciences*, 282(1801):20142039.

[26] Rebaudo, F., Struelens, Q., and Dangles, O. (2018). Modelling temperature-dependent development rate and phenology in arthropods: The `devRate` package for R. *Methods in Ecology and Evolution*, 9(4):1144–1150.

[27] Roznik, E. A. and Alford, R. A. (2015). Seasonal ecology and behavior of an endangered rainforest frog (*Litoria rheocola*) threatened by disease. *PLoS One*, 10(5):e0127851.

[28] Scheele, B. C., Pasmans, F., Skerratt, L. F., Berger, L., Martel, A., Beukema, W., Acevedo, A. A., Burrowes, P. A., Carvalho, T., Catenazzi, A., et al. (2019). Amphibian fungal panzootic causes catastrophic and ongoing loss of biodiversity. *Science*, 363(6434):1459–1463.

[29] Stefan, A., Geritz, H., and Kisdi, É. (2012). Mathematical ecology: why mechanistic models? *Journal of mathematical biology*, 65(6-7):1411.

[30] Stevenson, L. A., Alford, R. A., Bell, S. C., Roznik, E. A., Berger, L., and Pike, D. A. (2013). Variation in thermal performance of a widespread pathogen, the amphibian chytrid fungus *Batrachochytrium dendrobatidis*. *PloS one*, 8(9):e73830.

[31] Stevenson, L. A., Roznik, E. A., Greenspan, S. E., Alford, R. A., and Pike, D. A. (2020). Host thermoregulatory constraints predict growth of an amphibian chytrid pathogen (*Batrachochytrium dendrobatidis*). *Journal of Thermal Biology*, 87:102472.

[32] Team, R. C. et al. (2013). R: A language and environment for statistical computing.

[33] Vangansbeke, D., Audenaert, J., Nguyen, D. T., Verhoeven, R., Gobin, B., Tirry, L., and De Clercq, P. (2015). Diurnal temperature variations affect development of a herbivorous arthropod pest and its predators. *PloS one*, 10(4):e0124898.

[34] Vasseur, D. A., DeLong, J. P., Gilbert, B., Greig, H. S., Harley, C. D., McCann, K. S., Savage, V., Tunney, T. D., and O'Connor, M. I. (2014). Increased temperature variation poses a greater risk to species than climate warming. *Proceedings of the Royal Society of London B: Biological Sciences*, 281(1779):20132612.

[35] Verant, M. L., Boyles, J. G., Waldrep Jr, W., Wibbelt, G., and Blehert, D. S. (2012). Temperature-dependent growth of *Geomyces destructans*, the fungus that causes bat white-nose syndrome. *PloS one*, 7(9):e46280.

[36] Voyles, J., Johnson, L. R., Briggs, C. J., Cashins, S. D., Alford, R. A., Berger, L., Skerratt, L. F., Speare, R., and Rosenblum, E. B. (2012). Temperature alters reproductive life history patterns in *Batrachochytrium dendrobatidis*, a lethal pathogen associated with the global loss of amphibians. *Ecology and evolution*, 2(9):2241–2249.

[37] Voyles, J., Johnson, L. R., Rohr, J., Kelly, R., Barron, C., Miller, D., Minster, J., and Rosenblum, E. B. (2017). Diversity in growth patterns among strains of the lethal fungal pathogen *Batrachochytrium dendrobatidis* across extended thermal optima. *Oecologia*, 184(2):363–373.

[38] White, C. R. and Marshall, D. J. (2019). Should we care if models are phenomenological or mechanistic? *Trends in ecology & evolution*, 34(4):276–278.

[39] Woodhams, D. C., Alford, R. A., Briggs, C. J., Johnson, M., and Rollins-Smith, L. A. (2008). Life-history trade-offs influence disease in changing climates: strategies of an amphibian pathogen. *Ecology*, 89(6):1627–1639.

[40] Worner, S. P. (1992). Performance of phenological models under variable temperature regimes: consequences of the Kaufmann or rate summation effect. *Environmental Entomology*, 21(4):689–699.

Chapter 5

Modeling the amphibian chytrid fungus growth dynamics using optical density, MTT assay, and zoospore count data

Zachary Gajewski[1*], Jamie Voyles[2], Cierra Sheets[2], Leah R. Johnson[1,3]

1. Department of Biological Science, Virginia Tech, Blacksburg, VA, 24061
2. Department of Biology, University of Nevada Reno, Reno, NV 89557
3. Department of Statistics, Virginia Tech, Blacksburg, VA, 24061

∗ Corresponding author; e-mail: gzach93@vt.edu.

5.1 Abstract

Mathematical and statistical models are often used to explore biological processes and patterns that might not be straightforward to test in an experimental setting. Building these models with the right complexity and parameterizing them with enough appropriate data can be difficult. Some types of data can be time-consuming or expensive to collect, and therefore, a balance is needed between resources (i.e., time and money) and collecting enough data to fit the model. Often models are fitted with a single type of data that seems the most applicable to the model. However, using multiple data sources could potentially help parameterize models with limited data or reduce the need for collecting more time-intensive data. In this study, we use a model of the growth dynamics of the amphibian chytrid fungus, *Batrachochytrium dendrobatidis* (Bd), to test the effectiveness of adding two easier to collect data types (MTT assay and optical density data) to the more typically used (and more time-intensive to collect) zoospore count data. The amphibian chytrid fungus infects amphibians around the world and has been linked to declines in numerous amphibian populations. Bd starts as a mobile zoospore and develops into a zoosporangium inside the host skin, where more zoospore develop. Using simulated data, we examine if including these two extra data sources in the fitting procedure improves the accuracy of parameter estimation. Further, we

explore whether we can use less zoospore count data. We found that the addition of these two extra data sources does increase the accuracy of fitting Bd growth dynamics, especially zoosporangia dynamics. The more zoospore count data used, the better the model is at fitting Bd growth dynamics. However, with the use of MTT assay and optical density data, we can use less zoospore count data. This model still needs to be improved as model parameters were still poorly inferred in some cases, even with the additional data. We also attempted to perform inference on laboratory data and found similar patterns. By combining different data sources into a model we increased the accuracy of some model estimations.

5.2 Introduction

Models of ecological systems can help describe observed patterns and create hypotheses about why those patterns exist. However, matching up models with the appropriate complexity needed to understand biological patterns and parameterize models can be difficult [7, 9]. Some data can be time-consuming and expensive to collect. Therefore, it is important to consider the best way to use resources to maximize the data that can be collected. One potential way to supplement data is to use other types of data in the model. Here, we explore growth of a fungal pathogen using a model that combines three data sources, that vary in how informative and time-intensive they are to collect. We then test if we can still understand growth while limiting the amount of time-intensive data needed to fit the model by supplementing the data with other data.

The use of microorganism population growth models can be used to answer several important biological questions, include those related to disease ecology [24, 25, 26]. Data collected for microorganisms can vary in how time-intensive and expensive they are to collect. Cell counts are a relatively straightforward way of measuring the population growth of microorganisms grown in a lab. This often involves counting the number of cells in a sample using a hemocytometer and microscope [1]. Counting cells can provide detailed data on specific life stages and the viability of cells. However, this method can be time-intensive with dense cultures and multiple samples. An alternative is to measure the optical density of a sample by shining a specific wavelength of light through the samples to measure how much light gets refracted [2, 15]. The more light refracted, the higher the density of cells in the sample, and changes in optical density measurements allows us to observe growth in the sample. With the use of 96 well plates and a microplate reader, many optical density readings can be taken in a short period of time. However, everything in the well contributes to the optical density measurement, including both living and dead cells and detritus. [12]. Combined with optical density readings, MTT assays can be used to get a measure of cell metabolic activity within a sample [12, 14]. As the metabolic activity decreases in a sample, we relate this to decreased cell viability. An MTT assay involves the addition of MTT (3-(4,5-dimethylthiazol-2-yl)-2,5-diphenyltetrazolium bromide) into a sample, which is then broken down by viable cells into an insoluble formazan crystal [14]. The addition of a solubilization solution results in a

color change that can be measured with optical density readings. The more viable cells, the darker the color and the higher the optical density reading.

Cell counts, optical density measurements, and MTT assays have been used to quantify fungal population growth in the amphibian chytrid fungus system [12, 21, 24]. The amphibian chytrid fungus, *Batrachochytrium dendrobatidis* (Bd), is a fungal pathogen that infects amphibians and has been linked to amphibian population declines [19]. This fungal pathogen has two life stages, zoospores and zoosporangia. The fungal pathogen starts as a mobile zoospore. Upon encountering an amphibian, the zoospore encysts into the skin and develops into a zoosporangium. Inside the zoosporangium, new zoospores develop and are eventually released back into the water column or environment [3]. Optical density readings, which are often used to describe Bd growth *in vitro*, combine data on both live and dead zoospores and zoosporangia. This makes it difficult to build more detailed models about individual life stage patterns from optical density data.

When modeling Bd growth dynamics, more mechanistic models often model zoospore and zoosporangia dynamics. With these models, zoospore count data is more informative than optical density data due to it being directly related to a parameter being modeled [24]. Although zoospore count data can be used to build more detailed models useful for describing disease dynamics, count data can be time-consuming to collect. Additionally, zoospore counts also provide no information about the zoosporangia life stage, unlike optical density and MTT measurements. These two measurements group both life stages together, but provide information on both life stages. MTT assays provide the most information about zoosporangia due to viable zoosporangia being the most active in breaking down MTT [12].

In this study, we use data from multiple sources to try to improve our understanding of Bd growth dynamics. We do this by using a combination of optical density readings, MTT assays, and zoospore counts to parameterize a model comprised of delay differential equations that reflect what we know about Bd population dynamics. We explore the effects of using different types and amounts of data on our ability to parameterize the model using a Bayesian approach. More specifically, we simulated data from the model and fit this using different amounts of zoospore count data. We compared the fits and parameters values of the Bayesian model of the different data scenarios to determine how much and what zoospore count data is necessary. Lastly, we examined the performance and inferences we draw when fitting the model to real data. We used Bd growth data from two different constant temperature treatments. We then use the data to fit the Bayesian model with two different data scenarios for each temperature treatment and compared the amount of data to understand the different Bd growth dynamics in different temperatures.

5.3 Methods

5.3.1 Bd Growth Dynamic Model

We used zoospore count data to fit a series of differential equations that described the Bd growth cycle within a sample. The model has been modified from one originally described in [24] to included additional compartments, including one for non-zoospore producing zoosporangia, and subsequent cohorts of zoosporangia. The differential equations describing the dynamics are given by:

$$\begin{aligned}
\frac{dC}{dt} &= -(exp(ls_r) + exp(l\mu_z))C(t) \\
\frac{dS}{dt} &= ls_r(1 - f_s)C(t - T_{min}) - d_{s1}V(t) \\
\frac{dV}{dt} &= exp(ls_r)f_sC(t - T_{min}) - d_{s2}V(t) \\
\frac{dZ}{dt} &= \eta V(t) - (exp(ls_r) + exp(l\mu_z))Z(t) \\
\frac{dA}{dt} &= exp(ls_r)Z(t - T_{min}) - d_{s1}A(t) \\
\frac{dD_z}{dt} &= exp(l\mu)_z(C(t) + Z(t)) \\
\frac{dD_s}{dt} &= d_{s1}(S(t) + A(t)) + d_{s2}V(t),
\end{aligned} \tag{5.1}$$

where each compartment describes the time evolution of a portion of the Bd population in culture, and it is assumed that nutrient limitation will limit the population to 2 complete generations. The initial cohort of zoospores is denoted $C(t)$. These zoospores settle at a rate of s_r and die at a rate of μ_z. A fraction of zoospores (f_s) develop into zoosporangia that will produce zoospores ($V(t)$) or develop ($1 - f_s$) into zoosporangia that will not produce zoospores ($S(t)$). Both groups of zoosporangia take some time to develop from the original zoospores, T_{min}. Non-zoospore producing zoosporangia die at a constant rate d_{s1}, while zoospore producing zoosporangia have a faster dead rate d_{s2}. New zoospores, $Z(t)$, are produced by the active zoosporangia ($V(t)$), at a rate η. These zoospores either settle or die at the same rates as the original cohort and the new resulting zoosporangia are tracked in a final compartment $A(t)$. We also keep track of dead zoospores ($D_z(t)$) and dead zoosporangia ($D_s(t)$) in order to build the observation models that are parameterized from optical density and MTT data.

5.3.2 Bd Growth Observational Models

To supplement the zoospore count data, we use two observational models fit with MTT assay and optical density data. The first observational model is fit with optical density data. We assume that the optical density data follows a log-normal distribution, with the mean being the expected value from the optical density model and the standard deviation is $sdlog.O$. Observed optical density data at each time is assumed to be a linear combination of compartments in the dynamical model:

$$OD = (a)(C(t) + Z(t) + D_z(t)) + (e + f)(S(t) + V(t) + A(t)) + fD_s(t) + h. \tag{5.2}$$

Thus, we assume that optical density is comprised by a combination of live zoospores ($C(t)$ and $Z(t)$), live zoosporangia ($S(t)$,$V(t)$, and $A(t)$), and dead zoosporangia (D_s). The intercept, h, represents an optical density measurement with only the initial zoospore cohort and solution. The slope terms, a, e, and f, determine how much each Bd group contributes to the optical density measurement. For this model, we assume live and dead zoosporangia have different optical properties.

The second observational model is fit with MTT assay data and is a simple linear model. Again, we assume that the MTT data follows a log-normal distribution with a mean being the expected value from the MTT linear model, and the standard deviation set to $sdlog.M$ The observed MTT assay data at each time point is assumed to be a linear model with components from the dynamic model:

$$MTT = b(S(t) + V(t) + A(t)) + d. \tag{5.3}$$

Here we assume that MTT assay data is composed of only live zoosporangia components ($S(t)$ + $V(t)$ + $A(t)$) from the dynamic model. Additionally, all live zoosporangia components contribute the same amount to the observed MTT assay data at each time point. The parameter b scales the zoosporangia population to what is seen in MTT optical density readings (i.e., it is effectively the contribution per cell). Lastly, the intercept, d, represents an MTT optical density measurement with no zoosporangia in the well.

5.3.3 Bd Simulation Data

To simulate data, we set values for parameters in the Bd dynamic model (Table 5.1). Using these set parameters, we fit the delay differential equation (DDE) model for 30 days using the delay differential equation function in `deSolve`, a daily integration step, and the default integrator, `lsoda` in R [20, 23]. This gave simulated values for each component in the Bd dynamic model (i.e., C, Z, A) over time. The simulated values for each of the components in the DDE model and set parameter values were then used to solve the two observational models. This gave one MTT assay and optical density point at each time. We assume that zoospore counts follow a Poisson distribution, and MTT assay and optical density

data each follow their own log-normal distribution. We then set the solved values of the zoospore counts, MTT assay, and optical density as the expected values in their respective distributions for each time point. We set the optical density log-normal distribution standard deviation to 0.01 and we took 50 random draws at each time point. The MTT log-normal distribution set the standard deviation to 0.05 and we took 5 random draws at each time point. Lastly, we took 16 random samples from the Poisson distribution at each time point to get our simulated zoospore count data.

Parameters	Definition	Prior Distribution	Simulation Value
ls_r	Log Zoospore Settling Rate	$\mathcal{N}(0, 2)$	0
$l\mu_z$	Log Zoospore Death Rate	$\mathcal{N}(0, 2)$	-1.2
f_s	Fraction of Zoosporangia that Produce Zoospores	Beta$(2, 2)$	.9
d_{s1}	Death Rate of Non-Zoospore Producing Zoosporangia	Gamma$(1, 1)$	.1
d_{s2}	Death Rate of Zoospore Producing Zoosporangia	Gamma$(1, 1)$	7
$Tmin$	Development Time of Zoosporangia	Gamma$(1, 1)$	1
η	Zoospore Production Rate	Gamma$(200, 2.5)$	60
b	MTT Slope of Live Zoosporangia	$\mathcal{N}(-10, 4)$	-5
d	MTT Intercept	Fixed	0.1
$sdlog.M$	Log Standard Deviation of MTT assay	Exp(10)	0.05
a	Optical Density Slope of Live Zoospore	$\mathcal{N}(-10, 2)$	-11
e	Optical Density Slope of Live Zoosporangia	$\mathcal{N}(-10, 4)$	-8
f	Optical Density Slope of Dead Zoosporangia	$\mathcal{N}(0, 4)$	-9
h	Optical Density Intercept	Fixed	0.3
$sdlog.O$	Log Standard Deviation of Optical Density	$Exp(10)$	0.01

Table 5.1: Parameters for the DDE and observational models are shown along with the parameter definitions, prior distributions, and parameter values for the simulated data.

5.3.4 Data Scenarios

Using the simulated data, we used 6 different data scenarios (Figure 5.2), to determine how much zoospore count data is needed to fit this DDE model. In each case, the optical density and MTT were used, but the amount of zoospore count data used was varied. These scenarios were: 1) using all zoospore count data (full data scenario), 2) using only the observed zero zoospore count data days (zero data scenario), 3) using only the highest observed zoospore count data day (top data scenario), 4) using the top two highest observed zoospore count data days (two data scenario), 5) using the highest zoospore count and the first zero zoospore count data after days (top and bottom data scenario), and 6) using the highest zoospore count and two zero zoospore counts data (top and two bottom data scenario). Ideally, we

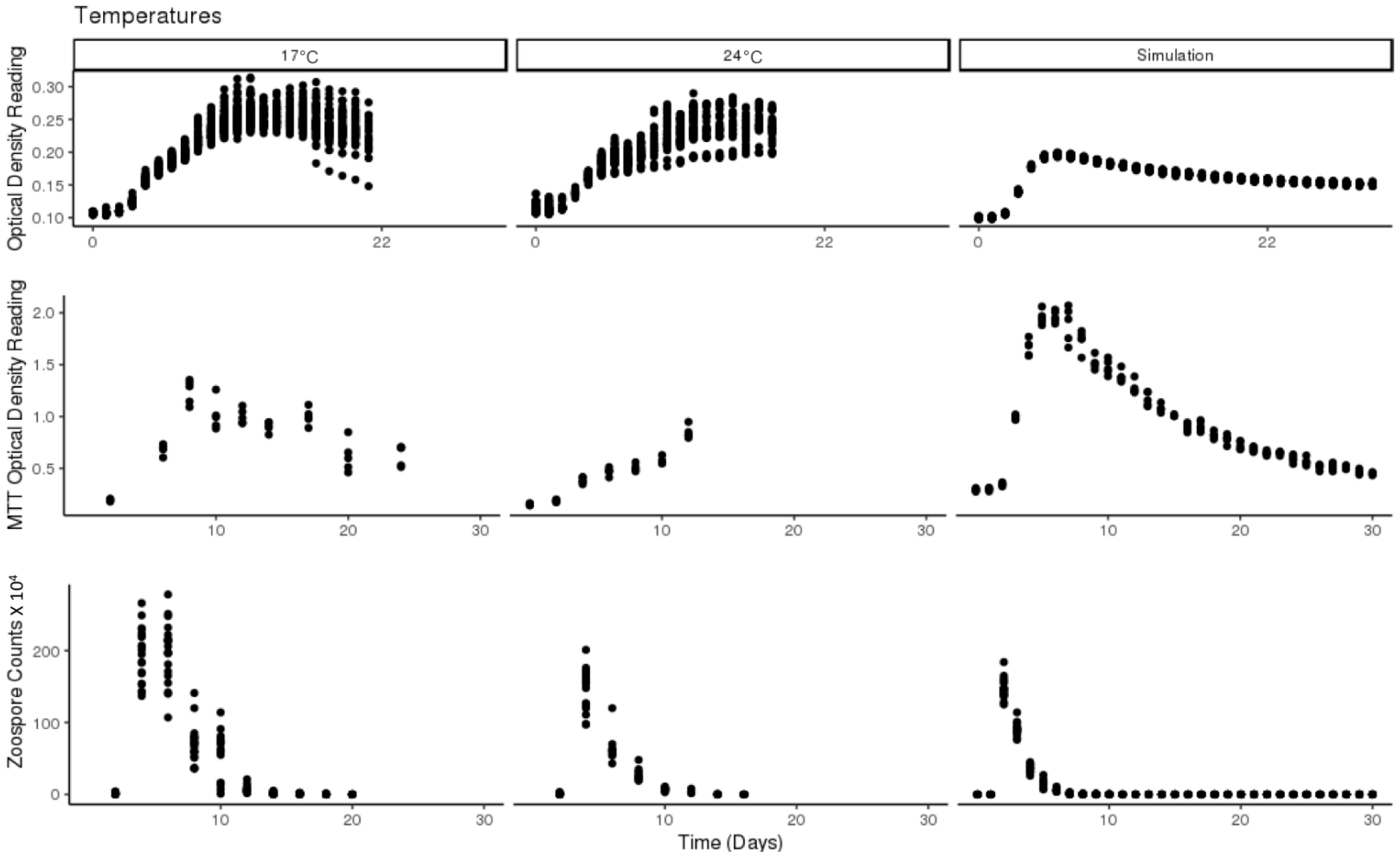

Figure 5.1: The zoospore count, MTT assay, and optical density data are plotted over time. We show the simulated data, 17°C data, and 24°C data.

would not need the highest zoospore count data day, as this requires the most work, and zero data scenairo was enough to accurately fit Bd growth dynamics.

Additionally, we tested the following 2 data scenarios that did not use any optical density or MTT data: 1) using all zoospore count data (reduced full data scenario) and 2) using the highest zoospore count and the first zero zoospore count data after days (reduced top and bottom). We used these scenarios to test how much zoospore count data is needed to describe Bd growth dynamics and the effect of incorporating the OD and MTT data.

5.3.5 Bd Temperature Growth Data

In addition to the simulated Bd growth data, we also wanted to test our inferential procedure with actual Bd growth data. We grew Bd at 2 constant temperatures (17°C and 24°C). The temperature treatments were conducted at the same time due to not having enough zoospores to inoculate all the 96 well plates. The initial setup was completed for the 17°C treatments and plates for 24°C were set up later when enough zoospores were available.

Bd strain CJB, isolated from *Rana muscosa* in the Serra Nevada Mountains, CA, was used for the temperature growth studies. Bd was grown in TGhL media (1 L deionized water, 16 g tryptone, 4 g gelatin hydrolysate, and 2 g lactose) in 25 cm ^{2} flasks (1ml of Bd and 14ml of TGhL) at 21°C. Fungal growth was monitored and zoospores were harvested at their peak density ($\sim$ 5 days). Zoospores were harvested by passing 13ml of the TGhL solution that the Bd was cultured in through sterile filter paper into a 50ml falcon tube. This filtered out zoosporangia, leaving only zoospores in the TGhL broth in the falcon tube. The remaining 2ml of the Bd culture was added to 13ml of TGhL and placed back into the 21°C incubator to keep the Bd culture growing to collect zoospore later for the 24°C treatment.

The filtered zoospore solution was used to set up 96 well plates used in the temperature trials. Using a hemocytometer, we found the concentration of zoospores in the filtered solution. Initial plate setup for the 17°C treatment was done with a concentration of 75×10^4 zoospore per ml. We tried to get the initial zoospore concentration for the 24°C plates as close to the first plates starting zoospore concentration. The 24°C plates started with an initial concentration of 67×10^4.

Two types of 96 well plates were set up for each temperature trial, optical density plates and MTT plates. All optical density 96 well plate setups had the same setup procedure. The plate's perimeter wells were all filled with 100 µl of TGhL to reduce evaporation in the inner experimental wells. The experimental wells were split in half for positive wells and negative wells. All positive wells received 50 µl of the positive zoospore solution and 50 µl of TGhL media. The negative wells were filled with 50 µl of the heat-killed zoospore solution (zoospore placed in 80°C for 10 mins) and 50 µl of TGhL media. The 96 well plates were then covered and wrapped in parafilm and placed in an incubator associated with their assigned temperature. While MTT plates consisted of 5 positive wells and 5 negative

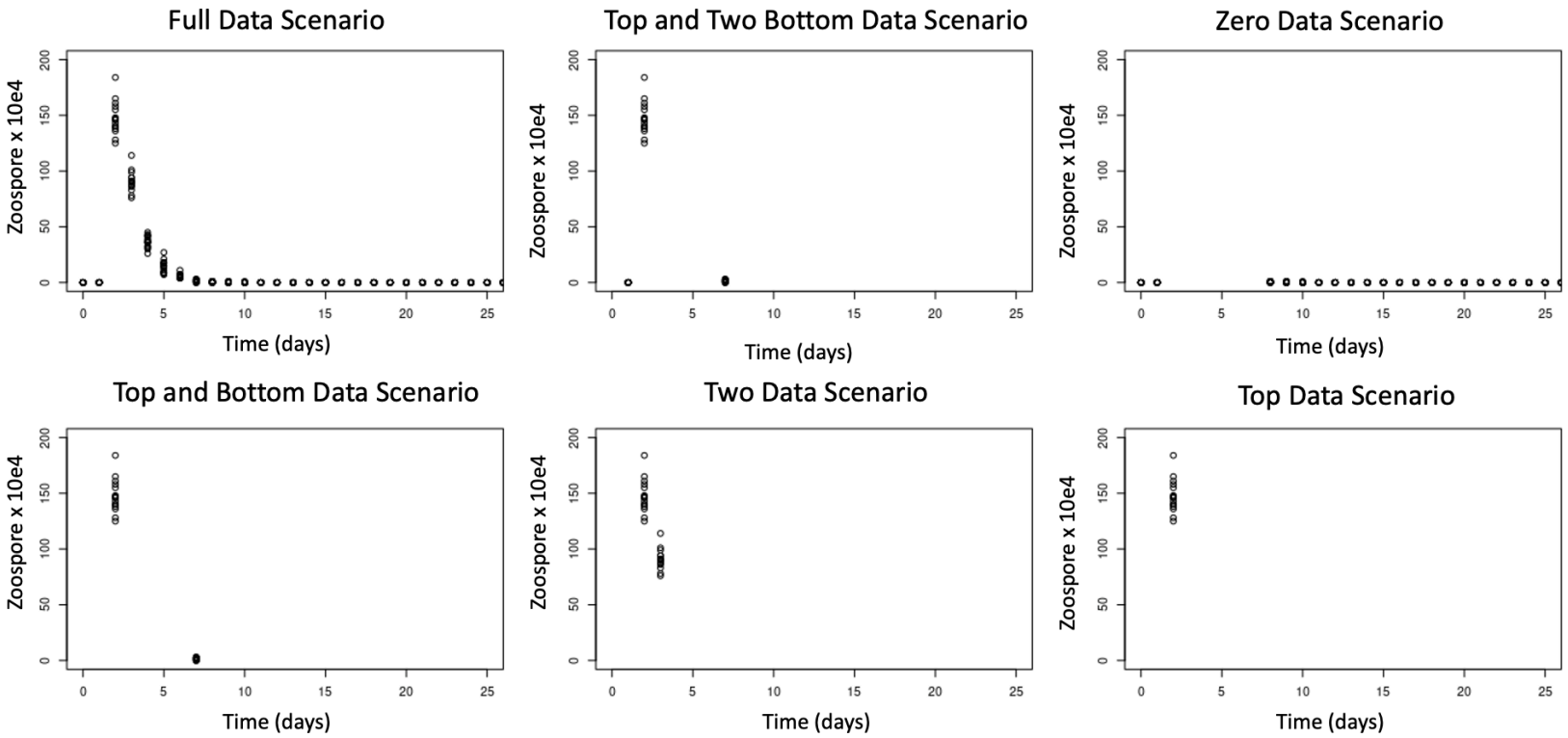

Figure 5.2: Shown are the different zoospore count data scenarios for the simulated data. We do not show the reduced full or reduced top and bottom data scenarios.The reduced full and reduced top and bottom scenarios use the full and top and bottom data scenario zoospore data, respectively.

wells surrounded by perimeter wells, as described above. MTT plates were also wrapped in parafilm and placed in the assigned temperature treatment.

We took zoospore counts every 2-4 days, depending on how fast Bd was growing. Zoospore counts consisted of choosing 5 random experimental wells to sacrifice from the optical density plates in the temperature treatment we were sampling. Each sacrificed well has 20 µl taken and pipetted onto a hemocytometer (10 µl per side). All zoospores were counted in the hemocytometer boxes twice per side, meaning that we had four counts per well. MTT measurements were taken along with the zoospore count measurements, every 2-4 days. For the MTT assay, each well (both positive and negative wells) had 20 µl of MTT solution (5mg 3-(4,5-dimethylthiazol-2-yl)-2,5-diphenyltetrazolium bromide per ml of phosphate-buffered saline (PBS)) added to them. The plate was then covered and placed in a dark area for 2 hours. After the 2 hours, 140 µl of SDS solution (140 µl sodium dodecyl sulfate in dimethylformamide solution [11]) was added into each well. We then took an optical density reading of the plate at 570nm and recorded the reading. Lastly, we recorded optical density readings, taken at 490nm, daily for all optical density plates in all temperature treatments. Plates were checked daily for contamination, indicated by unusually high optical density readings or cloudy wells. Any wells that were contaminated or had low TGHL volumes (> 50 µl due to evaporation) were not used in the analysis. Wells that were sacrificed for zoospore count measurements were removed from optical density data after they were sacrificed.

Using the real Bd growth data, we tested whether the same amount of zoospore count data is the same across temperature treatments. The two different data scenarios that we tested each used all the optical density and MTT data and were tested at both growth temperatures: 1) using all the zoospore count data, and 2) using only the highest observed zoospore count and the first zero zoospore count data after the highest zoospore count data.

5.3.6 Model Fitting

To fit the models with the different data scenarios, described above, we combined the three Bd growth measurements models using a Bayesian framework. We fit the delay differential equations (DDE) with zoospore count data, and we assumed that the optical density and MTT data were linear combinations of components from the DDE model. All zoospore count, MTT assay, and optical density data contributed to the Bayesian likelihood. A Poisson distribution was used for the zoospore count likelihood function, while log-normal

distributions were used for the optical density and MTT data:

$$
\begin{aligned}
\mathcal{L}(\lambda|Z) &= \prod_{i=1}^{n} \frac{\lambda^{z_i} e^{z_i}}{z_i!} \\
\lambda &= \eta V(t) - (exp(ls_r) + \mu_z) Z(t) \\
\mathcal{L}(\mu_1, \sigma_1^2|X) &= \prod_{i=1}^{n} \frac{1}{\sigma_1\sqrt{2\pi}} e^{-\frac{1}{2}(\frac{ln(x_i)-\mu_1}{\sigma_1})^2} \\
\mu_1 &= a(C(t) + Z(t)) + (e+f)(S(t) + V(t) + A(t)) + fD_s(t) + h \\
\mathcal{L}(\mu_2, \sigma_2^2|Y) &= \prod_{i=1}^{n} \frac{1}{\sigma_2\sqrt{2\pi}} e^{-\frac{1}{2}(\frac{ln(y_i)-\mu_2}{\sigma_2})^2} \\
\mu_2 &= (b+c)(S(t) + V(t) + A(t)) + bD_s(t) + d \\
\mathcal{L}(\theta|Z, X, Y) &= \mathcal{L}(\lambda|Z)\mathcal{L}(\mu_1, \sigma_1^2|X)\mathcal{L}(\mu_2, \sigma_2^2|Y)
\end{aligned} \tag{5.4}
$$

The reduced full and reduced top and bottom data scenarios only used the zoospore count Poisson distribution in the likelihood function. All data scenarios, both simulated and real data (described above), were fit the same way. Parameters were estimated using MCMC as implemented in the `deBInfer` package [6] in R [23]. Priors were chosen based on those used in [5] and modified to decrease how informative the priors were and allow for more MCMC mixing (Table 5.1). We adjusted proposal variances to achieve better MCMC mixing (all variance proposals are listed in the supplemental material). The same priors were used for all data scenarios and are listed in Table 5.1. Each model was run with two chains for 500,000 iterations of which the first 5,000 iterations were removed for burn-in. This was a total of 990,000 posterior samples per model. All models were checked visually for convergence. The autocorrelation (assessed using the acf function in R) between MCMC samples was high for each data scenario model. To reduce the autocorrelation, we took every 500^{th} sample from the MCMC chains. This left a total of 1980 samples per model for each data scenario.

Using the thinned samples, we assessed the correlation between model parameters for each data scenario model. We found a high correlation between some of the parameters in most models. Therefore, we used the 1980 samples per model to create a covariance matrix for those sets of parameters that had a positive or negative correlation greater than 0.8. Using this covariance matrix, we were able to rerun each model and jointly propose parameters that were highly correlated (Table 5.2) to sample more efficiently. Even though some parameters were jointly proposed, we still defined the same marginal prior distributions. We used the same methods as those described above, we only added in the joint sampling distribution. Therefore, we had a total of 1980 samples per data scenario again to analyze.

Data Scenario	Parameters Being Jointly Sampled
Full	ls_r, $l\mu_z$, and b
Top and Bottom	$Tmin$, d_{s1}, and b
Top and 2 Bottom	ls_r and $l\mu_z$
Top	None
Zero	ls_r, $l\mu_z$, and b
Reduced: Top and Bottom	None
Reduced: Full	ls_r and $l\mu_z$
Full 17°C	$l\mu_z$ and $d_{s2} + d_{s1}$ and b
Top and Bottom 17°C	d_{s1}, $Tmin$, and b
Full 24°C	ls_r, $l\mu_z$, and b
Top and Bottom 24°C	$Tmin$, b, and d_{s1}

Table 5.2: Shown in the table are the parameters that were highly correlated and jointly proposed for each data scenario. The full 17°C data scenario had two joint proposals.

5.3.7 Model Comparisons

To compare the simulated data scenarios, we used the 1980 posterior samples per data scenario to evaluate the DDE model 1500 times. We used these fits to determine how well the different simulated data scenarios were at fitting the true DDE component dynamics. We also used the 1980 samples to compare the posterior values of the DDE and observational model's parameters to the true parameter values, which are known since we simulated the data.

Next, we examined the model fits to the 17°C and 24°C data scenarios. To compare the data scenarios, we again used the thinned samples to fit the DDE model and compare the different component dynamics. We also plotted the posterior values of the DDE and observational models to compare the full data scenarios to the top and bottom data scenario for both temperature treatments.

5.4 Results

5.4.1 Simulation Results

None of the eight different simulated data scenarios fit all zoospore and zoosporangia components well (Figure 5.3). However, the full and the top and bottom data scenarios did better than others when estimating the new cohort of zoosporangia. The zero and two data scenarios were the most inaccurate at estimating zoospore and zoosporangia dynamics. The zero scenario underestimated almost all groups due to the fitted model assuming that Bd

didn't grow after the initial cohort of zoospores. The top data scenario had the largest uncertainty bands across all model compartments.

When closely examining the new zoospore dynamics (Z model compartment), most of the data scenarios accurately determined the timing and height of the maximum zoospore count (Figure 5.3). The addition of more zoospore count data, such as more zero zoospore counts, helped increase the certainty around the estimates of zoospore dynamics. Additionally, data scenarios that included the MTT assays and optical density data increased the certainty around zoospore dynamics. However, the opposite results are seen when examining model estimates for dead zoospore dynamics, D_Z. Dead zoospore estimates are less well constrained, and the reduced full data scenario, the scenario without MTT assay or optical density data, performed poorly. Removing optical density and MTT assay data improved the estimate of dead zoospores.

The non-zoospore producing and zoospore producing zoosporangia from the initial zoospore cohort were relatively low, and all data scenarios estimated these two groups well (Figure 5.3). However, other zoosporangia group estimates by the different data scenarios were less accurate. The top and bottom data scenario was the closest to accurately fitting the new zoosporangia group. When we removed the MTT assays and optical density data for the top and bottom scenario, the estimate accuracy decreased, and the uncertainty increased. The full data scenario estimated the new zoosporangia group relatively well. Removing MTT assays and optical density data from the full data decreased the new zoosporangia group estimate's accuracy (Figure 5.3). However, the estimates for the dead zoosporangia became more accurate without MTT or optical density in the full data scenario.

We also compared the predicted MTT assay and optical densities to the simulated observation used to fit the data. The full and top and bottom data scenarios performed the best at accurately fitting the MTT assay data (Supplemental Figure 6.3). The other data scenarios performed poorly when visually comparing model fits to the simulated data. All data scenarios underfit the optical density simulated data Supplemental Figure (6.2).

Lastly, we compared samples from the parameters' posterior distributions to the true parameter value, which we set to simulate the data (Figure 5.4). The zero data scenario had the parameter estimates that were the most off from the true parameter values. The full data, top and bottom, and top and two bottom data scenarios had the posterior distribution samples closest to the true parameter values. However, even these data scenarios overestimated the value of the zoospore production rate, η. The fraction of zoosporangia that produce zoospores, f_S, was typically underestimated.

All data scenarios had trouble identifying the correct optical density parameters (a, e, f) and generally underestimated them (Figure 5.5). The MTT parameter, b, was overestimated by all data scenarios except the full data scenario and the top and bottom scenario. The accuracy of these two data scenarios with identifying b explains why they fit the MTT assay data the best. Lastly, both log standard deviations for optical density, $sdlog.O$, and MTT assay, $sdlog.M$, parameters were overestimated when compared to the true parameter values.

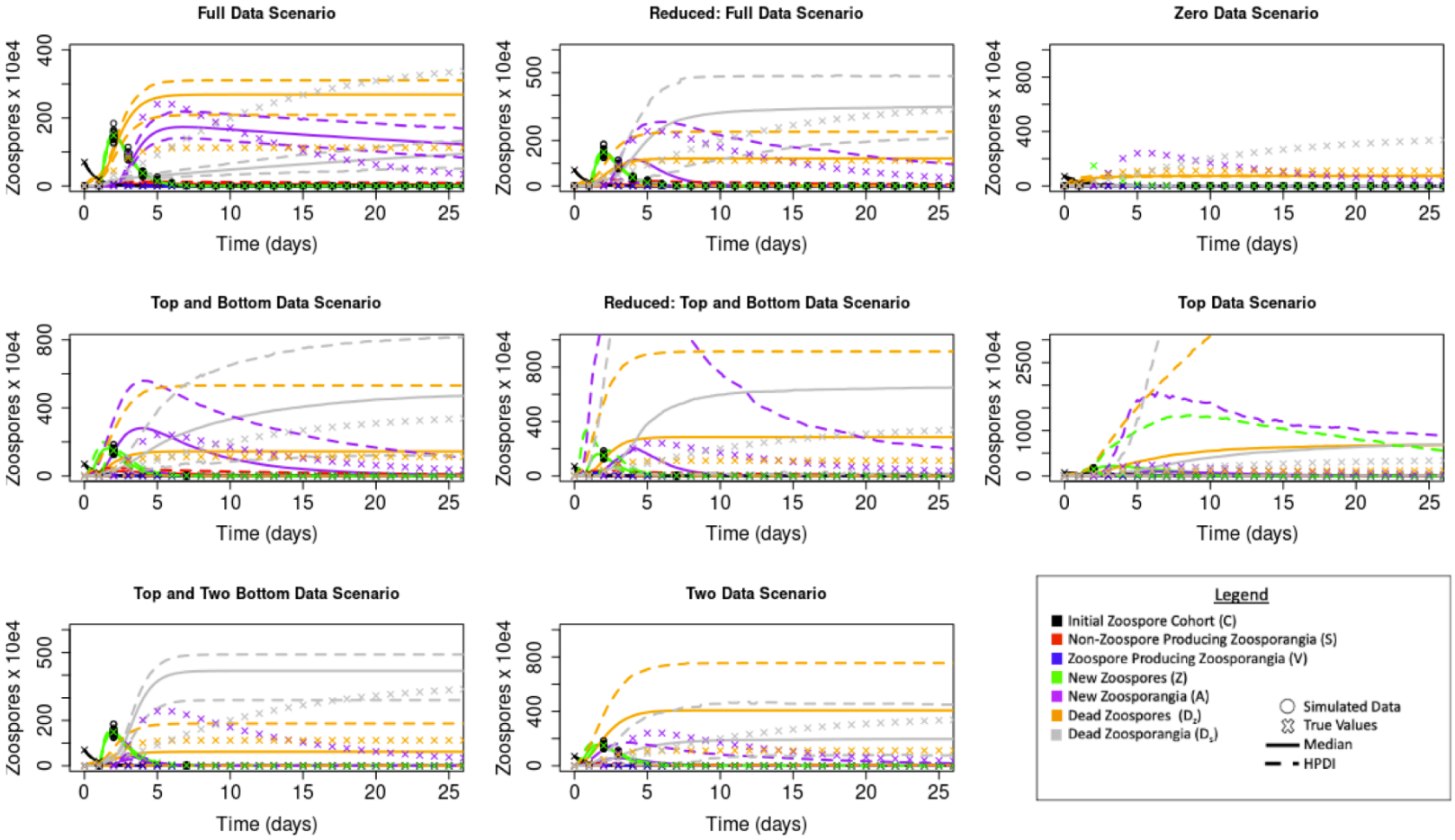

Figure 5.3: Panels show the estimated posterior medians (solid lines) and highest posterior density intervals, HPDI, (dashed lines) of the dynamical system for each of the explored data simulated scenarios, including the reduced data scenarios that do not include MTT or optical density data. The solution of the dynamical system based on the true parameters are shown as X's. Note the y-axes are not the same across panels but, have been scaled to enable examination of all/most of the HPDIs for all model compartments.

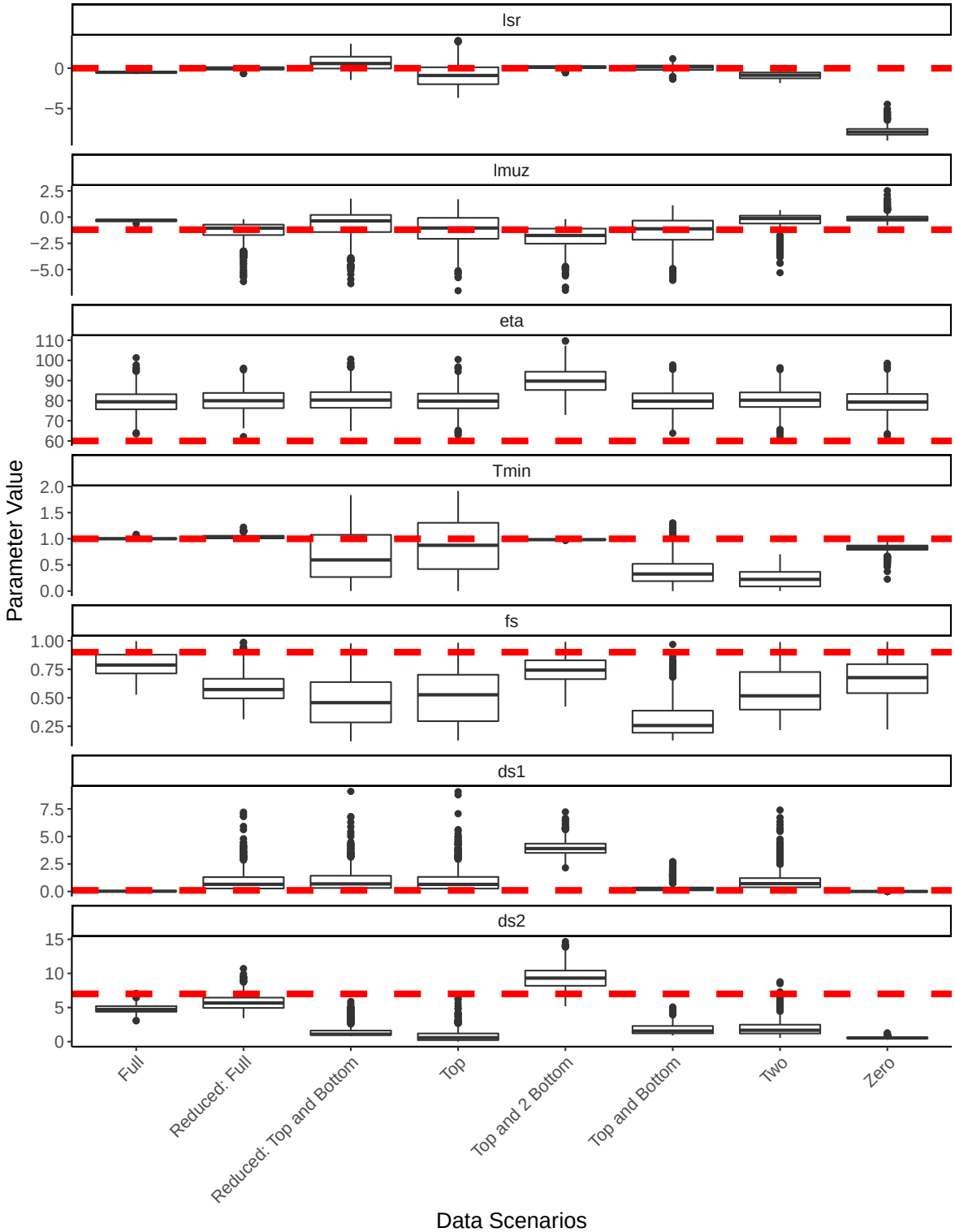

Figure 5.4: For each simulated data scenario, we plotted the posterior samples for each parameter in the DDE model. We marked the true parameter values for the simulated data with red dashed lines, for each parameter.

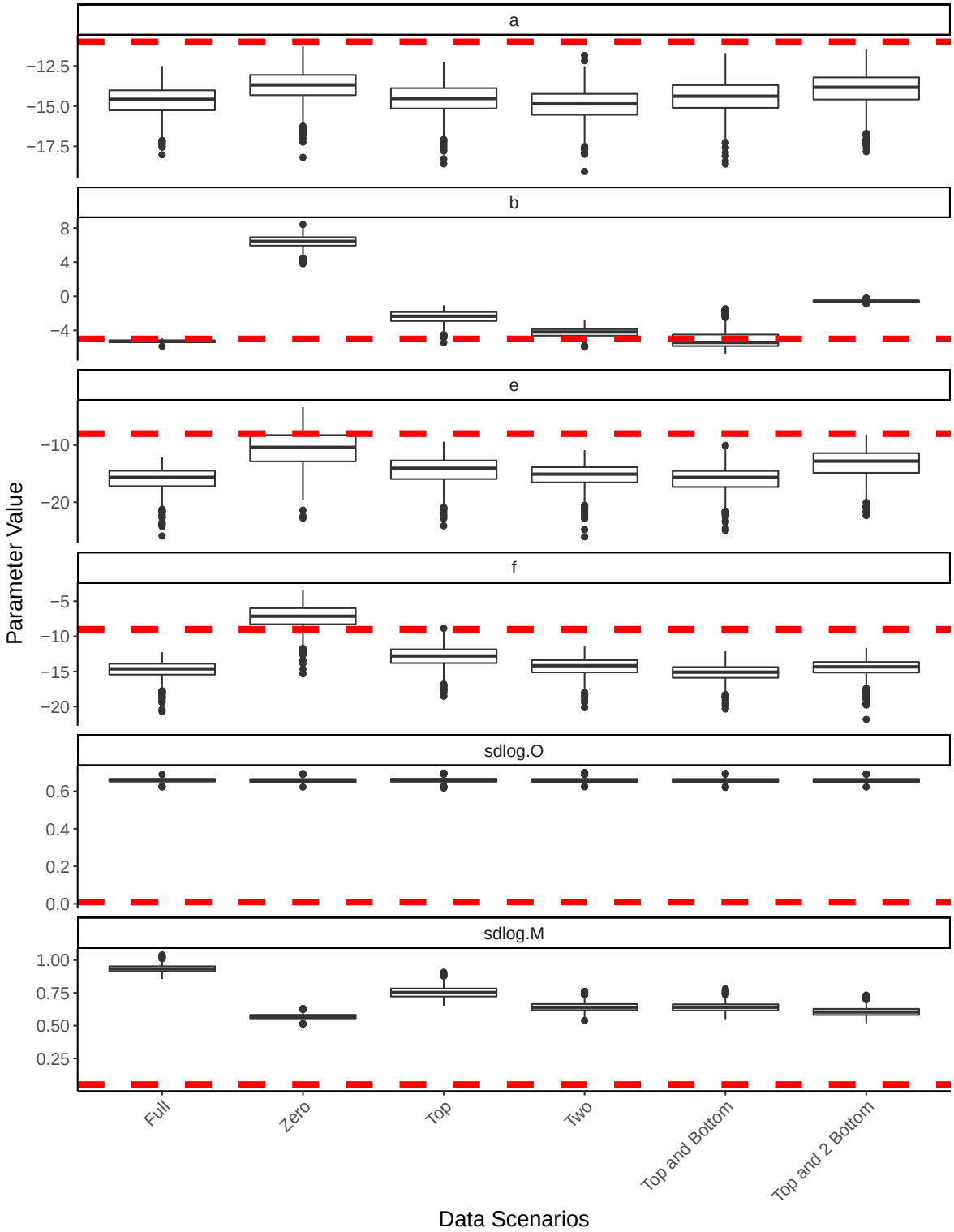

Figure 5.5: For each simulated data scenario that used all three types of data, we plotted the posterior samples for each parameter in the two observational models. We marked the true parameter values for the simulated data with red dashed lines, for each parameter.

5.4.2 Bd growth at 17°C and 24°C Results

In addition to fitting our model to simulated data, we fit the model to Bd growth data taken from a 17°C treatment and 24°C treatment. Although we do not know the true dynamics for the Bd components in the model, we can visually see that having all the zoospore data does decrease the width of the HPD intervals (although, as with the simulated data above, narrow intervals do not guarantee that the true dynamics have been captured). Uncertainty estimates around model fits increased without the MTT assay and optical density data; this is especially true in the 24°C treatment. When we fit the model with reduced 24°C zoospore count data, the new zoosporangia and dead zoosporangia components were dramatically different than fitting the model with all the zoospore count data.

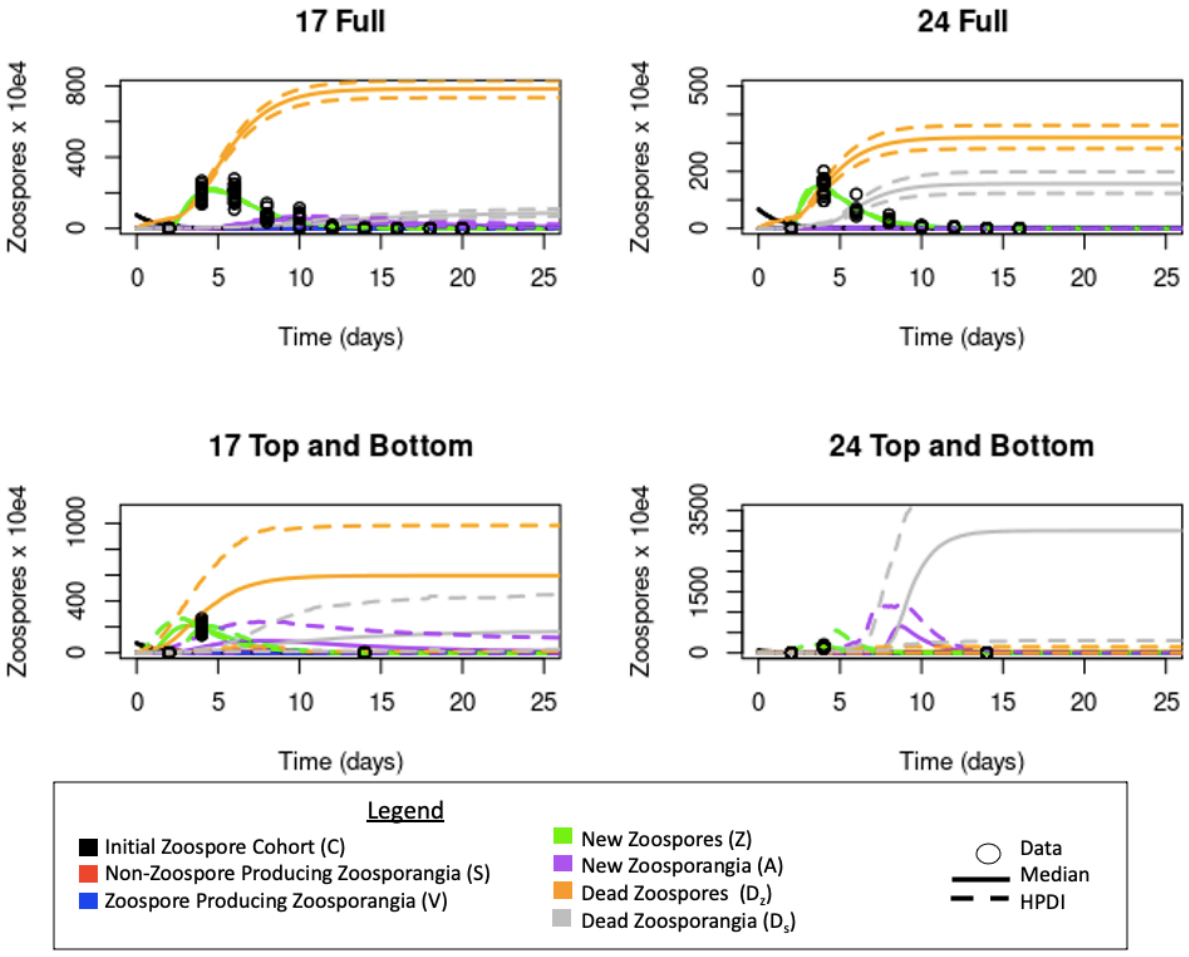

Figure 5.6: Panels show the estimated posterior medians (solid lines) and highest posterior density intervals, HPDI, (dashed lines) of the dynamical system for each of the explored data temperature scenarios. Note the y-axes are not the same across panels, but have been scaled to enable examination of all/most of the HPDIs for all model compartments.

The simulated data models had trouble estimating optical density dynamics well. This trend continued with the 17°C treatment, however, we got better optical density model fits in both 24°C data scenarios (Figure 6.4). But both 24°C data scenario models were unable to accurately fit the MTT assay data. The 17°C full data scenario did a much better job at fitting MTT assay data, although not when zoospore count data was limited (Figure 6.5).

We also compared parameter values of 17°C and 24°C full and limited zoospore count data scenarios. We can see that the 17°C treatment with limited zoospore count data has similar parameter estimates compare to the full 17°C data scenario. But when limiting the zoospore count data in the model at 24°C, the parameter values tend to change compared to the full 24°C data scenario (Supplemental Figures 6.6 and 6.7).

5.5 Discussion

In this study, we use a set of delay differential equations (DDEs) to describe the growth dynamics of the amphibian chytrid fungus. We developed a set of observation models that enabled us to use three complementary data types (zoospore counts, optical density, and MTT assay data) to fit the model and estimate data. Zoospore count data were used directly to fit the zoospore dynamics in the differential equations. The MTT assay and optical density data were assumed to represent a linear combination of some of the Bd life stages that were represented in the DDE model. By combining these three types of data, we improved the model fits for the unobserved zoosporangia components in the differential equations compared to model fits with only zoospore count data. We also showed that by supplementing zoospore count data with optical density and MTT assay data, the amount of zoospore count data needed to fit Bd growth dynamics was reduced. However, the data scenarios that required the least amount of work, such as the zero data scenario, did not provide the model with enough information to accurately fit Bd growth dynamics. To use these data scenarios, a lot of information about the particular strain of Bd's growth dynamics is needed to place strong priors on the model parameters.

Even with these three types of data, two of the DDE parameters, η and f_S, were unidentifiable. However, surprisingly, some data scenarios still accurately captured most zoospore and zoosporangia dynamics anyway. More specifically, the zoospore production rate, η, was overestimated in all data scenarios. This higher level should result in more zoospores produced, and we would expect the model to predict a higher number of zoospores than the observed zoospore count maximum. However, most models were able to correctly identify the zoospore dynamics. The estimation ends up trading off by underestimating f_S which controls the fraction of zoosporangia that produce zoospores. Therefore, even if the zoospores production rate is higher, fewer zoosporangia are producing zoospores. So although these two parameters are not uniquely identified, we can identify the components well.

The linear optical density model parameters were all incorrectly identified by the data sce-

narios. The lower estimates for the optical density observation model parameters lead to all the data scenarios underfitting the optical density data, and instead, the fitting procedure attributes effectively all of the pattern to noise (very high estimated observation variance). The poor fit to the optical density data and the model having difficulty identifying the true parameter values while being able to estimate the dynamics of the system could indicate that the optical density data is not contributing much to the inference. However, the MTT assay slope parameter, b, can be identified in a couple of data scenarios. With the MTT assay linear model, we made assumptions based on the literature and only had live zoosporangia contribute to the measurement. This simpler linear model could be why MTT assay parameters were correctly identified, and optical density parameters were not.

Even with some parameter identification issues with the MTT assay and optical density linear observational models, having them included in the inference procedure helped constrain the inferred zoosporangia dynamics. The data scenarios, full and top and bottom, performed the best at estimating the new zoosporangia cohort. However, without the MTT assay and optical density data, both data scenarios made inaccurate estimates and had more uncertainty. This indicates that despite not fitting the optical density data well, having these data sources does help fit Bd growth dynamics and increase certainty around model parameters and Bd growth projections.

In this study, we also explored using varying amounts of zoospore count data to fit our model. The zoospore count data is labor intensive to collect, so we wanted to determine if it is necessary to collect the full suite of data to fit the model. We found, generally, that more is better; full zoospore count data was always the best at fitting live zoospore and zoosporangia dynamics. Data scenarios that combined the highest zoospore count day with any information about zoospore counts after the peak improves the model estimations. The best model estimations from limited zoospore count data were from the top and bottom data scenario. However, it is possible that strong prior information (in contrast to the weakly informative priors used here) would enable more robust inference with fewer data.

We also determine in this study that different growth conditions, such as temperature, alter how the model performs when less zoospore count data is included in the inference process. The 17°C top and bottom data scenario did have increased uncertainty around the model fit to the DDE components (i.e., the HPD intervals were wider). However, it also predicted DDE model component dynamics that were similar to the 17°C full data scenario. This was not true for the 24°C top and bottom scenario, which predicted very different Bd growth dynamics than the 24°C full data scenario. Both of these temperatures are more intermediate growth temperatures for Bd, and yet there seem to be differences in the amount of zoospore count data needed to pin down dynamics[16, 21, 25]. Futures studies should investigate different data scenarios at a wider range of temperatures, include more extreme growth temperature for Bd, such as 28°C or 4°C [16, 21, 25]. Additionally, future studies can also examine the temperature sensitivity of the parameters in this model to determine the specific effects temperature has on Bd growth. Temperatures influence Bd growth dynamics and amphibian morbidity and mortality in the field [4, 8, 18, 21, 25]. Variations in temperature

also influence Bd growth, but current models have not been able to accurately predict the effect of varying temperatures on Bd growth ([10, 13, 17, 22]; Chapter 3; Chapter 4). We hope that this more mechanistic model that uses data from three different sources can be used to address this question and similar questions that need a better modeling approach or more data.

Before drawing any firm conclusions based on this model or continuing to use it to model/fit Bd growth dynamics, issues with parameter identification and model accuracy need to be addressed. Future iterations of the model should address the problems with fitting the optical density data by either using stronger priors or modifying the linear observational model. For example, we can try enforcing that zoosporangia contribute more than zoospores to the optical density measurement. Alternatively, we could assume that zoospores do not significantly contribute to optical density measurements and remove them from the observational model. We also added some complexity to the DDE model by adding more components and allowing non-zoospore producing zoosporangia and zoospore producing zoosporangia to have different death rates (d_{s1} and d_{s2}). Without the added complexity (and assuming only a single reproductive cohort), the previous version of the DDE model in [24] was able to identify all the model parameters. We need to determine if this added complexity is necessary or if we can remove some of the extra components (and therefore the extra parameters) in the model. By adjusting this model and addressing some of the shortcomings, we can better use this model to look in-depth at Bd growth dynamics and better answer specific biological questions, such as how temperature impacts Bd growth.

Bibliography

[1] Absher, M. (1973). Hemocytometer counting. In *Tissue Culture*, pages 395–397. Elsevier.

[2] Beal, J., Farny, N. G., Haddock-Angelli, T., Selvarajah, V., Baldwin, G. S., Buckley-Taylor, R., Gershater, M., Kiga, D., Marken, J., Sanchania, V., et al. (2020). Robust estimation of bacterial cell count from optical density. *Communications Biology*, 3(1):1–29.

[3] Berger, L., Hyatt, A. D., Speare, R., and Longcore, J. E. (2005). Life cycle stages of the amphibian chytrid *Batrachochytrium dendrobatidis*. *Diseases of Aquatic Organisms*, 68(1):51–63.

[4] Berger, L., Speare, R., Hines, H., Marantelli, G., Hyatt, A., McDonald, K., Skerratt, L., Olsen, V., Clarke, J., Gillespie, G., et al. (2004). Effect of season and temperature on mortality in amphibians due to chytridiomycosis. *Australian Veterinary Journal*, 82(7):434–439.

[5] Boersch-Supan, P. H., Ryan, S. J., and Johnson, L. R. (2016). Bayesian inference for a population growth model of the chytrid fungus. *See https://cran. r-project. org/web/-packages/deBInfer/vignettes/chytrid_dede_example.pdf*.

[6] Boersch-Supan, P. H., Ryan, S. J., and Johnson, L. R. (2017). `deBInfer`: Bayesian inference for dynamical models of biological systems in R. *Methods in Ecology and Evolution*, 8(4):511–518.

[7] Drew, K., Cieri, M., Schueller, A. M., Buchheister, A., Chagaris, D., Nesslage, G., McNamee, J. E., and Uphoff Jr, J. H. (2021). Balancing model complexity, data requirements, and management objectives in developing ecological reference points for Atlantic Menhaden. *Frontiers in Marine Science*, 8:53.

[8] Forrest, M. J. and Schlaepfer, M. A. (2011). Nothing a hot bath won't cure: infection rates of amphibian chytrid fungus correlate negatively with water temperature under natural field settings. *PLoS One*, 6(12):e28444.

[9] Getz, W. M., Marshall, C. R., Carlson, C. J., Giuggioli, L., Ryan, S. J., Romañach, S. S., Boettiger, C., Chamberlain, S. D., Larsen, L., D'Odorico, P., et al. (2018). Making ecological models adequate. *Ecology Letters*, 21(2):153–166.

[10] Greenspan, S. E., Bower, D. S., Webb, R. J., Roznik, E. A., Stevenson, L. A., Berger, L., Marantelli, G., Pike, D. A., Schwarzkopf, L., and Alford, R. A. (2017). Realistic heat pulses protect frogs from disease under simulated rainforest frog thermal regimes. *Functional Ecology*, 31(12):2274–2286.

[11] Hansen, M. B., Nielsen, S. E., and Berg, K. (1989). Re-examination and further development of a precise and rapid dye method for measuring cell growth/cell kill. *Journal of Immunological Methods*, 119(2):203–210.

[12] Lindauer, A., May, T., Rios-Sotelo, G., Sheets, C., and Voyles, J. (2019). Quantifying *Batrachochytrium dendrobatidis* and *Batrachochytrium salamandrivorans* viability. *EcoHealth*, 16(2):346–350.

[13] Lindauer, A. L., Maier, P. A., and Voyles, J. (2020). Daily fluctuating temperatures decrease growth and reproduction rate of a lethal amphibian fungal pathogen in culture. *BMC Ecology*, 20:1–9.

[14] Mosmann, T. (1983). Rapid colorimetric assay for cellular growth and survival: application to proliferation and cytotoxicity assays. *Journal of Immunological Methods*, 65(1-2):55–63.

[15] Myers, J. A., Curtis, B. S., and Curtis, W. R. (2013). Improving accuracy of cell and chromophore concentration measurements using optical density. *BMC Biophysics*, 6(1):1–16.

[16] Piotrowski, J. S., Annis, S. L., and Longcore, J. E. (2004). Physiology of *Batrachochytrium dendrobatidis*, a chytrid pathogen of amphibians. *Mycologia*, 96(1):9–15.

[17] Raffel, T. R., Halstead, N. T., McMahon, T. A., Davis, A. K., and Rohr, J. R. (2015). Temperature variability and moisture synergistically interact to exacerbate an epizootic disease. *Proceedings of the Royal Society B: Biological Sciences*, 282(1801):20142039.

[18] Roznik, E. A., Sapsford, S. J., Pike, D. A., Schwarzkopf, L., and Alford, R. A. (2015). Natural disturbance reduces disease risk in endangered rainforest frog populations. *Scientific Reports*, 5:13472.

[19] Scheele, B. C., Pasmans, F., Skerratt, L. F., Berger, L., Martel, A., Beukema, W., Acevedo, A. A., Burrowes, P. A., Carvalho, T., Catenazzi, A., et al. (2019). Amphibian fungal panzootic causes catastrophic and ongoing loss of biodiversity. *Science*, 363(6434):1459–1463.

[20] Soetaert, K. E., Petzoldt, T., and Setzer, R. W. (2010). Solving differential equations in R: package `deSolve`. *Journal of Statistical Software*, 33.

[21] Stevenson, L. A., Alford, R. A., Bell, S. C., Roznik, E. A., Berger, L., and Pike, D. A. (2013). Variation in thermal performance of a widespread pathogen, the amphibian chytrid fungus Batrachochytrium dendrobatidis. *PloS One*, 8(9):e73830.

[22] Stevenson, L. A., Roznik, E. A., Greenspan, S. E., Alford, R. A., and Pike, D. A. (2020). Host thermoregulatory constraints predict growth of an amphibian chytrid pathogen (*Batrachochytrium dendrobatidis*). *Journal of Thermal Biology*, 87:102472.

[23] Team, R. C. et al. (2013). R: A language and environment for statistical computing.

[24] Voyles, J., Johnson, L. R., Briggs, C. J., Cashins, S. D., Alford, R. A., Berger, L., Skerratt, L. F., Speare, R., and Rosenblum, E. B. (2012). Temperature alters reproductive life history patterns in *Batrachochytrium dendrobatidis*, a lethal pathogen associated with the global loss of amphibians. *Ecology and Evolution*, 2(9):2241–2249.

[25] Voyles, J., Johnson, L. R., Rohr, J., Kelly, R., Barron, C., Miller, D., Minster, J., and Rosenblum, E. B. (2017). Diversity in growth patterns among strains of the lethal fungal pathogen *Batrachochytrium dendrobatidis* across extended thermal optima. *Oecologia*, 184(2):363–373.

[26] Wilber, M. Q., Langwig, K. E., Kilpatrick, A. M., McCallum, H. I., and Briggs, C. J. (2016). Integral projection models for host–parasite systems with an application to amphibian chytrid fungus. *Methods in Ecology and Evolution*, 7(10):1182–1194.

Chapter 6

Conclusion

Emerging infectious diseases have been linked to several wildlife population declines, including in bats [7], amphibians [18], coral [17], and Tasmanian devils [12]. In amphibians, population declines worldwide have been linked to the disease chytridiomycosis, caused by an amphibian chytrid fungus, *Batrachochytrium dendrobatidis* (Bd) [5, 18]. Temperature and amphibian skin microbial communities are factors that can mitigate Bd caused mortality and morbidity in amphibians [6, 16, 19, 21]. Although microbial communities have been well studied, we are just beginning to understand how host and environmental factors shape these vital microbial communities (amphibian skin microbial studies reviewed in [16]). In Chapter 2, I examined how host factors, such as development, host species, and infection, were associated with differences in amphibian skin bacterial communities. At Mianus River Gorge, in Bedford, New York, USA, I sampled amphibian skin bacterial communities of three closely related ranid amphibians and ranid tadpoles. I found host development (tadpoles vs. adult frogs) was associated with host bacterial community differences. However, adults of the closely related *Lithobates spp.* did not have differences in bacterial communities, and infected *L. palustris* skin bacterial communities were not different from uninfected *Lithobates palustris*. My results add to the literature that shows developmental differences in amphibians are associated with differences in skin bacterial communities [9, 14]. This research also supports the literature that shows that host phylogeny may only be significant at higher taxonomic levels [2, 3, 4]. In contrast with my results, other studies have shown differences in skin bacterial communities between infected and uninfected individuals [8, 15]. I think that infection intensity may have been low at my sampling site. Bacterial communities may only be different in infected individuals if infection intensity is high enough. Additionally, I had a low sample size and only *L. palustris* were really infected. If the sample size was increased and other species were looked at, there could be differences in bacterial communities between infected and uninfected individuals.

My field study only examined bacterial community structure changes. However, how the function of these communities change with structure is likely as important. Changes in the community functions due to host or environmental factors could have important consequences for resistance to invading pathogens, like Bd. Additionally, microbial communities are complex and are composed of more organisms than just bacterial species, which I did not consider. Other organisms such as fungi, protozoans, and viruses, could significantly contribute and influence these communities and should be considered in future studies.

Environmental variation, such as varying temperatures, has been shown to influence amphibian skin microbial communities [11]. Environmental temperatures and variation in these temperatures also impacts Bd growth. More studies are starting to examine and recognize the importance of varying temperatures on organisms' performance [1, 6, 13, 20]. Attempts have been made to predict varying temperature performance from constant temperature data with different degrees of success [1, 10, 13]. In Chapter3, I created a Bayesian hierarchical logistic growth model fit with constant temperature data and used it to predict Bd optical density growth in varying temperature environments. I examine how predictions were altered by using different thermal performance curves to constrain the logistic growth rate, the temperature-dependent aspect in the model. I found that even with the hierarchical Bayesian approach and a smaller organism, such as the amphibian chytrid fungus, I could not accurately predict population growth under varying temperatures. Therefore, use these methods to scale up to larger organisms, that might have an acclimation time to changing temperatures, would be more difficult and even more inaccurate. Even with temperature scenarios that had low fluctuations, my predictions still overestimated the growth of Bd. The use of different thermal performance curves to make predictions highlighted the importance of choosing a function that meets the biological assumptions of the system, as the different curves strongly influenced predictions.

In Chapter 4, I collected new constant and varying temperature Bd growth data. I also expanded the Bayesian hierarchical logistic growth model by keeping the logistic growth rate temperature-dependent and making the delay period temperature-dependent as well. However, model parameters could not be identified due to the added complexity to the model, with two temperature-sensitive parameters. Creating models that are informative enough to describe or predict biological patterns and using data that is informative enough can often be difficult. For example, the simpler hierarchical model in my 3rd Chapter did not make accurate predictions. Increasing the complexity of the model to capture more biological detail might have helped improve the model's predictive ability. However, more informative data than optical density data is needed. This is due to optical density data grouping different life stages of both live and dead cells into one measurement. This can be useful for creating some phenomenological models. However, predicting varying temperature population growth seems to require a more complex and mechanistic approach.

Building off insights in Chapter 4, in Chapter 5 I built a more mechanistic model describing Bd growth dynamics. I fit the model with optical density, MTT assay, and zoospore count data. I used this model to test whether combining these three data sources reduced model uncertainty. Using the model, I also tested if using optical density and MTT data, reduced the amount of zoospore count data needed to fit this model. I found that by combining optical density, MTT assays, and zoospore count data, we can increase the information about the state of the system and limit zoospore count data, the more time-intensive data to collect, needed to understand Bd growth dynamics. Additionally, this model is mechanistic, and how temperature impacts Bd growth dynamics can be examined more in-depth. Using this model and examining the temperature sensitivity of the new parameters, we can start

to build back to predicting Bd growth in varying temperature environments.

My temperature studies attempted to consider pathogen growth in more realistic thermal environments. I increased model complexity and combined different data sources to create models that can accurately determine Bd growth in varying temperature environments. However, all of my studies only considered Bd and ignored host response to varying temperature environments, which can be just as crucial for disease dynamics. How the host responds to environmental variations can either increase disease in an area, reduce disease in an area, or it can remain the same. Using a more holistic approach by combining pathogen and host traits, such as host skin bacterial communities, which are influenced by environmental variation, is needed to accurately predict disease dynamics.

Models that incorporate both host and pathogen traits will typically be very complex and need large amounts of informative data to fit and parameterize them. Exploring the assumptions made about each data type would help increase how informative the data is. For example, examining the optical properties of zoospores and zoosporangia, both live and dead, could help refine the optical density observational model in Chapter 5. Additionally, by combing data sources, like in Chapter 5, we can use simulation studies to identify what types of data are informative for model states and parameters so that we can focus effort on collecting the most useful data for various models. By using these methods to increase the amount of information that can be gained from data, we can build more complex models that can combine host and pathogen traits into one model and accurately describe disease dynamics in a system.

Bibliography

[1] Bernhardt, J. R., Sunday, J. M., Thompson, P. L., and O'Connor, M. I. (2018). Nonlinear averaging of thermal experience predicts population growth rates in a thermally variable environment. *Proceedings of the Royal Society B: Biological Sciences*, 285(1886):20181076.

[2] Bird, A. K., Prado-Irwin, S. R., Vredenburg, V. T., and Zink, A. G. (2018). Skin microbiomes of California terrestrial salamanders are influenced by habitat more than host phylogeny. *Frontiers in Microbiology*, 9:442.

[3] Bletz, M. C., Archer, H., Harris, R. N., McKenzie, V. J., Rabemananjara, F. C., Rakotoarison, A., and Vences, M. (2017). Host ecology rather than host phylogeny drives amphibian skin microbial community structure in the biodiversity hotspot of Madagascar. *Frontiers in Microbiology*, 8:1530.

[4] Ellison, S., Rovito, S., Parra-Olea, G., Vásquez-Almazán, C., Flechas, S. V., Bi, K., and Vredenburg, V. T. (2019). The influence of habitat and phylogeny on the skin microbiome of amphibians in Guatemala and Mexico. *Microbial Ecology*, 78(1):257–267.

[5] Fisher, M. C. and Garner, T. W. (2020). Chytrid fungi and global amphibian declines. *Nature Reviews Microbiology*, 18(6):332–343.

[6] Greenspan, S. E., Bower, D. S., Webb, R. J., Roznik, E. A., Stevenson, L. A., Berger, L., Marantelli, G., Pike, D. A., Schwarzkopf, L., and Alford, R. A. (2017). Realistic heat pulses protect frogs from disease under simulated rainforest frog thermal regimes. *Functional Ecology*, 31(12):2274–2286.

[7] Hoyt, J. R., Kilpatrick, A. M., and Langwig, K. E. (2021). Ecology and impacts of white-nose syndrome on bats. *Nature Reviews Microbiology*, pages 1–15.

[8] Jani, A. J. and Briggs, C. J. (2014). The pathogen *Batrachochytrium dendrobatidis* disturbs the frog skin microbiome during a natural epidemic and experimental infection. *Proceedings of the National Academy of Sciences*, 111(47):E5049–E5058.

[9] Kueneman, J. G., Parfrey, L. W., Woodhams, D. C., Archer, H. M., Knight, R., and McKenzie, V. J. (2014). The amphibian skin-associated microbiome across species, space and life history stages. *Molecular Ecology*, 23(6):1238–1250.

[10] Liu, S.-S., Zhang, G.-M., and Zhu, J. (1995). Influence of temperature variations on rate of development in insects: analysis of case studies from entomological literature. *Annals of the Entomological Society of America*, 88(2):107–119.

[11] Longo, A. V. and Zamudio, K. R. (2017). Temperature variation, bacterial diversity and fungal infection dynamics in the amphibian skin. *Molecular Ecology*, 26(18):4787–4797.

[12] McCallum, H., Tompkins, D. M., Jones, M., Lachish, S., Marvanek, S., Lazenby, B., Hocking, G., Wiersma, J., and Hawkins, C. E. (2007). Distribution and impacts of Tasmanian devil facial tumor disease. *EcoHealth*, 4(3):318–325.

[13] Niehaus, A. C., Angilletta, M. J., Sears, M. W., Franklin, C. E., and Wilson, R. S. (2012). Predicting the physiological performance of ectotherms in fluctuating thermal environments. *Journal of Experimental Biology*, 215(4):694–701.

[14] Prest, T. L., Kimball, A. K., Kueneman, J. G., and McKenzie, V. J. (2018). Host-associated bacterial community succession during amphibian development. *Molecular Ecology*, 27(8):1992–2006.

[15] Rebollar, E. A., Hughey, M. C., Medina, D., Harris, R. N., Ibáñez, R., and Belden, L. K. (2016). Skin bacterial diversity of Panamanian frogs is associated with host susceptibility and presence of *Batrachochytrium dendrobatidis*. *Multidisciplinary Journal of Microbial Ecology*, 10(7):1682–1695.

[16] Rebollar, E. A., Martínez-Ugalde, E., and Orta, A. H. (2020). The amphibian skin microbiome and its protective role against chytridiomycosis. *Herpetologica*, 76(2):167–177.

[17] Richardson, L. L. (2004). Black band disease. In *Coral Health and Disease*, pages 325–336. Springer.

[18] Scheele, B. C., Pasmans, F., Skerratt, L. F., Berger, L., Martel, A., Beukema, W., Acevedo, A. A., Burrowes, P. A., Carvalho, T., Catenazzi, A., et al. (2019). Amphibian fungal panzootic causes catastrophic and ongoing loss of biodiversity. *Science*, 363(6434):1459–1463.

[19] Stevenson, L. A., Alford, R. A., Bell, S. C., Roznik, E. A., Berger, L., and Pike, D. A. (2013). Variation in thermal performance of a widespread pathogen, the amphibian chytrid fungus *Batrachochytrium dendrobatidis*. *PloS One*, 8(9):e73830.

[20] Stevenson, L. A., Roznik, E. A., Greenspan, S. E., Alford, R. A., and Pike, D. A. (2020). Host thermoregulatory constraints predict growth of an amphibian chytrid pathogen (*Batrachochytrium dendrobatidis*). *Journal of Thermal Biology*, 87:102472.

[21] Voyles, J., Johnson, L. R., Briggs, C. J., Cashins, S. D., Alford, R. A., Berger, L., Skerratt, L. F., Speare, R., and Rosenblum, E. B. (2012). Temperature alters reproductive life history patterns in *Batrachochytrium dendrobatidis*, a lethal pathogen associated with the global loss of amphibians. *Ecology and Evolution*, 2(9):2241–2249.

Appendix A Chapter 2 Supplemental Material

The Bray-Curtis (BC) dissimilarity matrix can be calculated with:

$$BC_{ij} = 1 - \frac{2C_{ij}}{S_i + S_j}, \tag{6.1}$$

where i and j are two different sites, S_i is the number of organisms at site i, S_j is the number of organisms at site j, and C_{ij} is the sum of the site with less counts for each species found in both sites.

The Jaccard (J) dissimilarity matrix can be calculated with:

$$J(X, Y) = \frac{|X \cap Y|}{|X \cup Y|}, \tag{6.2}$$

where X and Y represent two different sites, $|X \cap Y|$ is the number of species present at both sites, and $|X \cup Y|$ is the total number of species in present at either site.

Appendix B Chapter 3 Supplemental Figures

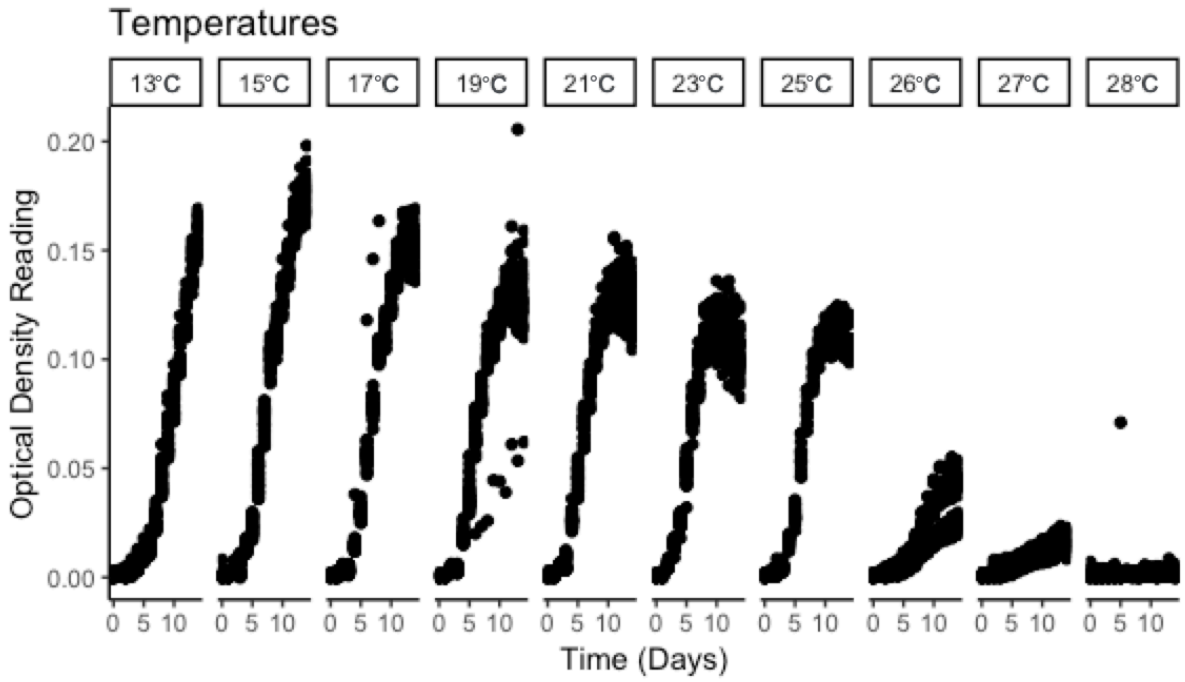

Figure 6.1: Optical density readings at 10 different temperatures, for a North Queensland isolate of Bd, over 14 days.

Appendix C Chapter 3 Supplemental Tables

Varying Temp Regime	r_T	K	d	Y_0
Dry Low Air	0.409 (0.388, 0.429)	0.196 (0.167, 0.227)	0.610 (0.132, 0.687)	0.0039 (0.0036, 0.0042)
Wet High Frog	0.443 (0.428, 0.460)	0.167 (0.154, 0.182)	0.156 (0.005, 0.339)	0.0035 (0.003, 0.0038)
Wet Low Frog	0.337 (0.321, 0.352)	0.125 (0.109, 0.146)	0.014 (0.00005, 0.058)	0.004 (0.004, 0.0041)

Table 6.1: A logistic growth model (Eq. 3.1) was fit to each of the three varying temperature regimes. The median and 95% highest posterior density interval for each of the logistic growth models are shown in the table.

Temperatures	Ratkowsky	Briere 2	Ikemoto	Logan 10	Stinner
Dry Low Air	1.084 (0.926, 1.165)	1.044 (0.934, 1.069)	0.972 (0.916, 1.004)	0.841 (0.788, 0.851)	0.8126 (0.8126, 0.8129)
Wet High Frog	1.163 (1.159, 1.166)	1.060 (1.045, 1.068)	0.935 (0.896, 0.966)	0.847 (0.839, 0.851)	0.81269 (0.81269, 0.81270)
Wet Low Frog	0.719 (0, 1.101)	0.666 (0, 0.973)	0.494 (0, 0.773)	0.563 (0, 0.800)	0.720 (0.003, 0.813)

Table 6.2: Based on the three temperature regimes, Dry Low Air (DLA), Wet High Frog (WHF), and Wet Low Fog (WLF), we calculated the median logistic growth rate that each thermal performance curve predicted. We also show the 95% highest posterior density interval, in parentheses, for each thermal performance curve.

Stinner $r_T = \frac{c}{1+e^{(k_1+k_2T)}}(T_{opt} < T) + \frac{c}{1+e^{(k1+k2(2Topt-T))}}(T_{opt} > T)$			
Parameters	Definition	Prior Distribution	Posterior Median
c	Constant	Gamma$(1,1)$	0.813 (0.789, 0.839)
k_1	Constant	$\mathcal{N}(32,1)T(30,40)$	32.364 (31.017, 33.983)
k_2	Constant	$\mathcal{N}(0,5)T(-5,10)$	-2.555 (-2.450, -2.680)
T_{opt}	Thermal Optimum	U$(13,25)$	19.234 (19.220, 19.250)

Table 6.3: The table shows the Stinner thermal performance curve and all its parameters, the priors given to them, and the posterior median and highest posterior density intervals. All normal distributions are given as $N(\mu, \tau)$, where $\tau = \frac{1}{\sigma^2}$.

Briere 2 $r_T = cT(T - T_{min})(T_{max} - T)^{\frac{1}{b}}$			
Parameters	Definition	Prior Distribution	Posterior Median
c	Constant	Gamma$(1,1)$	0.00049 (0.00044, 0.00055)
T_{min}	Minimum Temperature	$\mathcal{N}(4,0.5)$	7.214 (5.949, 8.403)
T_{max}	Maximum Temperature	U$(27,35)$	27.95 (27.806, 28.040)
b	Constant	Gamma$(10,1)$	0.966 (0.895, 1.043)

Table 6.4: The table shows the Briere 2 thermal performance curve and all its parameters, the priors given to them, and the posterior median and highest posterior density intervals. All normal distributions are given as $N(\mu, \tau)$, where $\tau = \frac{1}{\sigma^2}$.

Logan 10 $r_T = \alpha\frac{1}{1+ce^{-bT}} - e^{\frac{T_{max}-T}{\Delta_T}}$			
Parameters	Definition	Prior Distribution	Posterior Median
α	Constant	U$(0,2)$	0.134 (0.885, 0.957)
c	Constant	$\mathcal{N}(90,10)$	90.005 (89.409, 90.686)
b	Constant	Gamma$(1,1)$	0.384 (0.378, 0.390)
Δ_T	Breadth of Range	Gamma$(1,1)$	2.078 (1.995, 2.158)
T_{max}	Maximum Temperature	U$(27,35)$	27.001 (27.000, 27.005)

Table 6.5: The table shows the Logan 10 thermal performance curve and all its parameters, the priors given to them, and the posterior median and highest posterior density intervals. All normal distributions are given as $N(\mu, \tau)$, where $\tau = \frac{1}{\sigma^2}$.

Ratkowsky83 $r_T = c(T - T_{min})(1 - e^{(k(T-T_{max}))}))^2$			
Parameters	Definition	Prior Distribution	Posterior Median
c	Regression Coefficient	Gamma$(1, 1)$	0.069 (0.059, 0.082)
k	Regression Coefficient	Gamma$(1, 1)$	0.215 (0.181, 0.249)
T_{min}	Thermal Minimum	$\mathcal{N}(277, .5)$	274.6 (272.9, 276.5)
T_{max}	Thermal Maximum	U$(300, 308)$	301.6 (301.4, 301.7)

Table 6.6: The table shows the Ratkowsky 83 thermal performance curve and all its parameters, the priors given to them, and the posterior median and highest posterior density intervals. All normal distributions are given as $N(\mu, \tau)$, where $\tau = \frac{1}{\sigma^2}$.

Ikemoto $r_T = \frac{\phi \frac{T}{T_\phi} e^{\frac{\Delta H_A}{R}(\frac{1}{T_\phi} - \frac{1}{T})}}{1+e^{\frac{\Delta H_L}{R}(\frac{1}{T_L} - \frac{1}{T})}+e^{\frac{\Delta H_H}{R}(\frac{1}{T_H} - \frac{1}{T})}}$			
Parameters	Definition	Prior Distribution	Posterior Median
T_ϕ	Intrinsic Optimum Temperature	U$(286, 298)$	291.5 (286.5, 295.3)
T_H	$\frac{1}{2}$ Enzymes Active at High Temperature	Gamma$(310, 1)$	294.4 (294.3, 294.5)
T_L	$\frac{1}{2}$ Enzymes Active at Low Temperature	Gamma$(273, 1)$	282.7 (282.3, 283.1)
ΔH_A	Enthalpy of activation	$\mathcal{N}(16651, 5)$	16651.0 (16650.1, 16651.9)
ΔH_H	Change in Enthalpy at High Temperatures	$\mathcal{N}(67500, 5)$	67500.0 (67499.2, 67500.9)
ΔH_L	Change in Enthalpy at Low Temperatures	$\mathcal{N}(-72500, 5)$	-72500.0 (-72500.8, -72499.1)
ϕ	Developtment rate at T_{opt}	U$(0, 2)$	1.341 (0.781, 1.949)
R	Boltzman Gas Constant $\frac{cal}{Kmol}$	Fixed	1.987

Table 6.7: The table shows the Ikemoto thermal performance curve and all its parameters, the priors given to them, and the posterior median and highest posterior density intervals. All normal distributions are given as $N(\mu, \tau)$, where $\tau = \frac{1}{\sigma^2}$.

Appendix D Chapter 5 Supplemental Figures

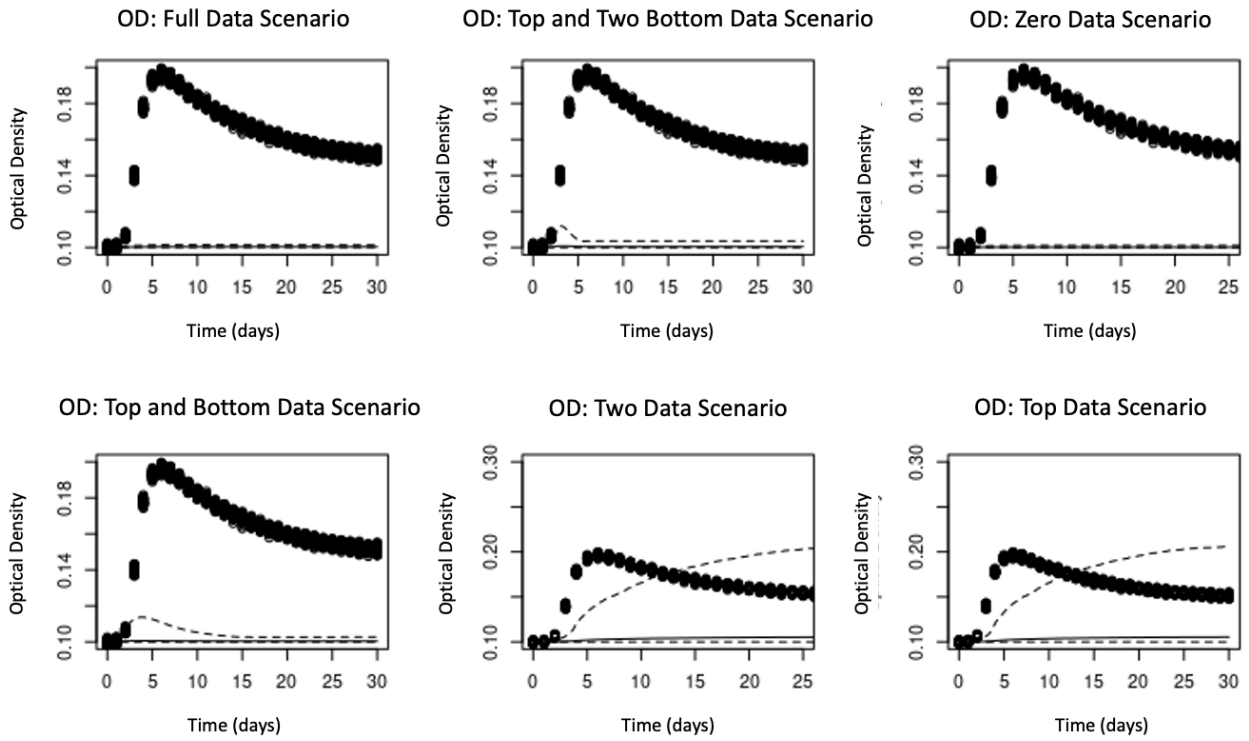

Figure 6.2: Shown are the estimated posterior medians (solid lines), highest posterior density intervals, HPDI, (dashed lines), and the simulated optical density data for each of the explored data simulated scenarios, excluding the reduced data scenarios that do not include MTT or optical density data. Note the y-axes are not the same across panels but, have been scaled to enable examination of all/most of the HPDIs for all model compartments.

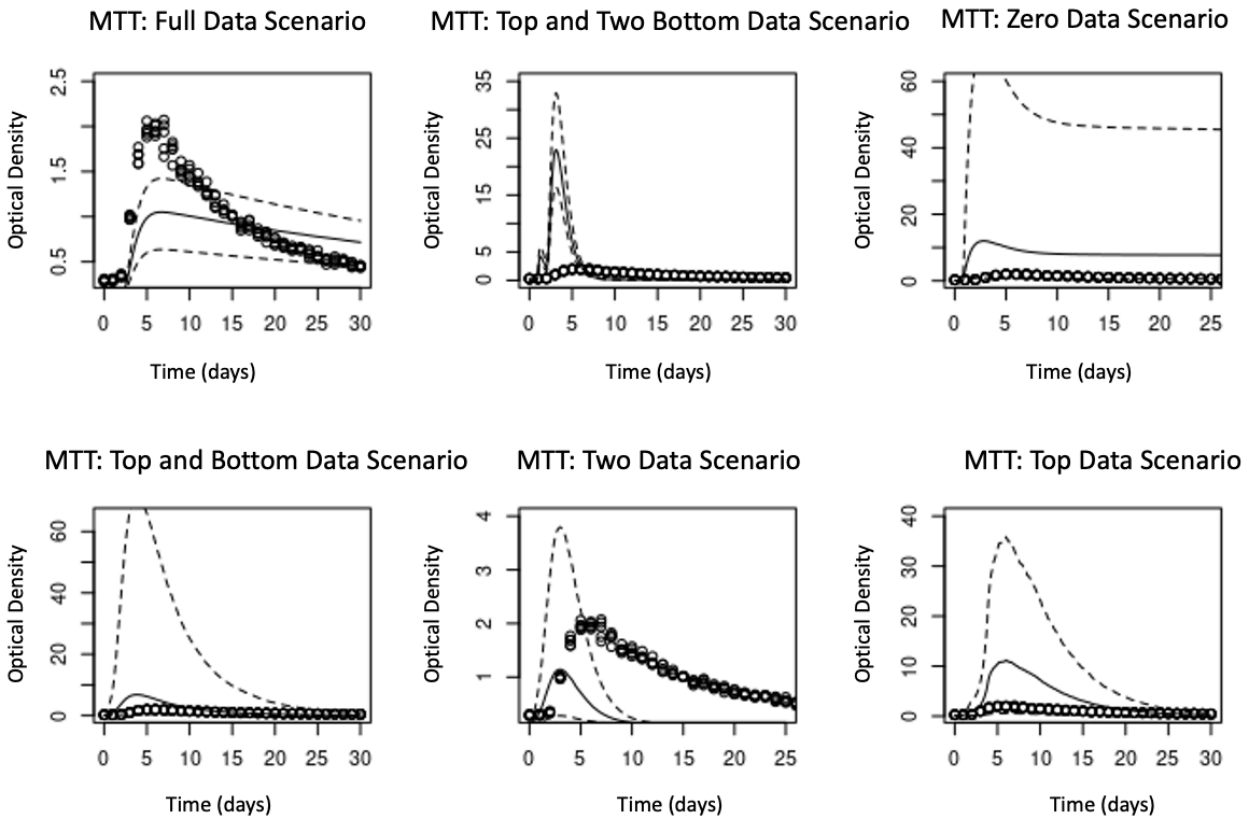

Figure 6.3: Shown are the estimated posterior medians (solid lines), highest posterior density intervals, HPDI, (dashed lines), and the simulated MTT assay data for each of the explored data simulated scenarios, excluding the reduced data scenarios that do not include MTT or optical density data. Note the y-axes are not the same across panels but, have been scaled to enable examination of all/most of the HPDIs for all model compartments.

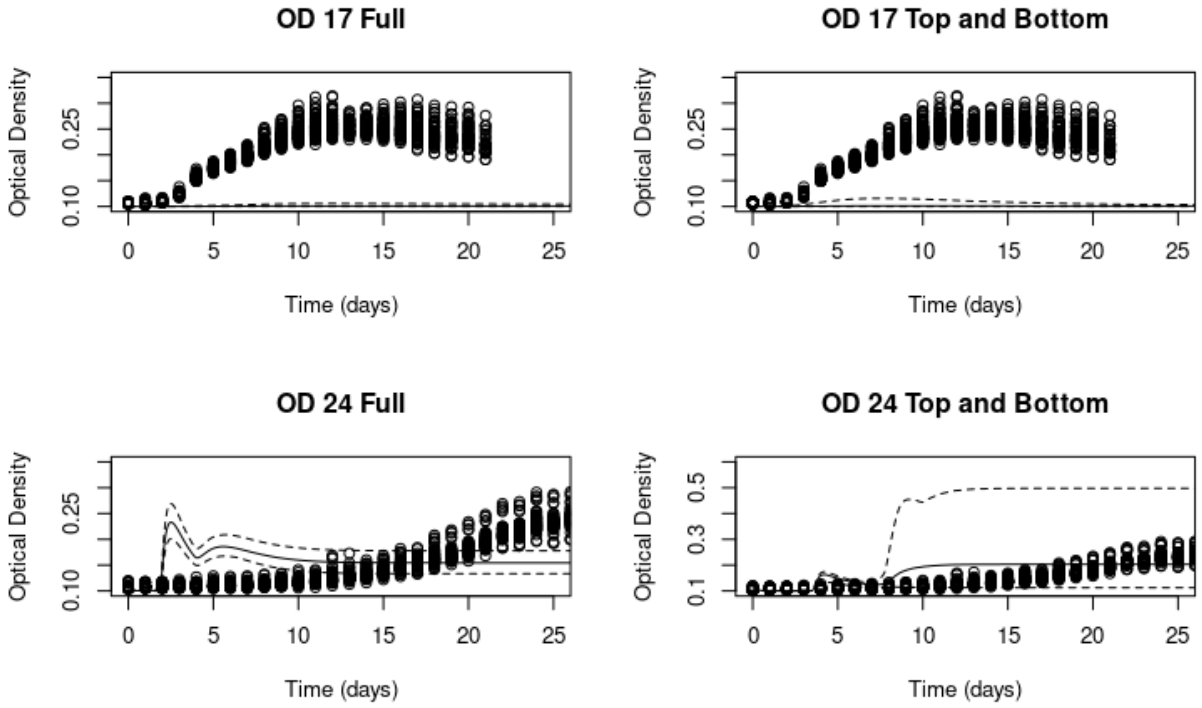

Figure 6.4: Shown are the estimated posterior medians (solid lines), highest posterior density intervals, HPDI, (dashed lines), and the simulated optical density data for each of the explored 17°C and 24°C data scenarios. Note the y-axes are not the same across panels but, have been scaled to enable examination of all/most of the HPDIs for all model compartments.

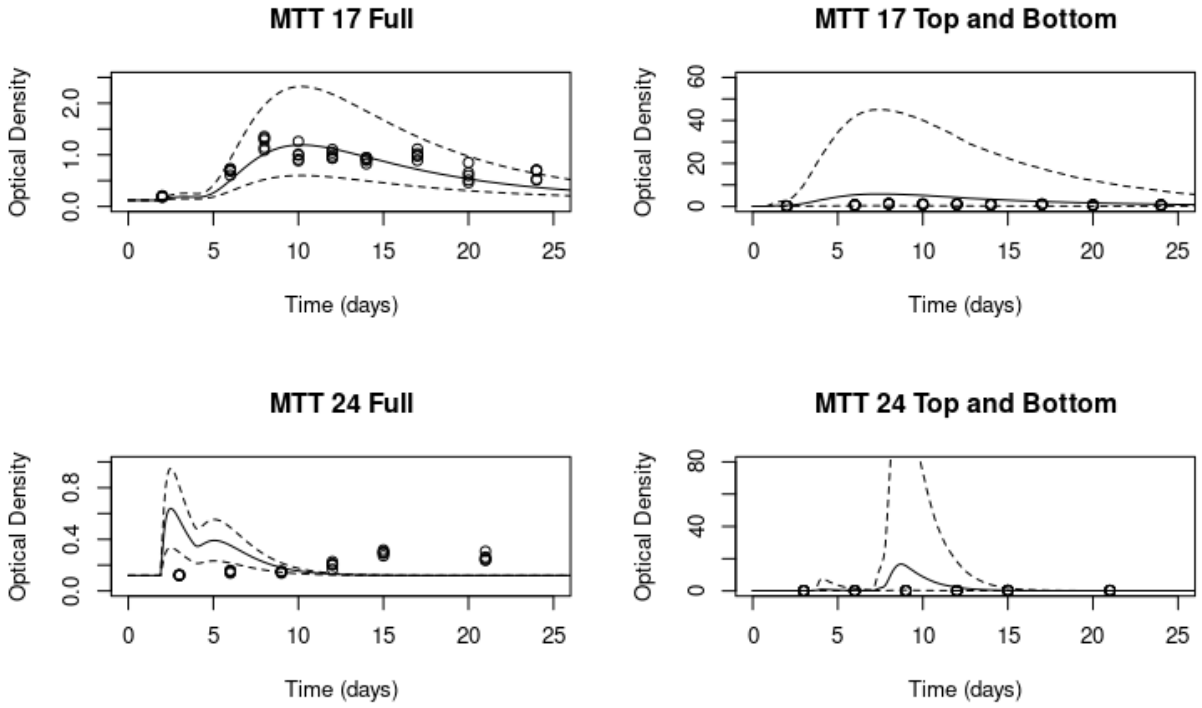

Figure 6.5: Shown are the estimated posterior medians (solid lines), highest posterior density intervals, HPDI, (dashed lines), and the simulated MTT assay data for each of the explored 17°C and 24°C data scenarios. Note the y-axes are not the same across panels but, have been scaled to enable examination of all/most of the HPDIs for all model compartments.

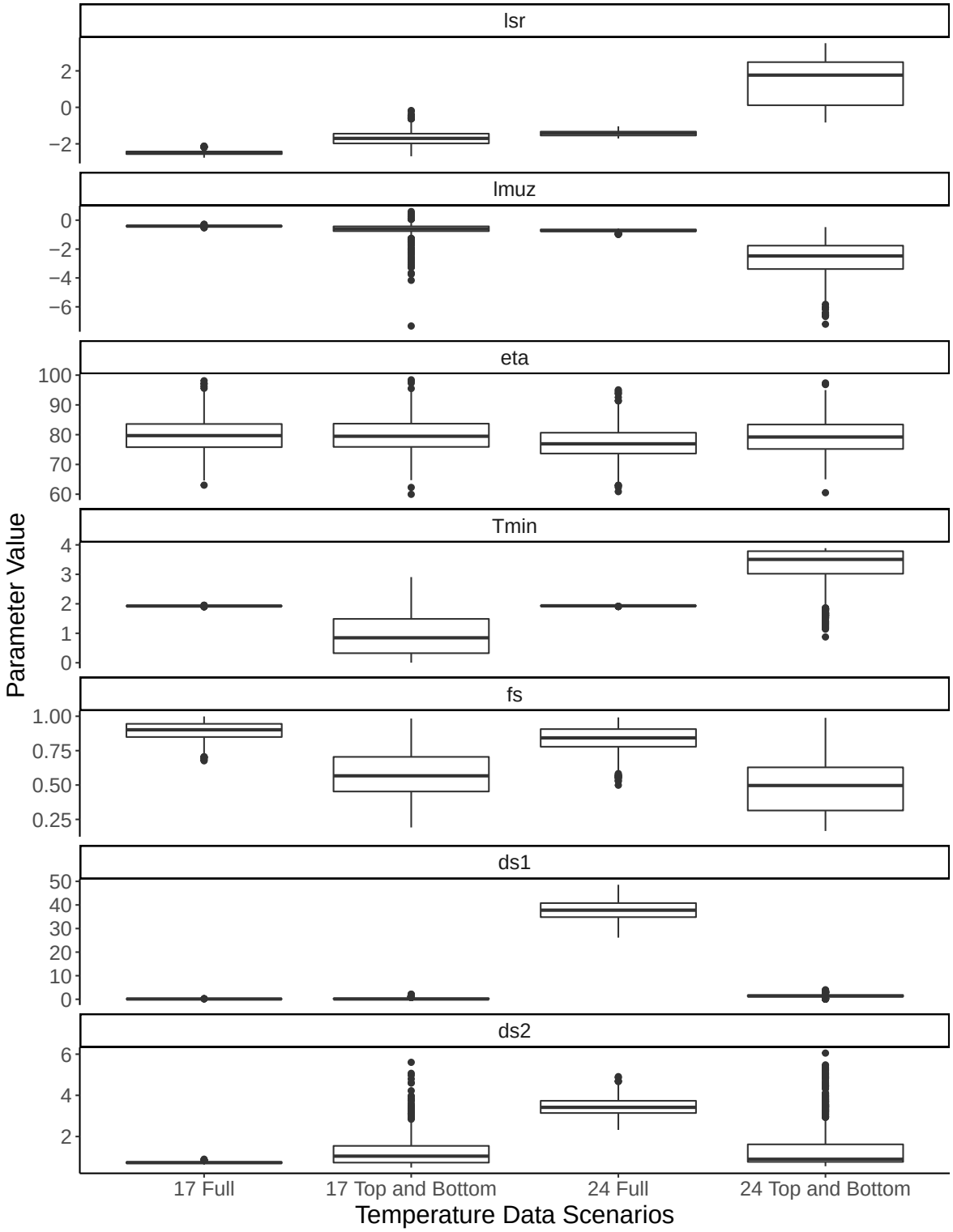

Figure 6.6: For both 17°C and 24°C data scenarios, we plotted the posterior samples for each parameter in the DDE model.

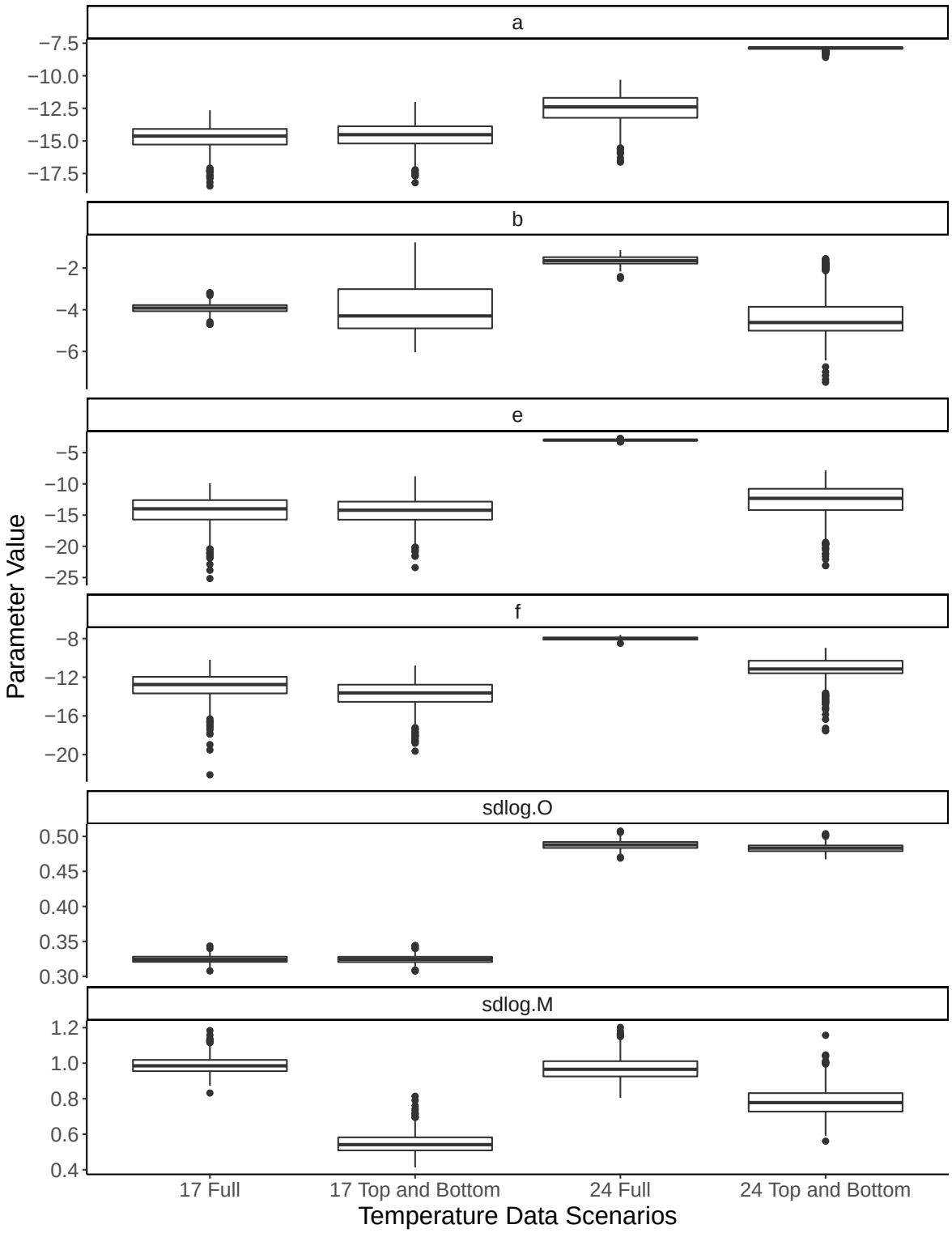

Figure 6.7: For both 17°C and 24°C data scenarios, we plotted the posterior samples for each parameter in the observational models.

Appendix E Chapter 5 Supplemental Tables

Data Scenario	lsr	$lmuz$	f_s	d_{s1}	d_{s2}	η	T_{min}	b	$sdlog.M$	a	e	f	$sdlog.O$
Full	0.00001	0.00001	-	0.00008	0.08	10	0.001	0.00001	0.01	6	15	8	0.002
Zero	0.01	0.01	-	0.00008	0.09	27	0.08	0.05	0.01	6	18	8	0.002
Top	0.01	0.03	-	0.8	0.08	12	0.003	0.06	0.01	6	20	8	0.002
Two	0.005	0.01	-	0.6	0.1	10	0.001	0.06	0.01	6	18	8	0.002
Top and Bottom	0.005	0.008	-	0.00001	0.05	11	0.00001	0.00001	0.01	6	19	8	0.002
Top and Two Bottom	0.00001	0.00001	-	0.3	0.8	13	0.00008	0.06	0.01	6	22	8	0.002
Reduced: Full	0.00001	0.00001	-	3	0.1	25	0.01	-	-	-	-	-	-
Reduced: Top and Bottom	0.01	0.01	-	2	0.05	25	0.01	-	-	-	-	-	-
17°C Full	0.003	0.01	-	0.6	0.1	10	0.001	0.06	0.01	6	18	8	0.002
17°C Top and Bottom	0.009	0.01	-	0.01	0.1	10	0.01	0.06	0.03	6	18	8	0.002
24°C Full	0.005	0.01	-	0.005	0.1	10	0.001	0.2	0.05	6	18	8	0.002
24°C Top and Bottom	0.005	0.01	-	0.01	0.1	10	0.008	0.2	0.05	6	18	8	0.002

Table 6.8: Shown are the tuned variance proposals for each parameters in each simulated and temperature data scenario. We we used a random walk to sample all parameters, except f_s, which was an independent sampler; and therefore we do not have a variance proposal. The top of the table shows the simulated data scenarios and the bottom of the table shows the temperature treatment data scenarios.